Modelling road traffic impact on pollutant concentrations in urban area

Thibaud Sarica

École des Ponts
ParisTech

THÈSE DE DOCTORAT
de l'École nationale des ponts et chaussées

Modélisation de l'impact du trafic routier sur les concentrations de polluants en zone urbaine

École doctorale N°531, Sciences, Ingénierie et Environnement – SIE

Spécialité : Sciences et Techniques de l'Environnement

Thèse préparée au Centre d'Enseignement et de Recherche en Environnement Atmosphérique (CEREA)

Thèse soutenue le 8 juin 2023, par

Thibaud SARICA

Composition du jury:

Isabelle, COLL Professeure, Université Paris-Est Créteil	*Présidente*
Guy, BRASSEUR Professeur, Max Planck Institute for Meteorology	*Rapporteur*
Oriol, JORBA Docteur, Barcelona Supercomputing Center	*Rapporteur*
Yao, LIU Docteure, Université Gustave Eiffel	*Examinatrice*
Lionel, SOULHAC Professeur, INSA Lyon	*Examinateur*
Karine, SARTELET Docteure, École nationale des ponts et chaussées	*Directrice de thèse*
Yelva, ROUSTAN Docteur, École nationale des ponts et chaussées	*Co-encadrant de thèse*
Christophe, CHAILLOU Docteur, Aramco	*Invité*

THÈSE DE DOCTORAT
de l'École nationale des ponts et chaussées

Soutenue publiquement le 8 juin 2023 par

Thibaud SARICA

pour l'obtention du grade de
Docteur de l'École nationale des ponts et chaussées

Spécialité : Sciences et Techniques de l'Environnement
École doctorale Sciences, Ingénierie et Environnement – SIE

Modélisation de l'impact du trafic routier sur les concentrations de polluants en zone urbaine

Modelling road traffic impact on pollutant concentrations in urban area

---

Jury composé de

P[r] Isabelle COLL	Université Paris-Est Créteil	Présidente
P[r] Guy BRASSEUR	Max Planck Institute for Meteorology	Rapporteur
D[r] Oriol JORBA	Barcelona Supercomputing Center	Rapporteur
D[r] Yao LIU	Université Gustave Eiffel	Examinatrice
P[r] Lionel SOULHAC	INSA Lyon	Examinateur
D[r] Karine SARTELET	École nationale des ponts et chaussées	Directrice de thèse
D[r] Yelva ROUSTAN	École nationale des ponts et chaussées	Co-encadrant de thèse
D[r] Christophe CHAILLOU	Aramco	Invité

"THERE IS AS YET INSUFFICIENT DATA FOR A MEANINGFUL ANSWER."
Isaac Asimov, The Last Question, 1956

Remerciements

Ce manuscrit de thèse représente l'aboutissement de plus de trois années de travail durant lesquelles j'ai eu la chance de rencontrer, d'échanger et de travailler avec de nombreuses personnes. Tout d'abord, je tiens à remercier les membres de mon jury de thèse pour leur disponibilité et leur bienveillance ; Guy Brasseur et Oriol Jorba pour avoir accepté la charge de rapporteur et Isabelle Coll, Yao Liu et Lionel Soulhac celle d'examinateur.

Je remercie tout particulièrement ma directrice de thèse, Karine Sartelet, et mon co-encadrant de thèse, Yelva Roustan. Merci pour votre patience et votre aide tout au long de ce projet. J'ai pu, grâce à tous nos échanges, grandir scientifiquement et également développer tout un panel de compétences et connaissances précieuses.

Merci à l'équipe d'Aramco, en particulier Christophe Chaillou, Clément Larrieu et Salah-Eddine Wali, de m'avoir fait confiance et d'avoir participé activement à mes travaux. J'ai grandement apprécié notre collaboration et nos échanges.

Je remercie également Steen Solvang Jensen et Matthias Ketzel, ainsi que toute l'équipe de l'Université d'Aarhus, pour notre collaboration et votre accueil pendant ma visite à Roskilde.

À tous mes collègues/amis du CEREA, merci pour tous les moments que nous avons passés ensemble. Un merci tout particulier à Youngseob pour nos discussions et ton aide précieuse pour me guider dans les méandres de Polyphemus et à Lydie pour ton aide sur les questions administratives et nos discussions entre deux bureaux. Je remercie Quentin de m'avoir supporté tout ce temps en partageant mon bureau et pour toutes nos conversations scientifiques, et beaucoup moins scientifiques. Merci à tous pour les agréables pauses thé (et café !), notamment Aurélie, Clémentine et Pierre.

J'ai une pensée toute particulière pour ma famille et mes amis, qui ont toujours été présents, de près comme de loin. Merci pour votre soutien, votre inspiration et la force que vous me transmettez. Sans vous, je ne serais pas allé aussi loin, merci !

Résumé

En milieu urbain et en particulier dans les rues, les personnes sont exposées à de fortes concentrations de dioxyde d'azote (NO_2), et de particules dont les aérosols organiques (OM) et le carbone suie (BC). Afin de mieux comprendre les sources et représenter l'évolution des concentrations dans les rues, une modélisation multi-échelle est utilisée, avec le modèle de réseaux de rues MUNICH couplé au modèle de chimie-transport régional Polair3D et au module chimique SSH-aerosol pour représenter la formation des composés secondaires aux différentes échelles.

L'influence des émissions des composés organiques volatils (COV) du trafic routier, des émissions hors dues à l'usure des hors échappements et des émissions d'asphalte est étudiée avec des scénarios de sensibilité. La simulation de référence utilise des facteurs d'émission standards obtenus de la méthodologie COPERT. L'utilisation de données récentes de mesure de spéciation permet de mieux caractériser les COV émis, en particulier les composés organiques intermédiaires, semi et faiblement volatils (COVI/S/F), engendrant une réduction des concentrations de OM allant jusqu'à 27 %. Une augmentation de 219 % des émissions de BC dues à l'usure des pneus, cohérente avec la littérature, double les concentrations de BC. Les émissions d'asphalte augmentent fortement les émissions de COVI/S/F. Les concentrations de particules simulées en prenant en compte ces émissions se comparent bien aux observations, soulignant l'importance de mieux caractériser cette source manquante dans les modèles.

Des simulations sont ensuite réalisées pour l'année 2030 afin d'évaluer les impacts futurs des émissions du trafic sur les concentrations. L'introduction de véhicules à très faibles émissions, conformes aux futures normes européennes d'émissions, induit une forte réduction des émissions par rapport à une flotte représentative de l'année 2014. Les émissions de NO_2 et de BC sont réduites de 70 %, entrainant une diminution des concentrations de 52 % pour le NO_2, 42 % pour le BC, et 20 % pour les particules. Les émissions d'une flotte composée uniquement de véhicules à très faibles émissions sont 99 % et 80 % plus faibles pour le NO_2 et le BC respectivement, réduisant les concentrations de NO_2 de 80 % et celles de BC de 45 %.

Pour représenter les gradients de concentrations dans les rues et mieux estimer l'exposition des personnes, une nouvelle version de MUNICH est développée. Plutôt que de considérer les concentrations homogènes dans chaque segment de rue, le volume des rues est discrétisé avec trois niveaux verticaux. Une discrétisation horizontale en deux zones est également introduite sous certaines conditions avec une paramétrisation tirée du modèle OSPM. Les concentrations simulées dans les rues de Copenhague et de l'est parisien avec cette version discrétisée de MUNICH se comparent mieux aux observations que celles simulées avec la version homogène, et les concentrations de NO_2, BC et OM sont plus élevées en bas des rues.

Mots-clés : qualité de l'air, modélisation numérique, trafic routier, émissions, milieu urbain, polluants primaires et secondaires

Abstract

In urban areas and in particular in the streets, populations are exposed to high concentrations of nitrogen dioxide (NO_2), and particulate matter including organic aerosols (OM) and black carbon (BC). In order to better understand the sources and to represent the evolution of the concentrations in the streets, a multiscale modeling is used, with the street-network model MUNICH coupled to the regional chemistry-transport model Polair3D, and to the chemical module SSH-aerosol to represent the formation of the secondary compounds at the different scales.

The influence of volatile organic compound (VOC) emissions from road traffic, non-exhaust emissions due to tire wear and asphalt emissions are studied with sensitivity scenarios. The reference simulation uses standard emission factors obtained from the COPERT methodology. The use of recent speciation measurement data allows for a better characterization of the emitted VOCs, in particular intermediate, semi and low volatile organic compounds (I/S/LVOC), resulting in a reduction of OM concentrations of up to 27 %. A 219 % increase in BC emissions from tire wear, consistent with the literature, doubles BC concentrations. Asphalt emissions strongly increase I/S/LVOC emissions. The simulated PM concentrations taking into account these emissions compare well with observations, highlighting the importance of better characterizing this missing source in the models.

Simulations are then performed for the year 2030 to assess the future impacts of traffic emissions on concentrations. The introduction of ultra-low emission vehicles, compliant with future European emission standards, results in a large reduction in emissions compared to a representative fleet of 2014. NO_2 and BC emissions are reduced by 70 %, resulting in a decrease in concentrations of 52 % for NO_2, 42 % for BC, and 20 % for PM. Emissions from a fleet of only ultra-low emission vehicles are 99 % and 80 % lower for NO_2 and BC respectively, reducing NO_2 concentrations by 80 % and BC concentrations by 45 %.

To represent the concentration gradients in the streets and to better estimate the population exposure, a new version of MUNICH is developed. Instead of considering homogeneous concentrations in each street segment, the street volume is discretized with three vertical levels. A horizontal discretization into two zones is also introduced under specific conditions with a parameterization from the OSPM model. The concentrations simulated in the streets of Copenhagen and eastern Paris with this discretized version of MUNICH compare better with observations than those simulated with the homogeneous version, and the concentrations of NO_2, BC and OM are higher at the bottom of the streets.

Keywords: air quality, numerical modeling, road traffic, emissions, urban area, primary and secondary pollutants

Contents

List of acronyms

Chapter 1

Introduction

Contents

1.1 Atmospheric composition and pollution

1.1.1 Atmospheric compounds and their origin

Air pollutants include a wide variety of compounds that can be observed in the gas and/or particulate phases. In this context, the term aerosols refers to systems composed of particles and the surrounding gases. When directly emitted in the atmosphere, compounds are classified as primary pollutants. Among them, carbon monoxide (CO) and primary organic aerosols (POAs) can be found. On the other hand, compounds that are formed in the atmosphere through physicochemical transformations are classified as secondary pollutants, such as ozone (O_3) and secondary organic aerosols (SOAs). For some pollutants the concentrations have both a primary and a secondary contribution, as for nitrogen dioxide (NO_2).

The volatile organic compounds (VOCs) consist of compounds existing only in the gas phase, i.e. with saturation vapor pressure higher than that of dodecane with 12 atoms of carbon. Organic compounds with relatively low vapor pressure are further classified as intermediate-volatile organic compounds (IVOCs), semi-volatile organic compounds (SVOCs) and low-volatile organic compounds (LVOCs) (Gentner et al. 2017).

Primary pollutants originate either from natural sources or anthropogenic sources, i.e. emitted through human activities. Natural sources of particles include wind erosion, volcanic eruptions and suspension of sea salts by waves. Particles emitted can be inert, such as mineral dust and black carbon (BC). If they interact in the atmosphere, they are further classified as organic, such as organic matter (OM), or inorganic, such as sea salts composed of sodium, chlorine and sulfate. Natural

particles have in general diameters larger than 1 µm, thus limited atmospheric lifetimes. Among the natural sources, emissions by the organic matter like soil, trees and plants, namely biogenic emissions, are also an important source of gases and particles, in particular of VOCs.

Anthropogenic sources of gases and particles encompass all human activities, from the industrial sector to road traffic and residential heating. The diameters of the emitted particles are usually lower than 1 µm, but the ones emitted by abrasion processes (tire, brake and road) or by agriculture and construction processes are typically coarser, with diameters superior to 2.5 µm.

Secondary pollutants are formed from gas precursors through gas-phase chemistry and aerosol dynamics (nucleation, coagulation, condensation/evaporation). Secondary particles are composed for the majority of ammonium, nitrate, sulfate and OM. Gas precursors originate mainly from fossil fuel combustion, agriculture and biomass burning, but also from biogenic emissions. The oxidation of the VOCs can also lead to the formation of lower-volatility compounds that may partition more easily to particles. Their diameters are generally lower than 2.5 µm.

Air pollutants present a wide variety of physicochemical characteristics (Putaud et al. 2010; Seinfield et al. 2016; Franzin et al. 2020). They are related to the origins of the pollutants and induce different impacts on the environment and the human health.

1.1.2 Impacts of atmospheric pollution

1.1.2.1 Impacts on the environment

Impacts of the air pollutants on the environment are numerous. They range from impacts on the climate, due to interactions between particles and incoming solar radiation, to impacts at the scale of the city and the street.

Interactions between atmospheric particles and the incoming solar radiation are complex and classified into direct, indirect and semi-direct effects. The direct effects on the solar radiative forcing are caused by the absorption and scattering of the solar radiation. Some species, such as BC, are able to absorb the solar radiation It induces a positive radiative forcing, thus the warming of the atmosphere (Roberts et al. 2004; Bond et al. 2013). On the contrary, other species, such as desert dusts, scatter the incoming solar radiation, resulting in a negative radiative forcing, i.e. cooling of the atmosphere (Myhre et al. 2013a). Indirect effects are the result of the modification of cloud properties due to the presence of particles able to act as cloud condensation nuclei (CCN). These new CCN induce an increase in the number of cloud droplets while reducing their size (Twomey 1977; Koehler et al. 2009). The solar radiation is then more reflected, and the radiative forcing is negative. Due to the reduced size of the could droplets, more time may be needed for them to grow enough to precipitate. The semi-direct effects are related to aerosols, with absorption properties, that are able to modify cloud properties without acting as CCN. Figure 1.1 presents the mean radiative forcing in 2011 in regard to 1750, estimated by the intergovernmental panel on climate control (IPCC) (Myhre et al. 2013b). Overall, aerosols have a cooling effect; but the warming effect of BC is visible.

The reduction of the visibility, especially in urban areas, can be caused by high concentrations of NO_2 or particulate matter (PM) (Wan et al. 2011; Manisalidis et al. 2020). In the PM, BC is particularly declared as a strong contributor to this effect (Chen et al. 2016; Li et al. 2022b).

Atmospheric pollution is responsible for other negative effects on the environment. It can contribute to the acidification of precipitation, through species such as sulfur dioxide (SO_2), which impacts both the natural and build environments (Singh et al. 2008; Xie et al. 2013; Manisalidis et al. 2020). The growth and yield of the vegetation can also be impacted when concentrations of O_3, NO_2 an SO_2 are high (Agrawal 2005; Fares et al. 2013). The progressive deposition of PM affect both vegetation growth and human constructions (Kuzmichev et al. 2016).

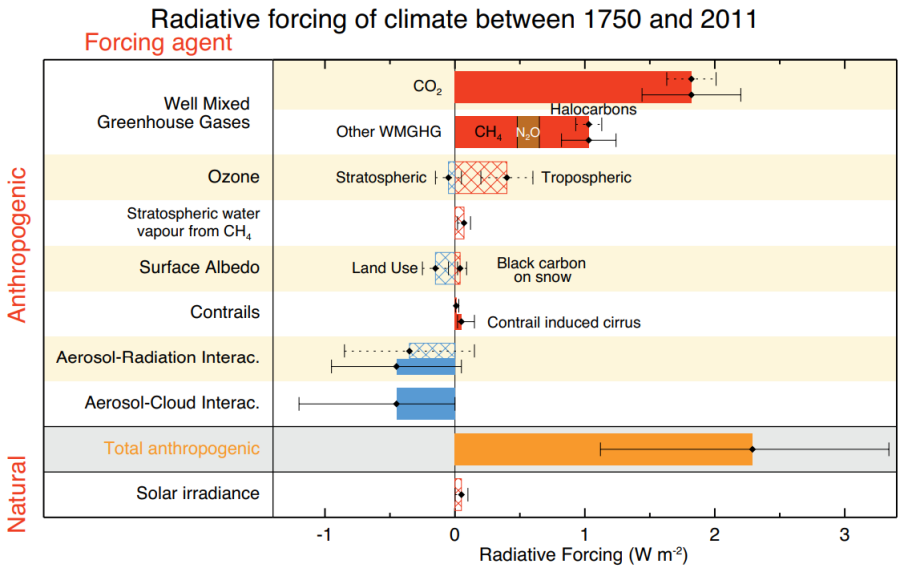

Figure 1.1: Mean radiative forcing in 2011 compared to 1750 for the main atmospheric compounds and mechanisms, estimated by the IPCC. Blue bars indicate a cooling effect, and red bars a warming effect (Myhre et al. 2013b).

1.1.2.2 Impacts on human health

In 2020, in Europe, exposure to high concentrations of NO_2, O_3 and fine particulate matter ($PM_{2.5}$) led to more than 300 000 premature deaths (EEA 2023). The impacts of atmospheric pollution on human health are related to the interactions between the pollutants and the metabolism. Among the harmful pollutants, NO_2, O_3, CO and PM can be cited. PM is considered to be the most harmful of them (Lelieveld et al. 2015).

Gaseous pollutants are responsible for various negative impacts on human health, mainly on the respiratory and cardiovascular systems. Limited exposure to high concentrations leads to both reversible and non-reversible effects, such as coughing, headache and the development of asthma. Long-term exposure to high concentrations of gaseous pollutants can have non-reversible impacts on the human body, e.g. chronic lung disease and cardiovascular disease (Manisalidis et al. 2020). NO_2 (Khaniabadi et al. 2017), O_3 (Zhang et al. 2019) and CO (Chen et al. 2007) are able to deeply penetrate into the lungs. Other compounds, parts of the VOCs, such as benzene, as also known to be highly toxic and classified as carcinogenic (Boeglin et al. 2006).

Impacts of particles on human health depends on their penetration in the respiratory system. Figure 1.2 presents the levels of penetration in regard to the particle diameter. Particles with a diameter larger than 10 µm are mainly blocked in the nose and the throat, and thus are not considered harmful. Particulate matter less than 10 µm in diameter (PM_{10}) are able to penetrate the air ways down to the lungs and cause irritation and difficulties to breathe for vulnerable people. Even smaller particles, with a diameter inferior to 2.5 µm and 0.1 µm, can infiltrate the vascular system and impacts other organs (Loaiza-Ceballos et al. 2021). Chemical composition of the particles also plays an important role in the impacts on human health. Particles of BC and OM are known to cause heart problems, lung cancer and the aggravation of preexisting heart and lung disease (Dons et al. 2012; Daellenbach et al. 2020; Ali et al. 2021; Chen et al. 2022). An explanation for the development of lung cancer in never-smokers and light smokers from $PM_{2.5}$ has recently been published in Hill et al. (2023).

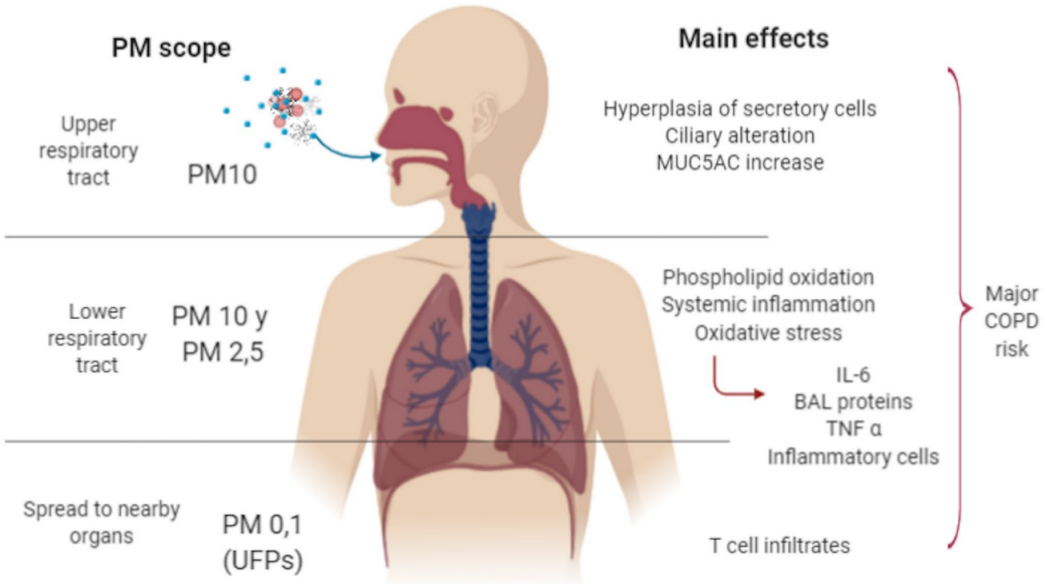

Figure 1.2: Penetration of particles in the respiratory system and their impacts on health. COPD stands for chronic obstructive pulmonary disease (Loaiza-Ceballos et al. 2021).

1.1.3 Air pollution regulations

In urban areas, concentrations of atmospheric pollutants are generally higher than those observed in more rural areas (Strosnider et al. 2017; Milojevic et al. 2017; Crippa et al. 2021). This is related to the concentration of the population in a dense urban fabric that limits the dispersion of pollutants. Anthropogenic emissions of nitrogen oxides (NO_x), PM and VOCs are particularly predominant in urban areas due to the proximity to road traffic and residential heating (Dios et al. 2010; Trombetti et al. 2018).

In an effort to reduce the adverse effects of air pollution on the populations exposed, the European Union (EU) and the World Health Organization (WHO) have set air quality standards (EU 2015; WHO 2021, respectively). Table 1.1 presents these two standards for the main atmospheric pollutants (NO_2, O_3, CO, $PM_{2.5}$ and PM_{10}). The limit values enforced by the EU were updated in 2015. The values proposed by the WHO, updated in 2021, are guidelines based on the recent discovery of the impacts of air pollution on the environment and the human health. They are more stringent than the European limit values, in particular for $PM_{2.5}$ and PM_{10}.

In 2020, despite reductions in emissions, 96 % of the European urban population was exposed to concentrations of $PM_{2.5}$ above the WHO guidelines. In contrast, less than 1 % was exposed to $PM_{2.5}$ concentrations above the EU directives, illustrating the discrepancy between current EU policy objectives and the scientific evidence on when health effects occur[1].

In addition, other compounds are regulated, such as SO_2, benzene, lead and arsenic. Specific types of PM, such as BC and ultrafine particles (particles that are less than 100 nm in diameter), are not yet regulated. This is due to the insufficient quantitative evidence on independent adverse health effects at the time of deriving the air-quality standards. However, good practice statements are shared until guidelines are defined (WHO 2021).

[1] https://www.eea.europa.eu/highlights/vast-majority-of-europes-urban (last visited 2023-04-21)

Table 1.1: Air quality standards set by the EU and the WHO (EU 2015; WHO 2021, respectively).

		European Air Quality Directives		WHO Air Quality Guidelines	
Pollutant	Averaging period	Concentration (objective)	Comments	Concentration	Comments
NO_2	Hourly	$200\,\mu g\,m^{-3}$ (limit value)	Not to be excessed on more than 18 hours/year	$200\,\mu g\,m^{-3}$	
	Annual	$40\,\mu g\,m^{-3}$ (limit value)		$10\,\mu g\,m^{-3}$	
O_3	Maximum daily 8-hour average	$120\,\mu g\,m^{-3}$ (target value)	Not to be excessed on more than 25 days/year (averaged over 3 years)	-	
	8 hours	-		$100\,\mu g\,m^{-3}$	99th percentile (i.e. 3-4 exceedance days per year)
CO	Maximum daily 8-hour average	$10\,\mu g\,m^{-3}$ (limit value)		$10\,\mu g\,m^{-3}$	
	24 hours	-		$4\,\mu g\,m^{-3}$	99th percentile (i.e. 3-4 exceedance days per year)
$PM_{2.5}$	24 hours	-		$15\,\mu g\,m^{-3}$	99th percentile (i.e. 3-4 exceedance days per year)
	Annual	$25\,\mu g\,m^{-3}$ (limit value)		$5\,\mu g\,m^{-3}$	
PM_{10}	24 hours	$50\,\mu g\,m^{-3}$ (limit value)	Not to be excessed on more than 35 days/year	$45\,\mu g\,m^{-3}$	99th percentile (i.e. 3-4 exceedance days per year)
	Annual	$40\,\mu g\,m^{-3}$ (limit value)		$15\,\mu g\,m^{-3}$	

1.2 Air quality modeling

Among the different approaches to study air quality, numerical models have been developed for several decades. They integrate our knowledge of the physicochemical processes taking place in the atmosphere to estimate pollutant concentrations. They can also be used as forecasting and prospective tools.

Numerical models are able to represent the dispersion and physicochemical transformations of pollutants at different spatial and time scales. Regional-scale chemistry-transport models (CTMs), such as Polair3D (Section 1.2.1), CHIMERE (Falasca et al. 2018; Menut et al. 2021) and CMAQ (Wong et al. 2012; Paz et al. 2015), are typically used to represent the urban background concentrations by solving the chemistry-transport equation. However, they are limited to spatial resolutions down to $\sim 1\,km^2$, and thus cannot represent concentrations in streets, where populations live close to emission sources.

To represent these concentrations, local-scale models are thus developed using different approaches. Computational fluid dynamics (CFD) models, such as code_saturne (Archambeau et al. 2004; Gao et al. 2018) and OpenFOAM (Lin et al. 2022), solve the Navier-stokes equations and mass conservation equations to represent pollutant concentrations with a fine spatial resolution. However, due to this fine definition of the buildings and streets, they suffer from high computational cost. Other models using approaches less accurate than CFD but that run faster are also developed. They are typically based on a Gaussian and/or an Eulerian approach (Vardoulakis et al. 2003; Liang et al. 2023). Among

these, can be mentioned the model of urban network of intersecting canyons and highways (MUNICH) (Section 1.2.2), the operational street pollution model (OSPM) (Berkowicz 2000b), SIRANE (Soulhac et al. 2011) and ADMS-Urban (McHugh et al. 1997; Hood et al. 2021).

Below are briefly described the two models used during this thesis, Polair3D and MUNICH. Both models are coupled to SSH-aerosol to represent the gas-phase chemistry and the physicochemical transformation undergone by aerosols in the troposphere. It is presented in Section 1.2.3.

1.2.1 Polair3D: regional-scale modeling

Polair3D is an off-line 3D Eulerian CTM from the Polyphemus air quality modeling platform[2] (Boutahar et al. 2004; Mallet et al. 2007). It is able to calculate pollutant concentrations from the regional scale down to city scale. It has been applied to several locations, providing accurate representations of gas and particle concentrations under different conditions (Sartelet et al. 2012; Zhu et al. 2016a,b; Sartelet et al. 2018; Abdallah et al. 2018).

Polair3D solves the time evolutions of pollutant concentrations on a regular grid taking into account the processes presented in Figure 1.3. The advection represents the three-dimensional transport by the wind, considering that the pollutant moves together with the mass of air in which it is located. The homogenization of concentrations due to turbulent diffusion is caused by the agitation of the air due to friction with the ground, but also by the vertical temperature gradient.

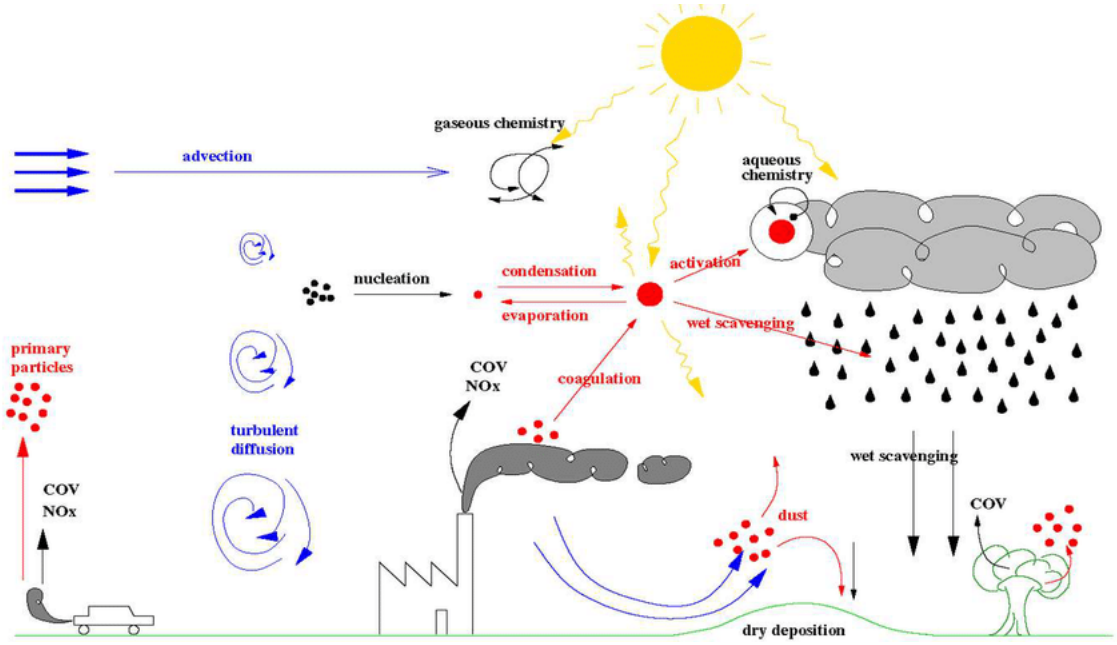

Figure 1.3: Processes taken into account in Polair3D (Sportisse 2010).

Emissions of gases and particles from natural and anthropogenic sources are both taken into account in the model. They are differentiated between surface emissions, happening near the ground such as road traffic emissions, and volume emissions, taking place higher in the atmosphere from the aviation and stacks on industrial plants for example. Dry deposition and wet scavenging remove gas and particle pollutants from the atmosphere. Dry deposition happens near the ground and is directly

[2] http://cerea.enpc.fr/polyphemus/ (last visited 2023-04-21)

proportional to the concentration above the ground. Wet scavenging is the loss by mass transfer with the aqueous phase (rain and in clouds).

The processes of gas-phase chemistry and aerosol dynamics (nucleation, coagulation, condensation/evaporation) are represented in Polair3D thanks to the coupling with SSH-aerosol (Section 1.2.3).

1.2.2 MUNICH: local-scale modeling

The model of urban network of intersecting canyons and highways (MUNICH)[3] is based on an Eulerian box-model approach to represent pollutant concentrations in the streets. It is extensively described in Kim et al. (2018, 2022); Lugon et al. (2020).

MUNICH has two components: a street segment and an intersection (respectively in red and green in Figure 1.4). Street canyons are represented by street segments in which pollutant concentrations are considered homogeneous. They are bounded by intersections with other streets at each end. The horizontal advection of air masses between streets is represented by these intersections.

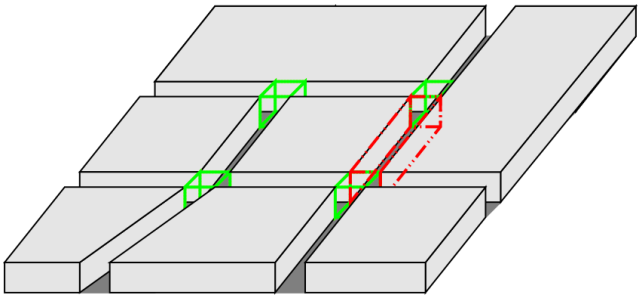

Figure 1.4: Representation of a street network in MUNICH with a street segment in red and intersections in green.

1.2.2.1 Street segment component

In MUNICH, a street segment is represented using an Eulerian box-model approach. With this approach, the resulting pollutant concentrations are considered homogeneous in the street segment. Each street segment is defined by a length L, a width W and an average building height H. This average height constrains MUNICH to be used in dense urban area.

The time variations of the mass M of a given pollutant rely on transport and chemistry processes, highlighted in Figure 1.5 and by the following mass conservation equation:

$$\frac{\mathrm{d}M}{\mathrm{d}t} = Q_{\mathrm{emis}} + Q_{\mathrm{inflow}} + Q_{\mathrm{outflow}} + Q_{\mathrm{vert}} + Q_{\mathrm{dep}} + Q_{\mathrm{chem}} + Q_{\mathrm{resusp}} \tag{1.1}$$

Q_{emis} is the flux emitted by traffic (light blue arrow in Figure 1.5). Q_{inflow} and Q_{outflow} are the incoming and outgoing fluxes via the intersections (light green arrows in Figure 1.5). Q_{vert} is the vertical turbulent exchange of pollutant with the background above the street (dark blue arrow in Figure 1.5). Q_{dep} is the flux of dry and wet deposition (orange arrow in Figure 1.5). Q_{chem} represents the physicochemical transformations undergone by the pollutant (red box in Figure 1.5). Q_{resusp} is the flux due to the resuspension of previously deposited materials on the road. It has been added in Lugon et al. (2021b), and has been estimated to be low for black carbon. The mass is expressed in µg and the fluxes in $\mu g\,s^{-1}$.

[3] http://cerea.enpc.fr/munich/ (last visited 2023-04-21)

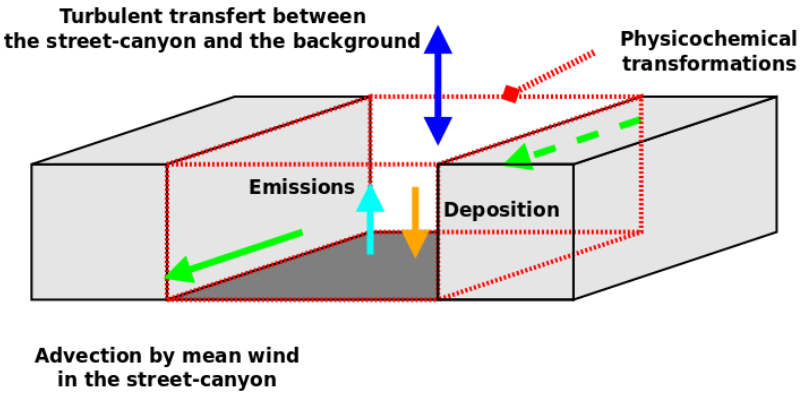

Figure 1.5: Representation of the processes taking place in a street segment of MUNICH.

Several meteorological parameters are needed to compute the evolution of pollutant concentrations in the street, e.g. planetary boundary layer height, surface pressure and temperature. Among them, wind information is crucial to determine the horizontal advection through the intersections and the vertical exchange with the background.

In the street, the wind direction is supposed to follow the street direction and the wind speed in the street is dependent on the wind speed at roof level. Two parameterizations are implemented in MUNICH to calculate the horizontal wind speed at roof level. The first one is based on a 2D parameterization of the wind field along the street axis (Soulhac et al. 2011). The second one, added in MUNICH v2.0 (Kim et al. 2022), corresponds to the application of an average vertical profile over a large homogeneous district or city. It is based on the calculation of a displacement height and a roughness length for the area considered (Macdonald et al. 1998). This second parameterization is used throughout this thesis.

To compute the mean horizontal wind speed in the street, MUNICH proposes three parameterizations (Maison et al. 2022). The first two, based on Soulhac et al. (2008) and Lemonsu et al. (2004), are exponential profiles that do not satisfy the no-slip condition at the ground. The third one, following Wang (2012, 2014), always satisfies this condition (Maison et al. 2022) and is thus used throughout this thesis.

The term Q_{vert}, which is the vertical turbulent exchange of pollutant with the background above the street, can also be calculated following three parameterizations in MUNICH. The first two, based on Soulhac et al. (2011) and Schulte et al. (2015), evaluate the vertical turbulent exchange at roof level, while the third one is able to calculate it at any height in the street. It is based on Wang (2012) with comparison to CFD (Maison et al. 2022). This parameterization is thus used throughout this thesis and more information is available in Chapter 5.

The physicochemical transformations Q_{chem} undergone by pollutants in the street are taken into account in MUNICH by the coupling with SSH-aerosol (Section 1.2.3). The model is thus able to represent aging of primary and formation of secondary gases and particles. A simple three-reaction mechanism involving solely nitric oxide (NO), NO_2 and O_3, known as the Leighton relationship is also implemented (Leighton 1961). This simplified mechanism is presented and used in Chapter 5.

1.2.2.2 Intersection component

In MUNICH, an intersection is considered to be a point in space connected to at least one street segment. Complete descriptions of the concept are available in Soulhac et al. (2009); Kim et al. (2018).

For an intersection and depending on the meteorological parameters, in particular wind direction and speed, the total air flow entering the intersection P_{in} is the sum of the incoming air fluxes from the windward street segments; and the total air flux exiting the intersection P_{out} is the sum of the outgoing air fluxes by the leeward street segments. Given that street segments have different widths and heights, the incoming and outgoing total air fluxes are not always equal. To overcome this, a vertical air flux P_{vert} is considered between the intersection and the overlying atmosphere on top of the intersection:

$$P_{\text{vert}} = P_{\text{in}} - P_{\text{out}} \tag{1.2}$$

This vertical flux is positive if the total incoming flux is superior to the total outgoing flux. In this case, the corresponding excess of pollutant concentrations is sent to the atmosphere. Otherwise, if the total outgoing flux is superior to the total incoming flux, the vertical air flux is negative and pollutant concentrations from the overlying atmosphere are sent to the leeward street segments through the intersection.

1.2.3 SSH-aerosol: aerosol dynamics modeling

SSH-aerosol[4] is a chemical model composed of three state-of-the-art modules to represent the evolution of primary and secondary aerosols in the atmosphere (Sartelet et al. 2020). Thanks to its modular approach, it can easily be coupled to air quality models, such as Polair3D and MUNICH, to consistently model physicochemical transformations during multiscale simulations. The general structure of SSH-aerosol is illustrated in Figure 1.6.

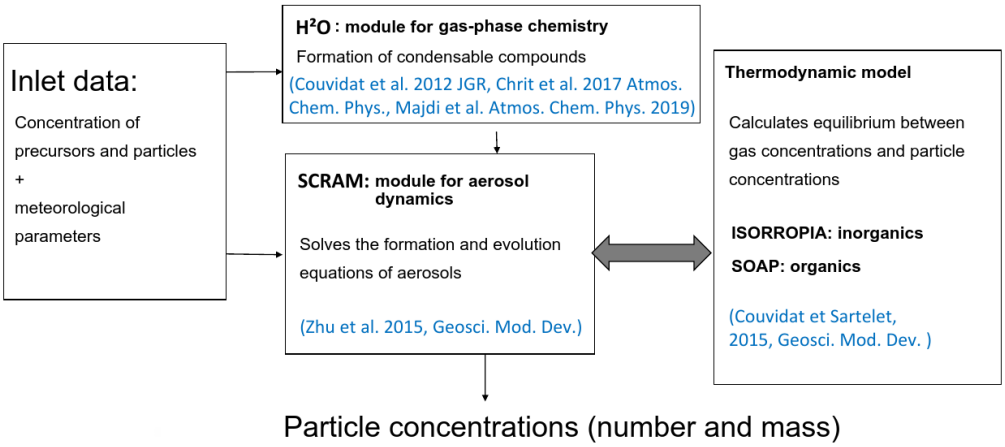

Figure 1.6: General structure of the SSH-aerosol model (Lugon 2021).

The size-composition resolved aerosol model (SCRAM) simulates the dynamics of externally and/or internally mixed atmospheric particles to classify them by both composition and size (Zhu et al. 2015). It includes the main processes involved in aerosol dynamics, which are coagulation, nucleation and condensation/evaporation. SCRAM represents the Brownian coagulation of particles thanks to the code of Dergaoui et al. (2013). For the nucleation, it uses the parameterization of Vehkamäki et al. (2002) for the homogeneous binary nucleation of water and sulfate. Finally, for condensation/evaporation, three methods are implemented. The dynamic method computes

[4] https://sshaerosol.wordpress.com/ (last visited 2023-04-21)

transfer rates for condensation/evaporation for all particles. The bulk-equilibrium method assumes a thermodynamic equilibrium between the bulk gas and particulate phases. The dynamic method is more accurate but the bulk-equilibrium method runs faster. In order to maintain both the accuracy of the dynamic method and the computational gain of the bulk-equilibrium method, a hybrid method is also implemented. It uses the bulk-equilibrium method for small particles and the dynamic method for larger ones, with a cutoff that can be set, e.g. 0.01 µm or 1 µm (Sartelet et al. 2020).

The secondary organic aerosol processor (SOAP) is a thermodynamic model used to compute the gas/particle partioning of organic compounds (Couvidat et al. 2015). Several processes involved in the formation of organic aerosols, such as hygroscopicity, absorption into the aqueous phase of particles and non-ideality and phase separation, are taken into account. Concerning the inorganic compounds, e.g. ammonium, nitrate and sulfate, the aerosol model ISORROPIA is used for the partioning between gas and particle phases (Nenes et al. 1998).

The hydrophilic/hydrophobic organics (H^2O) mechanism uses molecular surrogates to represent the formation of SVOCs through the oxidation of VOCs in the atmosphere (Couvidat et al. 2012). Different mechanisms can be used to represent the gas-phase chemistry. In this thesis, it is applied with a modified version of the gas-phase condensed chemical mechanism Carbon Bond 05 (Yarwood et al. 2005) to improve the representation of the oxidation of some VOCs, such as benzene, toluene, phenol and naphthalene (Majdi et al. 2019).

1.3 Objectives and plan of the thesis

High concentrations of NO_2 and PM, such as BC and OM are observed in urban areas and streets. This thesis focuses on improving our understanding of the sources of these high concentrations and their uncertainties, with the aim to reduce them. Concerning the uncertainties, modeling features that are poorly represented and strongly influence the local concentrations in the streets are identified. Since street concentrations are highly influenced by the urban background, multiscale modeling involving both regional and local scale modeling is necessary for sensitivity studies, as shown in Chapter 3. The multiscale modeling chain composed of Polair3D and MUNICH, coupled with SSH-aerosol, is thus used throughout this thesis.

The different assumptions identified as significant sources of uncertainties are related to traffic emissions, with the speciation of VOCs at exhaust, in particular the fractions of intermediate- and semi-volatile organic compounds (I/SVOCs) and the emissions of PM from tire wear, and also to the assumption of homogeneity of the concentrations in the streets of MUNICH. Road asphalt, a missing source of precursors of organic aerosols has been identified and added to the emissions. In previous studies (Roustan et al. 2011; André et al. 2019; Lugon et al. 2022), evolution of the vehicle fleet has been recognized as a major factor toward the decrease of urban concentrations. Here, in order to characterize the potential future evolutions, traffic impacts on air quality in 2030 are assessed by introducing very-low-emission vehicles in the fleet.

Chapter 2 briefly describes the sources of traffic emissions and the regulations in place. Then, the different approaches to model traffic emissions are presented. Finally, the development of a tool to calculate traffic emissions, Pollemission, is introduced.

In Chapter 3, the influence on pollutant concentrations of the uncertainties related to the modeling of traffic emissions (VOC speciations and tire wear) and asphalt emissions are studied over the Paris region. Sensitivity scenarios are defined to evaluate specific aspects of these uncertainties, and the importance of evaluating them at both the local and regional scales is shown.

Chapter 4 investigates the impacts of traffic emissions on air quality for the year 2030 over the Paris region. An evolution of emissions for all activity sectors is simulated, with the introduction of very-low-emission vehicles in the fleet.

Chapter 5 describes the development and validation of a new version of MUNICH taking into account concentration heterogeneities in streets. Traffic emissions are thus constrained in the lower part of the street instead of being artificially diluted in the whole street volume. The homogeneous and heterogeneous versions of MUNICH are applied to street networks in Paris and Copenhagen with comparisons to measurements and to the street model OSPM in Copenhagen.

Finally, Chapter 6 closes this manuscript by summarizing the results of the work carried out during this thesis and by offering perspectives to further improve the representation of the emission sources and for future developments of the models.

Chapter 2

Emissions from road traffic

Contents

In urban areas, road traffic is among the main polluting sectors, along with residential heating and industries (Trombetti et al. 2018). It is thus of importance to represent with accuracy road-traffic emissions and their impacts on air quality. Numerous laboratory and on-site measurements are performed in order to define emission inventories based on the characteristics of the vehicles (Gautam et al. 1998; Ropkins et al. 2009; Mathissen et al. 2012; Borucka et al. 2021; Zheng et al. 2022). However, the large number of vehicles in circulation, with different driving records and conditions, induces a wide variability in emissions. Traffic emission models that base their emission factors on these measurements are therefore subject to large uncertainties.

In this chapter, the different sources of emissions from vehicles are first described in Section 2.1. The European emission standards, which regulate traffic emissions in Europe, are then presented in Section 2.2. The different approaches to model traffic emissions are briefly described in Section 2.3. Finally, the tool used in this thesis to compute traffic emission factors, Pollemission, is presented in Section 2.4.

2.1 Sources of emissions from a vehicle

A motorized vehicle is "any power-driven vehicle which is normally used for carrying persons and goods by roads or for drawing, on the road, vehicles used for the carriage of persons or goods." (UN 1968). The term vehicle therefore includes cars, vans, trucks, buses and motorcycles. Despite their differences, vehicles equipped with an internal combustion engine (ICE) have the same emission sources, illustrated in Figure 2.1. Electric vehicles are different in that they do not emit pollutants at

exhaust and via evaporation, but only through non-exhaust emissions (tire and brake wear, road abrasion and resuspension).

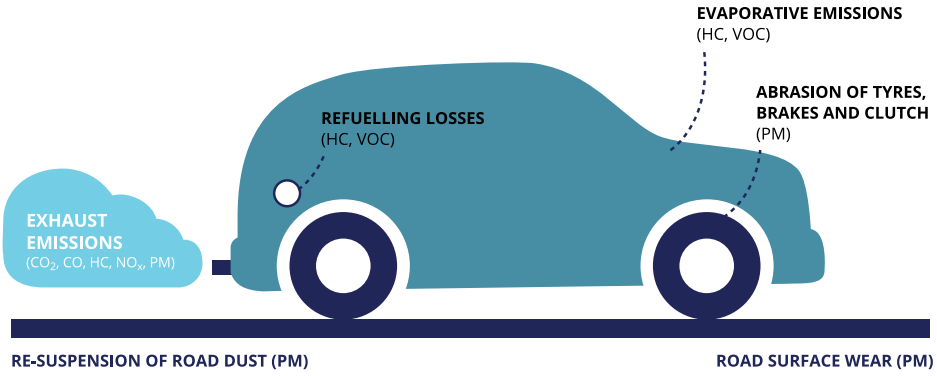

Figure 2.1: Sources of emissions from a vehicle (EEA 2016).

2.1.1 Exhaust emissions

Exhaust emissions arise from the combustion of fuel in the ICE. The main products of combustion are carbon dioxide (CO_2) and water (H_2O). However, several by-products are also produced, either from the incomplete fuel oxidation (CO, VOCs and PM) or from the oxidation of non-combustible species present in the combustion chamber (NO_x and SO_2). For the vehicle to be compliant with emission legislation, after-treatment devices are installed between the engine and the tailpipe. Unfortunately, as a result of their action, they may participate in the production of pollutants, such as ammonia (NH_3) (Westerholm et al. 1994; Alvarez et al. 2008; Kim et al. 2020; Gao et al. 2021).

Fuels with different compositions, e.g. petrol, diesel, compressed natural gas (CNG) and liquified petroleum gas (LPG), will impact the amount of pollutants emitted at exhaust (Perry et al. 1995; Pelkmans et al. 2011). Cold-start emissions, which occur before the engine and after-treatment devices have reached operating temperature, are known to be significantly higher than emissions under normal conditions, in particular with low ambient temperatures (Kyriakis et al. 1998; Pielecha et al. 2021).

The development of the engines to improve their efficiency also impacts exhaust emissions. For years now, vehicles running on petrol use predominantly gasoline direct injection (GDI) in place of the port-fuel injection (PFI). In GDI engines, the fuel injectors are mounted to the cylinder heads, delivering fuel directly into the combustion chambers, where it mixes with the air. On the contrary, in PFI engines, the fuel injectors are mounted outside the combustion chambers and the fuel is mixed with the air before entering the combustion chambers. The main advantage of the GDI system is the fuel efficiency due to higher injection pressures, resulting in smaller droplets that mix more easily with the air. While the emissions of gaseous pollutants are equivalent, PM emissions are higher with the GDI system (Jang et al. 2015; Lee et al. 2016; Saliba et al. 2017).

For diesel vehicles, a similar shift happened sooner than for petrol vehicles, from indirect injection (IDI) to direct injection (DI). As the GDI system, DI is much more fuel efficient. It also reduces the emissions of NO_x and PM, while increasing the emissions of VOCs (Stone 1999).

2.1.2 Evaporative emissions

Evaporative emissions are composed of VOCs emanating from the fuel system (tanks, injection system and fuel lines). They are specific to petrol vehicles. They are considered to be negligible for diesel vehicles due to the relatively low vapor pressure of this fuel and the presence of heavier hydrocarbons (Gaudioso et al. 1994; Dai et al. 2013; Yue et al. 2017).

Three mechanisms are usually considered when representing evaporative emissions:

- diurnal emissions, related to the variations in ambient temperature throughout the day. The fuel expands in the tank and, without an evaporative emission control system to trap the increasing volume of fuel vapor, some of the vapor leaks into the atmosphere.
- running losses, resulting from the vapor generated in the tank during vehicle operation. This mechanism is particularly important for old vehicles in which the temperature in the tank increases significantly. Now, with GDI and returnless fuel systems, running losses are very low.
- hot-soak emissions, which happen once the engine is turned off as the fuel temperature increases since it is no longer flowing.

The contribution of evaporative emissions to the total non-methane volatile organic compound (NMVOC) emissions has decreased considerably due to an optimization of the processes, such as GDI, and the development of evaporative emission control systems.

2.1.3 Non-exhaust emissions

Non-exhaust emissions of PM include emissions from tire and brake wear, road abrasion, and resuspension of previously deposited materials. Tires are subject to high stress, as they must carry the vehicle with the passengers, offer traction and steering, and absorb abnormalities of the road surface. The wear rates of tires depend on many factors, including vehicle traction configuration, tire and road condition, driving style and weather. PM emissions from tire wear are subject to large uncertainties in both size and composition. Emissions of tire wear are released to the atmosphere, but the main fraction is released to water or soil. According to Wik et al. (2009); Park et al. (2018); Baensch-Baltruschat et al. (2020) , emissions to the atmosphere may represent between 0.1 % and 10 % of the total PM_{10} emissions from tire wear. The tire-wear emission ratio $PM_{2.5}/PM_{10}$ may also present a wide variability, from 0.15 to 0.7 (Park et al. 2018; Ntziachristos et al. 2019a). The BC fraction of tire-wear emissions ranges from 15.3 % to 30 % (Thorpe et al. 2008; Ntziachristos et al. 2019a).

Two main brake systems are widely used in modern vehicles: disc brakes, in which flat brake pads are forced against a rotating metal disc, and drum brakes, in which curved brake shoes are forced against the inner surface of a rotating cylinder. The former is used in smaller vehicles, such as cars and motorcycles, while the latter is traditionally used for heavier vehicles. Wear rates of brakes depend on the relative position of brakes on the vehicles. For cars and motorcycles for example, the braking force is mainly applied to the front wheels. Wear rates also depend on the mechanism, pneumatic or electric, for brake actuation. As tire-wear emissions, PM emissions from brake wear are not emitted entirely to the atmosphere and are subject to large uncertainties. Emissions to the atmosphere may represent a large part of the total PM emissions from brake wear, with a contribution that could range between 63 % and 98 % for PM_{10}, and between 39 % and 70 % for $PM_{2.5}$ (Garg et al. 2000; Sanders et al. 2003; Thorpe et al. 2008; Grigoratos et al. 2015). The chemical composition of PM is largely dependent on the physical properties of the brake pad, the manufacturer and the

application. Nonetheless, they are mainly composed of metals, such as iron and copper, and OM (Garg et al. 2000; Sanders et al. 2003; Thorpe et al. 2008; Grigoratos et al. 2015; Ntziachristos et al. 2019a).

The quantification of emissions from road abrasion is more difficult than those for tire and brake wear. This is partly due to the chemical composition of the asphalt that is too complex to be quantified by mass balance, and partly because of the mixing of the primary wear particles with road dust and resuspended particles. Concerning the size resolution and chemical composition of PM from road-abrasion emissions, few studies have been performed; probably due to the same difficulties as for the quantification of emissions from brakes and tires (Thorpe et al. 2008; Ntziachristos et al. 2019a). The contribution of road abrasion to airborne PM_{10} of 50 % is suggested in Klimont et al. (2002).

Among the non-exhaust emissions, the resuspension of previously deposited particles probably presents the highest uncertainties. Amato et al. (2016) measured emission factors of PM_{10} ranging from 5.4 µg/veh/km to 17 µg/veh/km, in France. In Portugal, Alves et al. (2020) reported PM_{10} emission factor of 340 µg/veh/km and 41.2 µg/veh/km for cobblestone roads and asphalt pavement roads respectively. Fitz et al. (2002) reported PM_{10} emission factors ranging from 64 µg/veh/km to 124 µg/veh/km, in the USA. As the particles that are resuspended can originate from multiple sources, qualifying their chemical composition is extremely difficult (Thorpe et al. 2008; Casotti Rienda et al. 2021).

2.2 The European emission standards

Emissions from road traffic have been regulated in Europe since 1970, with the directive 70/220/EEC which presents the "measures to be taken against air pollution by gases from positive-ignition engines of motor vehicles" (CEU 1970). In 1992, the first stage of the European emission standards, Euro 1, came into force (CEU 1991). Since then, and to meet increasingly stringent regulations, vehicle manufacturers continually improve engine technologies and develop various emission-control systems.

European emission standards establish limits for all vehicle categories: passenger car (PC), light-commercial vehicle (LCV), heavy-duty vehicle (HDV) and motorcycles. Through the different stages, more and more air pollutants have been regulated. As of today, they include CO, NO_x, NH_3, total hydrocarbons (THCs), non-methane hydrocarbons (NMHCs), hydrocarbons (HCs)+NO_x, PM and particle number (PN). Road-traffic emissions of CO_2 are also regulated through CEU (2018).

Table 2.1 presents the evolution of the European emission standards for PC. For Euro 1 and Euro 2, solely CO, HCs+NO_x and PM were regulated. Since Euro 2, different emission limits are set for diesel and petrol vehicles. In Euro 2, CO limits were more stringent for diesel vehicles, but they allowed higher NO_x emissions. In Euro 3, HC+NO_x limits have been replaced by limits on THC for petrol vehicles. Diesel vehicles were exempted from THC and HC+NO_x limits. Petrol vehicles were also exempted from PM limits up to Euro 4. Starting at Euro 5, petrol vehicles equipped with DI are subject to regulation for PM. Regulations of PN has been introduced with Euro 5b for diesel vehicles and with Euro 6b for petrol vehicles.

Procedures to test emissions have been used, modified and replaced along the years. A chassis dynamometer is used to measure emissions during a test cycle. Over time, test cycles have evolved to stay up-to-date. The original test cycle, ECE15 + EUDC, includes urban and extra-urban segments. It is performed from a hot start. With Euro 3, it has been modified to represent cold-start emissions. This modified test is referred to as the New European Driving Cycle (NEDC). Between 2017 and 2019, the NEDC has been progressively replaced by the worldwide harmonized light vehicles test procedure (WLTP). Testing of the emissions on the real-driving emissions (RDE) test is mandatory since Euro

6d-Temp. The RDE test takes place on an open road and last from 90 to 120 minutes, including three segments: urban, rural and motorway, representative of the respective driving conditions, especially regarding vehicle speed.

A proposal for the next stage of the European emission standards, Euro 7, is currently submitted to the European Parliament and the Council (EC 2022). It should come into force at the beginning of July 2025. Emission limits are presented at the bottom of Table 2.1. Compared to the previous stages, it imposes the same limits for both diesel and petrol vehicles. THC and NMHC limits are now set for diesel vehicles. HCs+NO_x is no longed regulated. Two new compounds are added, NH_3 and PM_{10} from brake wear.

Table 2.1: European emission standards for passenger cars. Emission factors are expressed in g km^{-1}.

Stage	Date (first registration)	CO	THCs	NMHCs	NH_3	NO_x	HCs+NO_x	PM	PN [#/km]	Brake PM_{10}
Diesel										
Euro 1[a]	January 1993	2.72 (3.16)	–	–	–	–	0.97 (1.13)	0.14 (0.18)	–	–
Euro 2	01/1997	1.0	–	–	–	–	0.7	0.08	–	–
Euro 3	01/2001	0.66	–	–	–	0.50	0.56	0.05	–	–
Euro 4	01/2006	0.50	–	–	–	0.25	0.30	0.025	–	–
Euro 5a	01/2011	0.50	–	–	–	0.180	0.230	0.005	–	–
Euro 5b	01/2013	0.50	–	–	–	0.180	0.230	0.0045	6×10^{11}	–
Euro 6b	09/2015	0.50	–	–	–	0.080	0.170	0.0045	6×10^{11}	–
Euro 6c	09/2018	0.50	–	–	–	0.080	0.170	0.0045	6×10^{11}	–
Euro 6d-Temp	09/2019	0.50	–	–	–	0.080	0.170	0.0045	6×10^{11}	–
Euro 6d	01/2021	0.50	–	–	–	0.080	0.170	0.0045	6×10^{11}	–
Petrol										
Euro 1[a]	January 1993	2.72 (3.16)	–	–	–	–	0.97 (1.13)	–	–	–
Euro 2	01/1997	2.2	–	–	–	–	0.5	–	–	–
Euro 3	01/2001	2.3	0.20	–	–	0.15	–	–	–	–
Euro 4	01/2006	1.0	0.10	–	–	0.08	–	–	–	–
Euro 5a	01/2011	1.0	0.10	0.068	–	0.060	–	0.005[b]	–	–
Euro 5b	01/2013	1.0	0.10	0.068	–	0.060	–	0.0045[b]	–	–
Euro 6b	09/2015	1.0	0.10	0.068	–	0.060	–	0.0045[b]	6×10^{11}[c]	–
Euro 6c	09/2018	1.0	0.10	0.068	–	0.060	–	0.0045[b]	6×10^{11}	–
Euro 6d-Temp	09/2019	1.0	0.10	0.068	–	0.060	–	0.0045[b]	6×10^{11}	–
Euro 6d	01/2021	1.0	0.10	0.068	–	0.060	–	0.0045[b]	6×10^{11}	–
Petrol and diesel										
Euro 7 (proposed)	07/2025	0.50	0.10	0.068	0.02	0.060	–	0.0045	6×1011	0.007

[a] Values in parentheses are conformity of production (COP) limits.
[b] Applies only to vehicles with direct-injection engines.
[c] 6×10^{12}/km within first three years from Euro 6b effective dates.

2.3 Modeling road-traffic emissions

The main components of emission models are the emission factors. They can be defined as "empirical functional relations between pollutant emissions and the activity that causes them" (Franco et al. 2013). Emission factors are obtained through measurements both in the laboratory and under real-world operation. The main measurement techniques include engine dynamometer, remote sensing and road tunnel studies (Franco et al. 2013).

The applications of an emission model are defined by the level of detail with which it represents the emission and the corresponding activity. Consequently, emission models with high levels of detail require more information, i.e. input data. On the contrary, less detailed models assume typical and/or average emission conditions to present aggregated emission factors, which requires less information.

A wide variety of emission models exists, but, in the context of this thesis, the following focuses on three models. For more information, detailed reviews can be found in Masoud (2014) and Tsanakas (2019).

In the COPERT model[1] (Ntziachristos et al. 2009), emission factors depend on the vehicle and road types, and are defined as continous functions of the average vehicle speed. It takes into account exhaust emissions (both hot and cold), evaporative emissions, as well as non-exhaust emissions (except the resuspension of previously deposited particles). The approach based on the average vehicle speed may not be able to represent actual traffic conditions. Nonetheless, COPERT is well suited to compute national and regional emission inventories. As presented in Section 2.4, it can be adapted to compute emission factors in streets.

The HBEFA model[2] (Notter et al. 2019) relies on discrete emission factors predefined for different traffic situations. Traffic situations are determined based on four factors: (i) the road environnement (urban or rural), (ii) the road type (e.g. motorway, trunk road and access), (iii) the speed limit, and (iv) the service level (free flow, heavy, saturated and stop-and-go). Like COPERT, HBEFA is well suited to compute emission inventories at national and regionals scales, and can be adapted to lower scales. However, it requires more input data.

Finally, the PHEM model[3] (Zallinger et al. 2008) computes instantaneous emissions using a constant time step of 1 s. In order to do so, engine speed and power are first calculated, then, emissions are derived from the engine parameters, taking into account driving resistances and transmission losses. The temperature-dependent effects in the after-treatment devices can also be considered. PHEM calculates exhaust emissions only, and can be coupled with a dynamic traffic model.

2.4 Pollemission: Emission-factor computational tool

In this section, a tool to compute emission factors from traffic, Pollemission, is presented. It has been developed during this thesis to provide a flexible method that can be easily modified and adapted to meet the needs. It is used throughout this thesis to compute traffic emissions for simulations with MUNICH. Pollemission is freely available from Sarica (2021).

Pollemission is based on the 2019 version of the COPERT methodology, described in EMEP/EEA (2019). The methodology, originally developed to compute national emission inventories, has been adapted to compute emission factors in streets based on local traffic information. Pollemission takes into account emissions during transient thermal engine operation ("cold-start" emissions), vehicle wear (from tires and brakes) and road abrasion. Gasoline evaporation, included in the methodology, is not represented in Pollemission, because it is difficult to spatialise emissions precisely and thus as is it not suited for local computation.

First, the implementation of the COPERT methodology is described in Section 2.4.1. Then, Pollemission is validated against the official COPERT software in Section 2.4.2. Finally, Section 2.4.3 presents the speciations provided by the methodology for VOCs and PM.

[1] https://www.emisia.com/utilities/copert/ (last visited 2023-04-21)
[2] https://www.hbefa.net/e/index.html (last visited 2023-04-21)
[3] https://www.fvt.at/em/en/simulation/phem.html (last visited 2023-04-21)

2.4.1 Methodology implementation

The COPERT methodology differentiates four categories of vehicle: PCs; LCVs; HDVs, composed of heavy-duty trucks (HDTs) and buses; and mopeds & motorcycles (Lcat). These four categories are subdivided according to the fuel used, the engine size ("segment" in the methodology) and the European emission standard. In the following, a vehicle type is considered to represent a group of vehicles sharing the same attribute for each level of decomposition.

The methodology allows to compute emissions for the main atmospheric pollutants emitted by traffic: CO, NO_x, VOCs, PM, methane (CH_4) and NH_3. Emission factors for NMVOCs are computed as the difference between VOCs and CH_4 emission factors.

The total emission factor ef_{total} for a given vehicle type and a given pollutant is the sum of each contribution (exhaust and wear):

$$ef_{\text{total}} = ef_{\text{exhaust}} + ef_{\text{wear}} \tag{2.1}$$

Note that wear emission factors are provided for PM only, and following COPERT convention, emission factors are expressed in $\text{g}\,\text{km}^{-1}$.

2.4.1.1 Exhaust emission factors

Emission factors at exhaust are computed following the most accurate method of the methodology, Tier 3 (Ntziachristos et al. 2019b). However, some assumptions have to be made to adapt it to local computation. Firstly, corrections of the emission factors by fuel improvements are not considered as their implementation is complex and data are not available. Secondly, emission factors for HDVs are dependent on the road slope and their load, but in the absence of data, the road slope is considered to be zero and HDVs are considered to be charged at 50 % of their capacities. Thirdly, the decomposition by after-treatment devices proposed by the methodology is not taken into account, as the same coefficients are applied either way. Except for Euro 5 HDVs for which decomposition between selective catalytic reduction (SCR) and exhaust gas recirculation (EGR) makes a difference. Thus, for this vehicle type, it is considered that 75 % are equipped with SCR, as estimated by the methodology.

Exhaust emission factors are the sum of hot emission factors and cold-start emission factors:

$$ef_{\text{exhaust}} = ef^{\text{hot}}_{\text{exhaust}} + ef^{\text{cold}}_{\text{exhaust}} \tag{2.2}$$

Computable pollutants can broadly be separated into two groups depending on the computational method for cold-start emission factors:

- Group 1: CO, NO_x, VOCs, PM

  Cold-start emission factors are computed as over-emission factors of the hot emission factors.

- Group 2: CH_4, NH_3

  Cold-start emission factors are given as independent emission factors.

Note that cold-start emission factors are provided for PCs and LCVs only.

For exhaust emission, PM emission factors refer to $PM_{2.5}$ as the coarser fraction (from $PM_{2.5}$ to PM_{10}) is negligible in vehicle exhaust.

For some vehicle types and pollutants, the COPERT methodology provides only bulk emission factors. They correspond to the total emission factors ef_{exhaust} presented in Equation (2.2) without the possibility to compute hot and cold-start fractions separately. The formulation to compute these bulk emission factors are similar to the ones for hot emission factors.

To represent the deterioration of the performance of petrol PC and LCV equipped with three-way catalysts, correction factors are calculated using the following emission degradation function:

$$MC_{\mathrm{C},i} = A_{\mathrm{M}} + M_{\mathrm{mean}} + B_{\mathrm{M}} \tag{2.3}$$

With $MC_{\mathrm{C},i}$ the mileage correction factor for a given pollutant i, A_{M} and B_{M} two coefficients provided by the methodology, and M_{mean} the mean mileage for the vehicle type considered.

Group 1

In this group, the computation of hot and bulk emission factors is based on the following equation, with coefficients that depend on the vehicle type and pollutant:

$$ef^{\mathrm{hot}}_{\mathrm{exhaust}} = \frac{\alpha.V^2 + \beta.V + \gamma + \delta/V}{\epsilon.V^2 + \zeta.V + \eta}.(1 - RF) \tag{2.4}$$

With V the average speed (in $\mathrm{km\,h^{-1}}$). Other coefficients are directly provided by the methodology.

When cold-start emission factors are available, they are based on the following equation:

$$ef^{\mathrm{cold}}_{\mathrm{exhaust}} = ef^{\mathrm{hot}}_{\mathrm{exhaust}}.(\xi - 1).b.S_{\mathrm{cold}} \tag{2.5}$$

Where ξ is given by the methodology. b is also provided and introduced to reduce emission factors for more recent Euro standards. $\mathrm{S_{cold}}$ is the share of cold-running vehicles.

As the methodology does not give a way to compute PM cold-start emission factors for petrol PCs and LCVs, they are inferred from the corresponding diesel vehicle type. PM cold-start emissions from petrol vehicles are known to represent a higher part of the total PM emissions than for diesel vehicles. To take this into account, a ratio of cold emission/total emission for petrol vehicles (about 46 %) and diesel vehicles (about 37 %) is taken from André et al. (2019). Thus, PM cold emission factors for petrol PCs and LCVs can be computed by:

$$ef^{\mathrm{cold,PM}}_{\mathrm{exhaust}} = ef^{\mathrm{hot,PM}}_{\mathrm{exhaust}} \cdot \left.\frac{ef^{\mathrm{cold,PM}}_{\mathrm{exhaust}}}{ef^{\mathrm{total,PM}}_{\mathrm{exhaust}}}\right|_{\mathrm{diesel}} \cdot \frac{46}{37} \tag{2.6}$$

Group 2

In this group, the computation of all emission factors is based on Equation (2.7) and Equation (2.8), with a twist only to take into account the share of cold-running vehicles. Thus, hot and bulk emission factors for a given vehicle type and pollutant are computed using:

$$ef^{\mathrm{hot}}_{\mathrm{exhaust}} = (\alpha.C_m + \beta).\gamma.(1 - RF).(1 - S_{\mathrm{cold}}) \tag{2.7}$$

And cold-start emission factors using:

$$ef^{\mathrm{cold}}_{\mathrm{exhaust}} = (\alpha.C_m + \beta).\gamma.(1 - RF).S_{\mathrm{cold}} \tag{2.8}$$

In the formulae above, C_{m} is the mean cumulative mileage of the vehicle type. S_{cold} is the share of cold-running vehicles. Other coefficients are provided by the methodology.

For PCs running on CNG, cold-start emission factors of methane are considered to represent 62 % of the corresponding VOC emission factors, as indicated in the methodology.

2.4.1.2 Vehicle wear and road abrasion

Emission factors of total suspended particles (TSPs) from tire and brake wear, and road abrasion are directly given by the method Tier 2 of the methodology (Ntziachristos et al. 2019a). They do not take into account the resuspension of previously deposited materials.

Speed correction factors are provided for tire and brake wear emissions. These factors are introduced to represent the higher emissions at low speeds, typical of urban areas.

2.4.2 Validation

In order to validate our implementation of the Tier 3 method for exhaust emissions, emission factors from Pollemission are compared to emissions from the official COPERT program[1], developed by EMISIA SA. Several parameters must be set to ensure a fair comparison:

- COPERT computations are set to one vehicle driving 1 km for every vehicle type. A unit conversion is then applied to correspond to Pollemission's unit (from ton to $\mathrm{g\,km^{-1}}$);
- The mean speed is set to $20\,\mathrm{km\,h^{-1}}$ for every vehicle type;
- The ambient temperature is set to 15 °C;
- The COPERT program does not take the percentage of cold-running vehicles $\mathrm{S_{cold}}$ as an input but the average trip length $\mathrm{l_{trip}}$. $\mathrm{S_{cold}}$ is computed internally using the following formula:

$$S_{\mathrm{cold}} = 0.6474 - 0.02545 \times l_{\mathrm{trip}} - (0.00974 - 0.000385 \times l_{\mathrm{trip}}) \times t_a$$

  With t_a the ambient temperature. A $\mathrm{S_{cold}}$ of 30 % corresponds to a $\mathrm{l_{trip}}$ of about 10.23 km.

Taking into account all the potential sources of uncertainties between Pollemission and the COPERT program, only relative differences of absolute value larger than 15 % are considered. Table 2.2 presents the relative differences in emissions between the COPERT program and Pollemission for vehicle types with relative differences higher than 15 %. Among the 380 vehicle types included in the methodology, only 18 are significantly different. Furthermore, the fuels of these vehicle types (LPG and CNG) are not preponderant in the case of a complete fleet. NMVOC emission factors are computed as the differences between VOC and $\mathrm{CH_4}$ emission factors, thereby relative differences in VOC or $\mathrm{CH_4}$ are passed down to NMVOC emission factors.

Non-exhaust emission factors being directly provided by the methodology, with only speed correction, they do not need validation.

Pollemission is thus validated by comparison to the official COPERT program.

2.4.3 Speciation of $\mathrm{NO_x}$, VOCs and PM

Emission factors of NO and $\mathrm{NO_2}$ are determined from the emissions of $\mathrm{NO_x}$ using mass fractions of $\mathrm{NO_2}$ given by the COPERT methodology (Ntziachristos et al. 2019b).

The COPERT methodology provides five generic speciations for NMVOCs following vehicle category, fuel and European emission standard. Table 2.3 shows the distribution by group of NMVOCs according to the five speciations.

The compositions of the two speciations for petrol vehicles Euro I and on, and diesel PCs are rather different for some groups, but others are relatively identical. In fact, alkanes (respectively 30 % and 25 % for petrol and diesel vehicles) and alkenes (about 17 % for both speciations) represent an

Table 2.2: Relative differences (in %) between emissions from the COPERT program and Pollemission for the vehicle types with relative differences higher than 15 %. A negative relative difference indicates that Pollemission emission is higher.

Category	Fuel	Segment	Euro Standard	CO	VOCs	NMVOCs
Passenger Cars	LPG	Mini	Euro 4	18.74	-31.13	-37.06
Passenger Cars	LPG	Mini	Euro 5	18.74	-31.13	-37.06
Passenger Cars	LPG	Mini	Euro 6	18.74	-31.13	-37.06
Passenger Cars	LPG	Small	Conventional			
Passenger Cars	LPG	Small	Euro 1			
Passenger Cars	LPG	Small	Euro 2			
Passenger Cars	LPG	Small	Euro 3	19.37	-30.80	-33.90
Passenger Cars	LPG	Small	Euro 4	18.74	-31.13	-37.06
Passenger Cars	LPG	Small	Euro 5	18.74	-31.13	-37.06
Passenger Cars	LPG	Small	Euro 6	18.74	-31.13	-37.06
Passenger Cars	LPG	Medium	Conventional			
Passenger Cars	LPG	Medium	Euro 1			
Passenger Cars	LPG	Medium	Euro 2			
Passenger Cars	LPG	Medium	Euro 3	19.37	-30.80	-33.90
Passenger Cars	LPG	Medium	Euro 4	18.74	-31.13	-37.06
Passenger Cars	LPG	Medium	Euro 5	18.74	-31.13	-37.06
Passenger Cars	LPG	Medium	Euro 6	18.74	-31.13	-37.06
Passenger Cars	LPG	Large	Conventional			
Passenger Cars	LPG	Large	Euro 1			
Passenger Cars	LPG	Large	Euro 2			
Passenger Cars	LPG	Large	Euro 3	19.37	-30.80	-33.90
Passenger Cars	LPG	Large	Euro 4	18.74	-31.13	-37.06
Passenger Cars	LPG	Large	Euro 5	18.74	-31.13	-37.06
Passenger Cars	LPG	Large	Euro 6	18.74	-31.13	-37.06
Passenger Cars	CNG	Mini	Euro 4			
Passenger Cars	CNG	Mini	Euro 5			
Passenger Cars	CNG	Mini	Euro 6			
Passenger Cars	CNG	Small	Euro 4			
Passenger Cars	CNG	Small	Euro 5			
Passenger Cars	CNG	Small	Euro 6			
Passenger Cars	CNG	Medium	Euro 4			
Passenger Cars	CNG	Medium	Euro 5			
Passenger Cars	CNG	Medium	Euro 6			
Passenger Cars	CNG	Large	Euro 4	28.60		
Passenger Cars	CNG	Large	Euro 5	28.60		
Passenger Cars	CNG	Large	Euro 6	28.60		

important part of the two speciations. On the contrary, aromatics constitute the majority of the speciation for petrol vehicles (almost 45 %), whereas they constitute less than 20 % of the speciation for diesel vehicles. The contribution of cycloalkanes is twice as large for petrol vehicles compared to diesel vehicles. For diesel vehicles, aldehydes represent the largest contribution (about 31 %) and the

contribution of ketones is larger (4 % against 0.6 %) for petrol vehicles.

Table 2.3: NMVOC speciations provided by the COPERT methodology. The acronym PAH refers to polycyclic aromatic hydrocarbon (PAH), and POP to persistent organic pollutant (POP).

Fraction [%]	Petrol 4 stroke		Diesel PCs & LCVs	HDVs	LPG
Group	Conventional	Euro I & on	IDI & DI		
Alkanes	17.29	29.8	24.53	31.53	77.1
Cycloalkanes	0.88	1.14	0.65	1.16	0.1
Alkenes	21.3	17.22	17.17	13.33	11.7
Alkynes	6.31	3.1	2.34	1.05	1.28
Aldehydes	4.32	3.32	31.1	24.47	5.27
Ketones	0.32	0.66	4.14	0	0.78
Aromatics	49.56	44.41	19.49	25.17	3.75
PAHs & POPs	0.02	0.35	0.58	3.29	0.02
Total	100	100	100	100	100

PM emission factors from exhaust consists of BC, OM and dust. The COPERT methodology provides two ratios: BC/$PM_{2.5}$ and OM/BC (Ntziachristos et al. 2019b). However, associated uncertainties can be high, ranging from 5 % to 50 %. It is interesting to note that the majority of exhaust PM emissions for petrol vehicles is OM whereas for diesel vehicles, the majority is BC.

For emission factors of PM from non-exhaust sources, the COPERT methodology also provides information about size and chemical speciations (Ntziachristos et al. 2019a). Both tire- and brake-wear emissions are mainly composed of dust, at 49 % and 87 % respectively. While 60 % of the tire-wear emissions are ranging in size between 1 µm and 2.5 µm, 60 % of the brake-wear emissions are between 2.5 µm and 10 µm. Emissions from road abrasion are considered to be only composed of dust with a size distribution between 1 µm and 10 µm. More information can be found in Section 3.2.

Chapter 3

Sensitivity of the concentrations to the representation of traffic emissions in the models

Contents

In air quality modeling, there are many sources of uncertainties that can influence concentrations to a greater or lesser extent. Some are related to the parameterization of the model, with the representation of the flow field and of the aerosol processes. Others are induced by the input data of the model, such as boundary conditions and missing sources. For simulations at the street scale, the representation of road traffic emissions strongly influences the street concentrations of pollutants emitted or formed from traffic emissions, such as NO_2 and BC, but it is attached to uncertainties. As detailed in chapter 2, road traffic emissions can be represented using different approaches (Section 2.3).

The choice of the representation depends on the information available to compute these emissions, such as vehicle number and speed. The COPERT methodology is one of the main European tool to help countries build national emission inventories by calculating emission factors from traffic (EMEP/EEA 2019). However, it can easily be adapted to generate emissions from traffic at a lower resolution (see Pollemission in Section 2.4).

Although the COPERT methodology is based on numerous laboratory and real-situation measurement studies, some uncertainties persist. The VOC speciations provided by the methodology for exhaust emissions are based on measurements performed on vehicles compliant with old emission standards (pre-Euro 1 and Euro 1) and poorly describe the emitted intermediate-, semi- and low-volatile organic compounds (I/S/LVOCs). Non-exhaust emissions are also subject to high uncertainties, in particular tire-wear emissions. Emissions of organic aerosol precursors from road asphalt is a source that is currently ignored in air quality modeling but which could impacts the concentrations of OM.

This chapter thus investigates the sensitivity of the concentrations in streets to these uncertainties through emission scenarios. Section 3.1 presents a first study that simulates the month of April 2014 taking into account only the modification of traffic emissions at the local scale, i.e. for the MUNICH simulation. It is published as a chapter of the *Air Pollution Modeling and its Application XXVIII* (Sarica et al. 2022). However, the influence of the emission scenarios on the background concentrations are not modeled. The second study tackles this issue in Section 3.2 by simulating impacts on concentrations for year 2014 at both regional and local scales using Polair3D and MUNICH respectively. It is published in *Environmental Pollution* (Sarica et al. 2023c).

Table 3.1: Influence of background concentrations on the concentrations in the streets. The *fixed* and *modified* keywords represent the first and second study for which the background concentrations were not modified and modified respectively. Average concentrations are expressed in µg m^{-3}. NMB represent the bias in regard to the respective reference simulation S0/SCN0, in %.

		S2/SCN2		S3/SCN3		S4/SCN4	
	Background	fixed	modified	fixed	modified	fixed	modified
PM_{10}	mean	23.3	22.1	26.3	29.3	25.3	26.2
	NMB	-1.5	-5.3	9.8	23.0	6.6	11.8
$PM_{2.5}$	mean	21.0	20.4	21.6	23.3	22.9	24.4
	NMB	-1.7	-5.5	1.0	7.2	7.3	12.7
BC	mean	1.5	1.4	2.1	2.9	1.5	1.4
	NMB	0.0	0.0	34.9	89.9	0.0	0.0
OM	mean	3.9	3.9	5.3	7.6	5.8	8.0
	NMB	-7.5	-23.5	20.5	40.6	36.1	53.5

To highlight the impacts that background concentrations have on concentrations in the streets, modeled concentrations from the two studies are compared for the month of April 2014. Table 3.1 presents this influence on the particulate pollutants for scenarios S2/SCN2, S3/SCN3 and S4/SCN4. Scenarios S2, S3 and S4 refer to the first study without modification of the background concentrations (Table 3.2). Scenarios SCN2, SCN3 and SCN4 refer to the second study with modification of the background concentrations (Table 3.5). Scenarios S1 and SCN1 cannot be compared as they differ by their emissions. Scenario SCN1 uses a more recent VOC speciation for diesel passenger cars that is not in scenario S1. Since the biases are systematic, only the normalized mean bias (NMB) is presented as it has the same numerical value as the normalized mean error (NME). The formulation

of both NMB and NME is outlined in Appendix A2.

Taking into account the impacts of the emission scenarios on the background concentrations, through regional-scale simulations with Polair3D, and their feedback on the concentrations in the streets greatly amplify the impacts of the emission scenarios on street concentrations. For scenarios S2/SCN2, which modify exhaust emissions of I/S/LVOCs, the reductions observed in S2 are amplified in SCN2, from 1.5 % to 5.3 % for PM_{10}, and from 7.5 % to 23.5 % for OM. For scenarios S3/SCN3 and S4/SCN4, the increases in concentrations are higher when considering the modification of the background concentrations. Concentrations of BC and OM are especially impacted in SCN3, and they increase from 35 % to 90 % and 20.5 % to 40.6 % respectively when the change of background concentrations is taken into account. The road-asphalt emissions of organic aerosol precursors in scenarios S4/SCN4 greatly impact OM concentrations with an increase from 36.1 % to 53.5 %, leading to an increase from 7 % to 12 % of PM_{10} concentrations.

3.1 Modelling pollutant concentrations in streets: a sensitivity analysis to asphalt and traffic related emissions

Higher concentrations of NO_2 and particles (OM and BC) are often observed in streets compared to urban background. Road traffic is generally seen as one of the dominant sources of emissions in streets. The main goal of this work is to evaluate the impact of uncertainties of traffic emissions (speciation of VOCs at exhaust and non-exhaust emissions) on pollutant concentrations in streets, and to evaluate the potential impact of asphalt-related emissions, which are usually ignored.

3.1.1 Introduction

Despite increasingly stringent regulations, road transport remains a source of air pollution (NO_2 and particles to a lesser extent) in urban areas. The European emission standards (Euro norms) drive in Europe the reduction of automobile-related emissions through several regulations, from Euro 1 in 1992 to the Euro 7 regulation expected for 2025. However, only emissions at exhaust are considered by these regulations and non-exhaust emissions are omitted. The COPERT methodology, described in the EMEP/EEA air pollution emission inventory guidebook (EMEP/EEA 2019), lists traffic-related pollutant emission factors for the different Euro norms and vehicle technologies. It is often used in Europe to build emission inventories. However, uncertainties remain high for some emission factors, such as those linked to non-exhaust emissions, and the methodology lacks a detailed speciation of some emitted pollutants such as VOCs. Non-exhaust emissions and VOC speciation may influence particle concentrations (BC and OM respectively) (Lugon et al. 2021b; Sartelet et al. 2018). Depending on the speciation, VOCs may contain precursors of organic aerosols (I/SVOCs, toluene, xylenes etc.).

Numerical modelling is an effective tool to evaluate the impacts of emission changes but also the importance of urban topology on pollutant concentrations at street scale. In this work, MUNICH is used to compute concentrations of pollutants at street scale (Kim et al. 2018; Lugon et al. 2020). MUNICH is coupled with the modular box model SSH-aerosol (Sartelet et al. 2020) to represent formation and aging of primary and secondary gases and particles in streets. Four sensitivity scenarios are designed to study uncertainties in the COPERT methodology linked to VOC speciation at the exhaust, non-exhaust emissions and asphalt emissions.

3.1.2 Simulated scenarios

Simulations are performed over the month of April 2014 using the street network presented in Kim et al. (2018). This street network is composed of 577 street segments representing a district of Le Perreux-sur-Marne, a suburb 13 km east of Paris. Meteorological parameters and background concentrations originate from Lugon et al. (2021b). Deposition and scavenging of both gas and particle phases are taken into account. The size distribution of particulate species are represented in the model by 6 size bins of diameters ranging between 0.01 µm and 10 µm (Lugon et al. 2021b).

Fleet composition and traffic flows and speeds have been determined for a typical weekday and a typical weekend day from simulations using the traffic simulator SymuVia (André et al. 2020). The fleet is composed on average by 77 % of PCs and 14 % of LCV. Diesel is the most widespread fuel in the fleet representing respectively 65.2 % and 97.5 % of PCs and LCVs. Traffic flows of PCs are higher during the weekday than weekend day with peaks at up to 1 400 vehicles per hour at morning and afternoon rush hours over the main street section of interest for this study. During the weekend day, the maximal flow is about 200 vehicles per hour. For both days the PC speed profiles are similar, and vary between 24 $km\,h^{-1}$ and 32 $km\,h^{-1}$.

Table 3.2: List of the simulations performed.

Scenario	Description
S0	Reference simulation - COPERT methodology only
S1	More recent NMVOC speciations for petrol PCs and LCVs
S2	I/S/LVOCs are estimated from Sartelet et al. (2018)
S3	Higher tire-wear emissions following Lugon et al. (2021b)
S4	Emissions from road asphalt derived from Khare et al. (2020)

Table 3.2 presents the reference simulation S0 and the four sensitivity scenarios, S1 to S4, performed in this study. The reference simulation S0 is based on the COPERT methodology described in EMEP/EEA (2019) for exhaust emissions of CO, NO_x ($NO + NO_2$), VOCs, CH_4 and $PM_{2.5}$, and non-exhaust emissions of PM_{10}. NO_2 fractions, VOC speciations and PM decomposition into BC, OM and dust are also provided by the COPERT methodology. At exhaust, the "cold-start" emissions when the operational temperature of the internal combustion engine and after-treatment devices have not yet been reached are taken into account. In all scenarios, only the street emissions for the local-scale simulation with MUNICH are modified. The impact of the scenarios on the background concentrations is not taken into account.

Scenario S1 evaluates the impacts of using finer and more recent NMVOC speciations for petrol PCs and LCVs. These new speciations originate from laboratory measurements performed during the MAESTRO project[1]. With these new speciations, the fractions of IVOCs and SVOCs are reduced from 6.0 % to less than 2.0 % and from 4.9 % to less than 0.2 % compared to COPERT respectively. Scenario S2 investigates the implications of estimating I/S/LVOC emissions from the NMVOC emissions as presented in Sartelet et al. (2018), with formulae based on chamber measurements performed in the United-States for petrol and diesel vehicles. The primary organic aerosols emitted in S0 are not considered in this scenario, as they are assumed to be LVOCs. Using this method, the averaged total emission of I/S/LVOCs is reduced by 71 % compared to the reference S0, 78 $\mu g\,s^{-1}$ against

[1] Modélisation/caractérisation des précurseurs gazeux et des AErosols Secondaires du Transport Routier – joint project between LCE-AMU, IRCELYON, UGE-EASE and CEREA

272 µg s^{-1}. The volatility distribution is also modified with a larger fraction of IVOCs and a lower fraction of LVOCs. Non-exhaust emissions originating from tire, brake and road wears are bound to high uncertainties partly due to the difficulties to differentiate the origin of the measured materials. Following Lugon et al. (2021b), the tire emission factors are multiplied by 9 in scenario S3 as the simulation S0 underestimates the concentrations of BC compared to observations. Furthermore, the chemical speciation of tire-wear emissions assumes 25 % of BC (compared to 15.3 % in simulation S0). Finally, scenario S4 considers emissions of SOA precursors in the gas phase from road asphalt due to pavement heating and exposure to sunlight, as detailed in Khare et al. (2020). As a first assessment, these emissions are assumed to occur during daytime at a constant rate of 0.025 mg/min/kg asphalt. This rate is derived assuming a temperature of the road asphalt of 20 °C during the simulation period.

3.1.3 Concentration levels

The reference S0 is compared to observations, performed on one segment of the street network, using the statistical criteria presented in Hanna et al. (2012). Although NO_x and NO concentrations are underestimated, NO_2 concentrations are well modelled and satisfy the strictest criteria. Particles are also well modelled: PM_{10} and $PM_{2.5}$ both comply with the strictest criteria, although PM_{10} are slightly underestimated and $PM_{2.5}$ are slightly overestimated. However, BC concentrations are significantly underestimated and none of the criteria are satisfied. These results and comparisons to observations are in accordance with previous works (Kim et al. 2018; Lugon et al. 2021b).

Scenario S1 with the use of more recent speciations for NMVOC emissions of petrol PCs and LCVs has low impacts on pollutant concentrations. PM_{10} and $PM_{2.5}$ average concentrations are decreased by about 0.12 % compared to the reference S0. Organics in the particle phase are impacted with a reduction of the average concentration of 0.6 %. The gas-phase concentrations of IVOCs and SVOCs are also reduced by 12.6 % and 5.2% respectively. This low sensitivity was expected as petrol is not the preponderant fuel in the fleet. 30 % and 2 % of the PCs and LCVs respectively are running on petrol. Scenario S2 PM_{10} and $PM_{2.5}$ average concentrations are 1.6 % and 1.8% lower compared to the reference S0 respectively. Organics are the most impacted compounds of PM with a reduction of 8.7 %, showing that the IVOC and SVOC speciation of VOCs may have a large influence on organic concentrations in the particles.

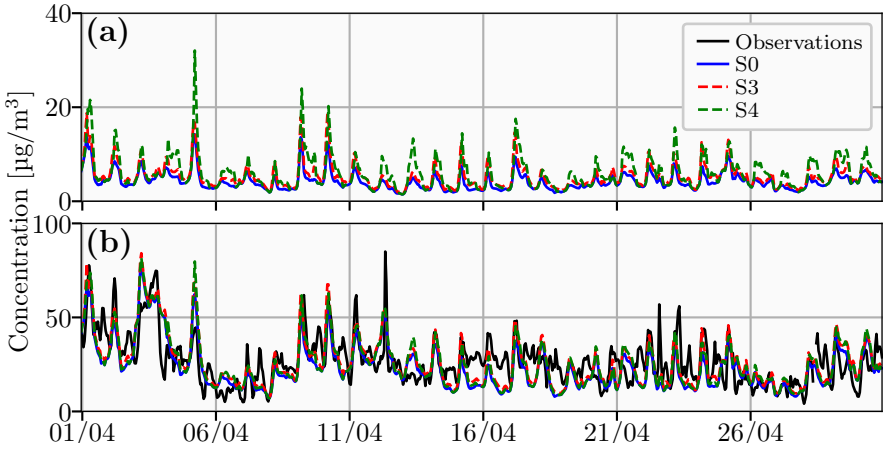

Figure 3.1: Hourly simulated concentrations of organics (a) and PM_{10} (b) at a segment of the street network for the reference simulation S0 and scenarios S3 and S4. PM_{10} concentrations are compared to observations [µg m^{-3}].

There is a high increase in the PM concentrations in scenario S3, due to higher emission factors and modified chemical speciation of tire wear. PM_{10} and $PM_{2.5}$ average concentrations are 10.9 % and 1.1 % higher compared to the reference S0 respectively. BC and organics are the particle compounds that increase the most by 41.9 % and 23.8 % respectively. In scenario 4, taking into account road asphalt emissions results in a large increase of the concentrations of gas-phase IVOCs and SVOCs by as much as 492.0 % and 321.5 % respectively. The impacts on particle-phase organics are not as high, 36.0 % for the organics. The PM_{10} and $PM_{2.5}$ average concentrations increase by 6.6 % and 7.4 % respectively, compared to the reference S0. These results are plausible and confirm the conclusion of Khare et al. (2020) that road asphalt can be a major missing source of SOA precursor emissions.

3.1.4 Conclusion

The impacts of different sources of uncertainties linked to traffic emissions on pollutant concentrations in streets have been evaluated using the street network model MUNICH, coupled with the complex chemistry module SSH-aerosol. The reference simulation S0 presents concentrations that compare well to the observed concentrations and previous works.

The impacts of considering more recent NMVOC speciations for petrol PCs and LCVs in scenario S1 are limited as petrol is not the preponderant fuel in the fleet. Nevertheless, slight reductions of PM and organics are observed, as the fraction of IVOCs and SVOC are lower in the new speciations than in COPERT. Computing IVOC and IVOC emissions using the method presented in Sartelet et al. (2018), which is not specific to European cars, in scenario S2 results in larger modifications of organic concentrations in streets compared to the reference S0. Having access to more recent NMVOC speciations for diesel European vehicles is decisive to fully assess the impacts of NMVOC speciation on pollutant concentrations.

The simulated BC concentrations are closer to observation in the scenario S3, which has higher emission factors and modified chemical speciation for tire wear. This indicates the necessity to better measure and characterize non-exhaust emissions. Taking into account SOA precursor emissions from road asphalt in scenario S4 results in a huge increase of the gas-phase IVOC and SVOC concentrations. Nonetheless, the impacts on PM and organics concentrations are in the range of the modifications induced by the other scenarios. Further work is needed to assess the significance and uncertainties of this source of emissions before systematically considering it in emission inventories.

The impacts of the scenarios on the background concentrations is not taken into account in this study. Because traffic emissions do affect background concentrations, the impacts on the street concentrations would be larger if the impacts on background concentrations were taken into account. Simulations using background concentrations modified accordingly to the scenarios have to be performed in order to fully assess the impacts of the scenarios on the concentrations in streets.

3.2 Sensitivity of pollutant concentrations in urban streets to asphalt and traffic-related emissions

The higher concentrations of atmospheric particles, such as BC and OM, detected in streets compared to the urban background are predominantly attributed to road traffic. The integration of this source of pollutant in air quality models nevertheless entails a high degree of uncertainty and some other sources may be missing. Through sensitivity scenarios, the impacts on pollutant concentrations of sensitivities related to traffic emissions and road asphalt emissions are evaluated. The 3D Eulerian model Polair3D and the street network model MUNICH are applied to simulate various scenarios

and their impacts at the regional and local scales. They are coupled with the modular box model SSH-aerosol to represent formation and aging of primary and secondary gas and particles. Traffic emissions are calculated by means of the COPERT methodology. Using recent VOC speciations for light vehicles with more detailed information pertaining to I/S/LVOCs leads to limited reductions of OM concentrations (10 % in streets). Changing the method of estimating I/S/LVOC emissions leads to an average reduction of 60 % at emission and a decrease of the OM concentrations of 27 % at the local scale. An increase in 219 % of BC emissions from tire wear, consistent with the uncertainties found in the literature, doubles the BC concentrations at the local scale, which remain underestimated compared to observations. Emissions of I/S/LVOCs are several orders of magnitude higher when considering emissions from road asphalt due to pavement heating and exposure to sunlight. However, simulated concentrations of PM at the local scale remain within acceptable ranges compared to observations. These results suggest that more information is needed on I/S/LVOCs and non-exhaust sources (tires, brakes and road abrasion) that impacts the concentration of particles. Furthermore, currently unconsidered emission sources such as road asphalt may have non-negligible impacts on pollutant concentrations in streets.

3.2.1 Introduction

In urban areas, populations are exposed to high concentrations of pollutants due to unfavorable dispersion conditions and proximity to traffic. In 2019, more than 90 % of the European urban population was exposed to concentrations of NO_2 and $PM_{2.5}$ exceeding the World Health Organization 2021 air quality guidelines (EEA 2022). The main components of PM include BC, dust, inorganic aerosols, organic aerosols and metals. As organic aerosols, BC has strong impacts on health, ranging from minor upper respiratory irritation to chronic respiratory and heart disease (Kampa et al. 2008; Mabahwi et al. 2014).

While BC is a chemically inert primary pollutant, organic aerosols, or OM, can be classified as POAs if directly emitted into the atmosphere, or SOAs if formed in the atmosphere from the oxidation of VOCs and/or the condensation of semi volatile organic compounds. VOCs consist of compounds existing only in the gas phase, i.e., with saturation vapor pressure higher than that of dodecane with 12 carbon atoms. Organic compounds with relatively low vapor pressure are further classified as IVOCs, SVOCs and LVOCs (Gentner et al. 2017). The oxidation of gas-phase organic compounds leads to the formation of lower-volatility compounds that may partition more easily to particles. This process is highly dependent on oxidant concentrations that are mainly governed by photochemical reactions of NO_x and VOCs.

Road traffic could be one of the main sources of pollutants explaining the high concentrations of NO_2, BC and OM observed in streets (Kamara et al. 2021; Saarikoski et al. 2021). Traffic-related emissions are categorized depending on their origins: exhaust and non-exhaust. Traffic exhaust emissions arise from the combustion of fuels such as petrol, diesel and LPG in ICE vehicles. Incomplete fuel oxidation, the oxidation of non-combustible species present in the combustion chamber and the various after-treatment devices to comply with emissions legislation produce several by-products: CO, CH_4, NH_3, NO_x, VOCs and PM. Traffic non-exhaust emissions include fuel evaporation and emissions which are not covered by existing emissions legislation, consisting of particles emitted as a result of tire wear, brake wear and resuspension.

The representation of traffic emissions in a modeling framework raises many questions concerning the representation of traffic characteristics and their temporal and spatial variations (Quaassdorff et al. 2022; Tsanakas et al. 2020; Lejri et al. 2018). The resulting emissions may depend on a great number of parameters and the way the corresponding information is aggregated over time

(Borge et al. 2012) and translated into emission factors as per the Computer Program to Calculate Emissions from Road Transport (COPERT) or the European Handbook Emission Factors for Road Transport (HBEFA) methodologies. The assessment of real-world emissions can be carried out directly for tailpipe emissions, but only for a few vehicles in a fleet. At the fleet level, it can be done indirectly through a combination of observational and modeling approaches (Wiesner et al. 2021; Krecl et al. 2017). For the current work we rely on the COPERT methodology which is described in the EMEP/EEA air pollutant emission inventory guidebook (EMEP/EEA 2019). It provides a formulation to calculate the emission factors of pollutants emitted by road traffic, both exhaust and non-exhaust. Exhaust emission factors are relatively well known and documented with numerous laboratory and real-situation measurements. However, the VOC speciations offered by the methodology are based on measurements made with vehicles compliant with old emission standards (pre-Euro 1 and Euro 1) and do not give detailed information about emitted I/S/LVOCs. Non-exhaust emissions are subject to higher uncertainties due to the difficulties in measuring emissions during vehicle use and differentiating the varying sources (e.g., tires, brakes, road abrasion and resuspension). Tire emissions are particularly poorly characterized (Luhana et al. 2004; Boulter 2005). Road asphalt emission could be an additional source of organic aerosol precursors that is currently ignored. Although (Zhang 2015; Nilsson et al. 2018), they may persist afterward and depend on temperature and incident solar flux, as recently suggested by Khare et al. (2020).

In air quality modeling, regional and street models can be used concomitantly to simulate concentrations down to the street scale, representing the multiscale evolution of concentrations (San Jose et al. 2022; Lv et al. 2022; Mu et al. 2022). For example, the 3D Eulerian model Polair3D may provide concentrations at the regional scale, to feed the street network model MUNICH (Kim et al. 2018, 2022) which calculates concentrations in streets. Modeled concentrations can be significantly affected by several sources of uncertainties linked to the representation of the flow field (Kim et al. 2022, 2015, 2013), of aerosol processes (Lugon et al. 2021a; Zhu et al. 2016b) and other missing sources/sinks (Sartelet et al. 2018). In order to evaluate the sensitivity of the concentrations to the most uncertain aspects of emission that are usually not considered, but that may be significant, four scenarios investigating the influence of VOC speciations, non-exhaust emissions and road asphalt emissions are presented and analyzed in this study. The following section presents the reference simulation with the model setups and parameterizations. Then, Section 3.2.3 introduces the four sensitivity scenarios and their impacts on emissions. Finally, the scenarios' impacts on concentrations are discussed in Section 3.2.4.

3.2.2 Simulation setup and reference simulation

This section presents the simulation setup of the reference simulation SCN0 and the methodology to compute emissions. The regional- and local-scale simulations are performed for the year 2014 using the Polair3D (Mallet et al. 2007) and MUNICH (Kim et al. 2022) models, as detailed below. They are both coupled with the box-model SSH-aerosol to simulate the evolution of gas as well as primary and secondary aerosols (Sartelet et al. 2020). As both Polair3D and MUNICH are coupled with SSH-aerosol, this modeling chain enables the assessment of impacts of traffic and asphalt emissions and their sensitivities on pollutant concentrations in streets, taking into account physicochemical transformations at all scales.

SSH-aerosol takes into account gas-phase chemistry and aerosol dynamics (coagulation, condensation/evaporation). Because this study focuses on mass concentrations of particles, and not on the number concentration, nucleation is not taken into account in aerosol dynamics. Indeed, it has a low impact on mass concentrations (Sartelet et al. 2022): nucleation forms nanometric particles, and

particles with a diameter of less than 20 – 30 nm have low mass. The smallest particle diameter represented here is 10 nm, to be able to account for ultra-fine particles emitted by traffic exhaust at around 60 nm. The size distribution of particles is represented in the models by 6 size sections of diameters ranging between 0.01 and 10 µm: [0.01 – 0.0398 µm], [0.0398 – 0.1585 µm], [0.1585 – 0.4 µm], [0.4 – 1 µm], [1 – 2.5119 µm] and [2.5119 – 10 µm]. In this study, SSH-aerosol is applied with a modified version of the gas-phase condensed chemical mechanism Carbon Bond 05 (Yarwood et al. 2005). It represents the oxidation of VOCs whose oxidation products may partition to particles to form SOAs (e.g., benzene, toluene, xylene, phenol, naphthalene, IVOCs and SVOCs) with low and high-NO_x reaction paths and yields based on smog chambers experiments (Majdi et al. 2019).

3.2.2.1 Local-scale simulations

A district of Le Perreux-sur-Marne, a suburb 13 km east of Paris, is taken into consideration (Kim et al. 2018). It consists of 577 street segments (see Figure 3.2). Simulations are performed from 10 January to 27 December 2014 using MUNICH (Kim et al. 2022). In each street segment, concentrations are assumed to be homogeneous, and evolve depending on chemistry, on exchanges between the street and the background, and from one street to the next via intersections. Dry deposition is modeled on the road, the pavement and the building walls and wet deposition corresponds to scavenging by precipitation, as detailed in Kim et al. (2022).

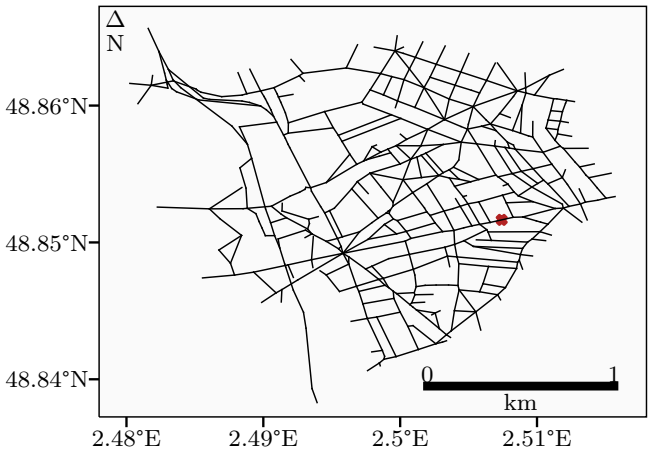

Figure 3.2: Local-scale simulation network representing a district of Le-Perreux-sur-Marne. The brown cross represents the position where observations have been performed.

In the streets of the network, emissions from road traffic are computed using Pollemission (Sarica 2021), which is based on the COPERT methodology, as described in the EMEP/EEA air pollutant emission inventory guidebook (EMEP/EEA 2019). It uses an average-speed approach to determine emission factors, both exhaust and non-exhaust. Five vehicle categories are considered: PCs, LCVs, HDTs, buses (Bus) and two-wheeled vehicles (Lcat). The most common fuels are differentiated, i.e., petrol and diesel, but also LPG and CNG. Electric vehicles are assumed to only emit non-exhaust pollutants. Finally, exhaust emissions depend on the cylinder size for PCs and Lcat, and weight for LCVs, HDTs and Bus, as well as on European emission standards, e.g., Euro 1 and Euro 5 norms, as each norm introduces new and/or improved powertrain technologies and after-treatment processes in the wake of the lowering of emission limits.

Cold exhaust emissions, i.e., transient exhaust emissions during the cold start occur before the operational temperatures of the ICE and after-treatment devices are reached. They are known to be

higher than hot-exhaust emissions and to increase with low ambient temperatures (Joumard et al. 1990; Pielecha et al. 2021). They are estimated using the COPERT methodology, except for the PM cold emission factors for petrol PCs and LCVs, which are absent from the methodology and are inferred from the corresponding diesel vehicle type using a ratio of 1.24 (André et al. 2020). The share of vehicles running during thermal transient operation is fixed to 30 %, following Kyriakis et al. (1998). Non-exhaust emissions related to tire and brake wear, and road abrasion consist of PM falling mainly into the coarse particle category (between PM_{10} and $PM_{2.5}$). Evaporation of VOCs from petrol vehicles that occurs partly during parking phase is not considered at the local scale.

Fleet composition and traffic conditions (vehicle speed and number) correspond to a typical urban fleet for the Île-de-France region for 2014 (André et al. 2019) (see Appendix 3.A for details). Diesel is the most predominant fuel, with more than 65 % of PCs. The complete fleet composition is presented in Table S1. The traffic conditions for each street segment of the network were obtained from simulations performed with the dynamic traffic model Symuvia (Leclercq et al. 2007), as detailed in Kim et al. (2022). On average over the traffic simulations, PCs represent the majority of the fleet at 77 %, followed by LCVs at 14 %. HDTs, Bus and Lcat are less present in the fleet at 3 %, 4 % and 2 % respectively.

NO_x emission factors are speciated into NO and NO_2 using the fractions of NO_2 provided by the COPERT methodology for each vehicle type. The speciation of PM exhaust emission factors also follows the COPERT methodology by using the fractions of BC and OM supplied for each vehicle type. The OM fraction of the PM emissions is assumed to be emitted in the form of LVOCs. If a fraction of PM remains after the BC and OM speciation, it is categorized as dust and unspeciated species. The PM size distribution at emission is assumed to be the same as in Lugon et al. (2021a,b), i.e., exhaust primary PM are assumed to be in the size bin [0.0398 – 0.1585 µm]. The emission factors of NMVOCs are calculated as the difference between VOC andCH_4 emission factors. In contrast to NO_x and PM, the COPERT methodology presents 5 NMVOC speciation profiles aggregated for pre-Euro and Euro petrol PCs and LCVs, diesel PCs and LCVs, HDTs and Bus, and vehicles running on LPG. These speciation profiles include about 60 different species and are presented in Table S2. For heavy compounds that may be considered as precursors of SOAs, only aggregated species are available. In the NMVOC speciations, the IVOC fraction regroups cycloalkanes, alkanes from C_{10} to C_{12}, and aromatics C_9 and C_{10}. Similarly, the SVOC fraction gathers the alkanes and aromatics containing at least 13 atoms of carbon.

Non-exhaust emissions of TSPs originate from tire, brake and road wear. The calculation of their emission factors follows Tier 2 of the COPERT methodology (Ntziachristos et al. 2019a). Table 3.7 presents the size distribution and speciation into BC, OM and dust of the non-exhaust emissions of particles, as specified by the methodology. Dust (and unspeciated species) are the most emitted species for all three sources. Road wear emits only dust materials, as suggested by Tier 1 of the methodology. The majority (90 %) of the emissions falls into PM coarse and $PM_{2.5\text{-}1}$. Appendix 3.B presents the size distributions for the six size sections used in this work.

3.2.2.2 Regional-scale simulations

Because background concentrations can have a strong impact on concentrations in streets, simulations at the regional scale are performed using the model Polair3D from the Polyphemus platform (Mallet et al. 2007), on an area centered on the Île-de-France region with a horizontal resolution of 0.02°x0.02° and 14 vertical levels from the ground to 12 km (see Figure 3.3). The simulation period is from 8 January to 27 December 2014. Biogenic emissions, boundary and initial conditions are taken from Sartelet et al. (2018). Meteorological conditions are modeled using the WRF model (version 3.9.1.1),

as detailed in Lugon et al. (2020). Dry and wet depositions are modeled as detailed in Sartelet et al. (2007).

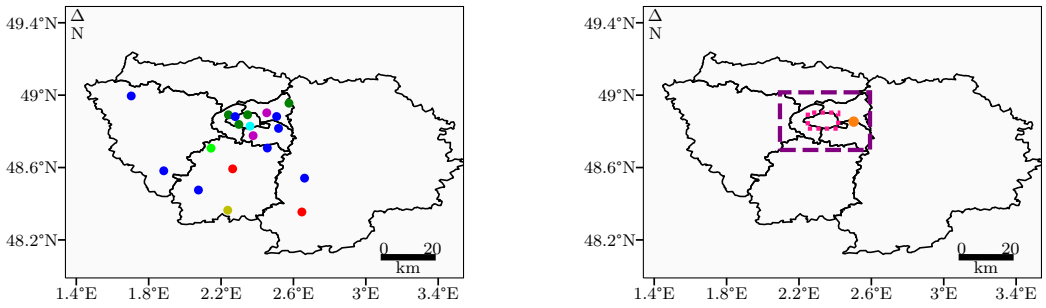

(a) **(b)**

Figure 3.3: (a) Regional-scale simulation domain with the position of the measurement stations. In blue, stations measuring only NO_2. In green, stations measuring NO_2 and PM_{10}. In red, stations measuring NO_2 and $PM_{2.5}$. In magenta, stations measuring NO_2, PM_{10} and $PM_{2.5}$. In cyan, the station measuring NO_2 and BC. In yellow, the station measuring BC. In light green, the station measuring OM. (b) Regional-scale simulation domain with the purple area corresponding to Paris suburbs for the study of the impacts of the various scenarios on emissions and concentrations. The pink area includes Paris city for assessment of the scenarios' impacts on concentrations. The orange hexagon indicates the position of the street network at local scale.

Anthropogenic emissions are retrieved from the EMEP gridded emission inventory[2]. Non-traffic emissions are processed as per Sartelet et al. (2018). Traffic emissions of NO_x, VOCs and PM are speciated similarly to the local scale (see Section 3.2.2.1 where details of the fleet composition are available), i.e., taking into account the fraction of each vehicle type in the fleet. Thus, NO_x emissions are composed of 27 % of NO_2. Because EMEP emissions do not distinguish exhaust from non-exhaust emissions, PM emissions are assumed to originate at 41 % from exhaust, 25 % from brake wear, 18 % from tire wear and 16 % from road abrasion, as at the local scale. Following André et al. (2019), 19 % of NMVOC emissions are considered to be evaporative emissions from petrol PCs and LCVs via evaporation of fuel in the tank during driving and parking, and fuel permeation/leakage. Speciation of these emissions are taken from the COPERT methodology considering ethanol blends.

3.2.2.3 Model evaluations

The reference simulation SCN0 is compared to observational data using the statistical indicators presented in Appendix A1 and the two criteria from Hanna et al. (2012) and Herring et al. (2018). The first criterion is the strictest, with $-0.3 \leq FB \leq 0.3$; $0.7 \leq MG \leq 1.3$; $VG \leq 1.6$; $NAD \leq 0.3$; $NMSE \leq 3$; $FAC2 \geq 0.5$. The second criterion is less strict, with $-0.67 \leq FB \leq 0.67$; $0.7 \leq MG \leq 1.3$; $VG \leq 1.6$; $NAD \leq 0.5$, $NMSE \leq 6$; $FAC2 \geq 0.3$. The most strict criterion is usually applied to rural areas while the less strict is applied to urban areas, as uncertainties are generally higher in these configurations.

At the regional scale, concentrations are compared to background and rural stations for NO_2, PM_{10}, $PM_{2.5}$, OM and BC (see Figure 3.3a for the position of the stations). These stations provide

[2] https://www.ceip.at/the-emep-grid/gridded-emissions (last accessed: 2023-03-15)

measured concentrations over the whole simulation period. They are compared to concentrations in the first vertical layer of the regional simulation. As shown in Table 3.3, the reference simulation compares well to observations for NO_2, PM_{10}, $PM_{2.5}$ and OM while satisfying the strictest criterion for the most part. NO_2, $PM_{2.5}$ and OM concentrations are slightly overestimated and PM_{10} concentrations underestimated. The underestimation is larger for BC, and the criteria are not respected for BC, although the model to measurement correlation is high. These results are comparable to previous studies with similar setups (Roustan et al. 2011; Sartelet et al. 2018; Lugon et al. 2020).

Table 3.3: Polair3D concentration evaluation against observations (*obs* and *sim* represent average observed and simulated concentrations respectively; in $\mu g\,m^{-3}$). Formulation of the indicators is presented in Appendix A1.

	Number of stations	*obs*	*sim*	Correlation	FB	MG	VG	NAD	NMSE	FAC2
NO_2 (hourly)	17	27.43	27.97	0.58	0.14	0.84	2.16	0.28	0.71	0.65
PM_{10} (daily)	6	21.66	18.53	0.68	0.12	0.89	1.15	0.16	0.26	0.93
$PM_{2.5}$ (daily)	4	13.94	15.77	0.65	-0.21	1.24	1.26	0.19	0.31	0.86
OM (daily)	1	3.15	4.14	0.46	-0.33	1.34	1.57	0.25	0.38	0.66
BC (daily)	2	1.18	0.62	0.82	0.62	0.52	1.87	0.33	1.00	0.50

At the local scale, measurements were performed at a section of Boulevard d'Alsace Lorraine from mid-March to mid-June (see Figure 3.2 for the position of the section in the network). It is shown in Table 3.4 that NO_2 and PM_{10} concentrations are underestimated but still mostly conform to the strictest criterion. The statistical indicators for $PM_{2.5}$ concentrations also meet most of the strictest criterion while slightly overestimating the observations. Concerning BC, although the concentration is underestimated at the regional scale, many criteria are satisfied (for example FB is 0.62). However, at the local scale, the underestimation is more significant, with none of the criterion satisfied. Uncertainties related to traffic emissions or the vertical transfer parameterization at rooftop in MUNICH can be potential explanations. All these verifications are comparable to previous studies (Kim et al. 2018, 2022).

Table 3.4: MUNICH hourly concentration evaluation against observations over a period of three months of a segment of Boulevard d'Alsace Lorraine (*obs* and *sim* represent average observed and simulated concentrations respectively; in $\mu g\,m^{-3}$). Formulation of the indicators is presented in Appendix A1.

	obs	*sim*	Correlation	FB	MG	VG	NAD	NMSE	FAC2
NO_2	52.16	47.86	0.54	-0.12	1.13	1.23	0.18	0.25	0.87
PM_{10}	23.42	21.45	0.59	-0.11	1.12	1.31	0.18	0.22	0.83
$PM_{2.5}$	12.72	19.62	0.39	0.36	0.68	1.63	0.27	0.55	0.68
BC	6.10	1.41	0.53	-1.16	4.08	9.65	0.63	3.65	0.09

3.2.3 Sensitivity scenarios and their impacts on emissions

Three scenarios are adopted for investigating traffic emission sensitivities related to the COPERT methodology and their impacts on the concentrations in the street. Two scenarios focus on exhaust emissions with the use of more recent and detailed VOC speciations for PCs and LCVs, or a different approach to compute I/S/LVOC emissions based on Sartelet et al. (2018). The third scenario assesses

sensitivities linked to tire wear emissions assuming that they are underestimated in the COPERT methodology. The fourth scenario tests the possibility that road-asphalt emissions of organic aerosol precursors are non-negligible using emission factors from Khare et al. (2020). Table 3.5 summarizes the simulations performed in this work. This section presents the differences between emissions of the reference simulation SCN0 and the sensitivity scenarios. A subset of the regional domain corresponding to the city of Paris and its outlying suburbs (see Figure 3.3b), is extracted to study the scenarios' impacts on emissions where urbanization and transportation are most prominent. Their impacts on total emissions of IVOCs and SVOCs in the gas phase and emissions of LVOCs and BC in the particle phase are presented in Table 3.6.

Table 3.5: List of the simulations performed.

Scenario	Description
SCN0	Reference simulation - COPERT methodology only
SCN1	More recent VOC speciations for light vehicles
SCN2	I/S/LVOC emissions estimated from total VOC emissions
SCN3	Higher tire wear emissions
SCN4	Addition of I/S/LVOC emissions from road asphalt

3.2.3.1 NMVOC speciation

The NMVOC speciations provided by the COPERT methodology are based on measurements performed on pre-Euro and Euro 1 vehicles and applied to all European emission standards up to Euro 6d. The first sensitivity scenario SCN1 evaluates the impact of using finer and more recent NMVOC speciations for PCs and LCVs. These new speciations originate from laboratory measurements on a PFI and a DI petrol Euro 5 PCs (Marques et al. 2022) and a diesel Euro 6 LCV using the Artemis cold urban cycle. These speciation profiles are detailed in Table S3, S4 and S5 for the petrol PFI, the petrol DI and the diesel vehicles respectively.

In terms of organic compounds that are known SOA precursors, the total BTEX (benzene, toluene, ethylbenzene and xylenes) fraction is higher for the PFI technology at more than 41 % against 26 % for the DI technology, partly because of the higher toluene fraction. For the COPERT petrol speciation, the total BTEX fraction is similar to that of the DI technology. The diesel LCV speciation presents a lower BTEX fraction at 3 % against 3.9 % for the COPERT speciation. This reduction happens despite the increase of the benzene fraction from 2 % to 2.6 %. The fractions of other functionalized compounds of between 6 and 11 atoms of carbon are higher in the recent speciations of the DI and PFI vehicles, at 25 % and 19 % respectively, compared to 7 % for the COPERT speciation. The diesel LCV speciation presents a lower fraction of these functionalized compounds: 1.7 % compared to 2.4 % for COPERT. The IVOC fractions are lower in the recent petrol speciations, at 1.7 % for the PFI technology and 2 % for the DI technology, compared to the COPERT speciation which is at 6 %. Similarly, the SVOC fractions are lower in the PFI and DI speciations, at 0.18 % and 0.01 % respectively, compared to 5 % for COPERT. For the diesel LCV speciation, IVOC and SVOC fractions are also lower than COPERT: 21 % and 0.6 % respectively compared to 31 % and 3.6 % for COPERT.

To evaluate the impact of these speciations, they are applied to all petrol and diesel PCs and LCVs from Euro 1 to Euro 6d. For petrol vehicles, it is assumed that all vehicles up to Euro 4 are

PFI designed, and that 20 % of Euro 5 and later norm vehicles are DI designed[3]. As detailed in the previous section, in the reference simulation SCN0, exhaust IVOCs and SVOCs are estimated as fractions of the NMVOC emissions following the COPERT data. Exhaust LVOC emissions are taken equal to the OM emissions of particles. In the scenario SCN1, LVOC emissions are not modified, but exhaust IVOCs and SVOCs are estimated using the NMVOC speciations presented above. Appendix 3.C presents the processing of these speciations, in particular the determination of the IVOC and SVOC fractions. The scenario SCN1 induces reductions in emissions of I/SVOCs of 46 % at the regional scale and 50 % at the local scale. The reduction is greater for the local scale as traffic is the only direct emission source considered in the street.

The second sensitivity scenario SCN2 implements the method presented in Sartelet et al. (2018) to estimate the IVOC, SVOC and LVOC emissions from the total NMVOC emissions, based on chamber measurements performed in the United States on petrol and diesel vehicles (Zhao et al. 2016). This method was successfully applied to represent exhaust aging in a Euro 5 petrol vehicle (Sartelet et al. 2018). Distinct formulations are available for diesel vehicles whether equipped or not with a diesel particulate filter. For petrol vehicles, cold-start emissions are treated individually. I/SVOC emissions are more impacted than in SCN1 with a reduction of 67 % at the local scale. LVOC emissions are also greatly reduced by 54 % at the local scale.

Table 3.6: Normalized mean bias (NMB) of emissions for the scenarios compared to the reference for the Paris suburbs and at local scale [%].

NMB		SCN1	SCN2	SCN3	SCN4
$IVOC_{gas}$	Polair3D	-45.6	-56.2	0.0	117.5
	MUNICH	-50.0	-66.6	0.0	3.2×10^5
$LVOC_{part}$	Polair3D	0.0	-59.8	194.0	0.0
	MUNICH	0.0	-53.6	219.4	0.0
BC	Polair3D	0.0	0.0	175.4	0.0
	MUNICH	0.0	0.0	213.4	0.0

3.2.3.2 Tire wear emissions

As previously observed in Lugon et al. (2021b), the reference simulation SCN0 tends to underestimate the concentrations of BC compared to observations. The third sensitivity scenario SCN3 follows scenario 4 presented in Lugon et al. (2021b), who argued that the underestimation of BC concentrations may in turn be due to an underestimation of tire wear emissions and uncertainties in the PM speciation of the COPERT methodology. The tire wear emission factor in PCs follows the literature (Malmqvist 1983; Luhana et al. 2004; Boulter 2005) and a value of 100 mg/km/veh is applied. This value is about 9 times higher than the COPERT value of 10.7 mg/km/veh. This ratio of 9 is also employed to increase tire wear emissions in the other vehicle categories. The chemical speciation of tire wear emissions assumes 25 % of BC, which is the average weight fraction between 22 % and 30 % indicated in Thorpe et al. (2008), against the 15.3 % provided by the COPERT methodology. The OM fraction remains consistent with the COPERT methodology (36 %) and the remaining 39 % are classified as dust and unspeciated compounds. The size distribution follows the reference SCN0 except for the $PM_{2.5}/PM_{10}$ ratio, which is taken from the NORTRIP model (10 %) (Denby et al. 2013). The size distributions and chemical speciations are presented in Table 3.7. As expected, this scenario has

[3] https://www.aftonchemical.com/Generic/PFI-vs-GDI (last accessed: 2023-04-21)

strong impacts on emissions. LVOC and BC emissions both increase by 194 % and 175 % respectively at the regional scale and even more at the local scale by 219 % and 213 % respectively.

Table 3.7: Fractions of the size distributions and chemical speciations of non-exhaust PM emissions from tire, road and brake wear. Dust refers to dust and unspeciated compounds. $PM_{10\text{-}2.5}$ represents coarse particles of diameters between 2.5 µm and 10 µm. $PM_{2.5\text{-}1}$ represents the particles of diameters between 1 µm and 2.5 µm.

Source	Scenario	Size distribution				Speciation		
		PM_{10}/TSP	$PM_{10\text{-}2.5}$	$PM_{2.5\text{-}1}$	PM_1	BC	OM	Dust
Tire	All except SCN3	0.6	0.3	0.6	0.1	0.153	0.36	0.487
	SCN3	0.6	0.9	0.086	0.014	0.25	0.36	0.39
Brake	All	0.98	0.6	0.3	0.1	0.026	0.107	0.867
Road	All	0.5	0.46	0.54	0.0	0.0	0.0	1.0

3.2.3.3 Road asphalt

Khare et al. (2020) highlight a possible major missing source of SOA precursors in streets: emissions of road asphalt due to pavement heating and exposure to sunlight. This emission of SOA precursors entails a high degree of uncertainty linked to: i) the mixture used in the process of producing the asphalt, ii) the meteorological conditions to which the asphalt is exposed (mainly temperature and solar radiation), iii) the time elapsed since the paving process. Measurements were performed (Khare et al. 2020), using real-world PG 64-22 asphalt[4] during road paving in New Haven, Connecticut. The derived emission factors were observed to decay exponentially after paving. Because of the freshness of the samples (hours to days after paving operations), these emission factors may be too high to represent an asphalt layer of several months or years old. In our study, as a first assessment, road asphalt emissions are assumed to only occur during daytime with a constant emission factor corresponding to the asymptotic value of 0.1 mg min^{-1} kg^{-1} asphalt presented in Fig. 3.A of Khare et al. (2020). This value, measured at an asphalt temperature of 60°C, is corrected by a factor 0.25 to take into account that temperatures are lower in our simulation than during the measurements. The factor 0.25 is determined from Fig. 1.B of Khare et al. (2020), which shows that the emission factor doubles between 20°C and 40°C, and between 40°C and 60°C. Finally, as per the Supplementary Material S8 in Khare et al. (2020), a factor 0.23 is applied to the total emission factor to take into account that only a fraction, the superficial layer, of the total road asphalt laid is exposed to solar radiation. The surface mass originates from the Office des Asphaltes in Paris,[5] while the averaged value of 80 kg m^{-2} is considered a typical representation of road asphalt in France. At the regional scale over the whole of Île-de-France, the street network in Lugon et al. (2021a) is used to calculate road asphalt emissions based on the quantity of road surface per cell of the domain (m^2 $cell^{-1}$). Only the Île-de-France region is represented as data are not available for its vicinity and that there are far fewer roads in the rest of the area. Asphalt emissions are speciated as IVOCs, SVOCs and LVOCs in the gas phase with a variable volatility distribution in line with Fig 3.C of Khare et al. (2020). At the local scale, I/SVOC emissions are about 15 times higher when asphalt emissions are considered. At

[4]The Performance Grade (PG) of an asphalt is defined by two numbers which represent pavement temperatures for optimal use conditions. The first number (64°C in this case) is the 7-day average maximum pavement temperature. The second number (-22°C in this case) is the minimal temperature.

[5]https://www.asphaltes.org/ (last accessed: 2023-03-15)

the regional scale, they are only two times higher than the average reference over the year, because of the significant contribution of other sources such as residential heating.

3.2.4 Impacts on concentrations

This section investigates the impacts of the scenarios on concentrations at both the regional and local scales. As for emissions, impacts at the regional scale are studied on a subset of the domain corresponding to Paris city and its suburbs, and also to Paris city alone for the impacts on dense traffic areas (see Figure 3.3b). Furthermore, the concentrations presented at the regional scale are surface concentrations, i.e., they correspond to those simulated in the first vertical level of the domain (from 0 m to 30 m). As the sensitivity scenarios influence the emissions of I/S/LVOCs and/or BC, the impacts on concentrations are presented for OM (Table 3.8) and BC (Table 3.9). The impacts on PM_{10} and $PM_{2.5}$ can be found in Appendix 3.D. Since the biases are systematic, only the normalized mean bias (NMB) is presented as it has the same numerical value as the normalized mean error (NME). The formulation of both NMB and NME is outlined in Appendix A2. The impacts of the scenarios on the size distribution of the particles and the concentrations of I/S/LVOCs are presented in Section 3.2.4.1. Seasonal variations of the reference simulation SCN0 and scenario SCN4 are described in Appendix 3.F.

Table 3.8: Impacts of the sensitivity scenarios on OM concentrations over the Paris suburbs and Paris city and at the local scale. Average concentrations are expressed in µg m^{-3} and NMB in %.

OM		SCN0	SCN1	SCN2	SCN3	SCN4
Polair3D	Average	4.6	4.3	3.9	5.4	4.9
Paris suburbs	NMB	-	-6.8	-15.7	15.9	6.5
Polair3D	Average	5.9	5.1	4.3	7.4	6.8
Paris city	NMB	-	-13.2	-27.2	25.1	15.3
MUNICH	Average	5.9	5.3	4.2	8.5	9.3
	NMB	-	-9.9	-27.0	39.7	58.9

Table 3.9: Impacts of the sensitivity scenarios on BC concentrations over the Paris suburbs and Paris city and at the local scale. Average concentrations are expressed in µg m^{-3} and NMB in %.

BC		SCN0	SCN1	SCN2	SCN3	SCN4
Polair3D	Average	0.7	0.7	0.7	1.2	0.7
Paris suburbs	NMB	-	-0.1	0.0	59.2	0.0
Polair3D	Average	1.1	1.1	1.1	2.0	1.1
Paris city	NMB	-	-0.1	-0.1	78.8	0.0
MUNICH	Average	1.5	1.5	1.5	3.1	1.5
	NMB	-	-0.1	0.0	98.3	0.0

The lower emissions of I/S/LVOCs in the first two scenarios lead to reductions in concentrations of OM, thus PM_{10} and $PM_{2.5}$. The concentrations of BC are not significantly influenced by these scenarios, because its emissions are not modified and it is an inert compound. The use of more recent speciations for NMVOC emissions of PCs and LCVs in the scenario SCN1 leads to limited impacts on

OM concentrations in average over the Paris suburbs with a decrease of 7 %. However, the influence of the speciations is higher in Paris city, with an average impact that reaches 13%. PM_{10} and $PM_{2.5}$ concentrations are almost identical to the reference SCN0 with a decrease of 3 % in average over the Paris suburbs reaching 6% over Paris city. At the local scale, OM concentrations are reduced by 10 % and PM_{10} and $PM_{2.5}$ concentrations by more than 4 % using the most recent SCN1 speciation.

Using a different formulation to determine I/S/LVOC emissions in SCN2 induces a decrease in PM_{10} and $PM_{2.5}$ concentrations by about 4.5 % over the Paris suburbs reaching more than 8 % over Paris city. At the local scale, the decrease is similar over Paris city at 8 %. Similarly to the scenario SCN1, the OM concentrations are the most impacted with a decrease of 16 % over the Paris suburbs, reaching 27 % over Paris city and at the local scale.

Considering higher tire wear emissions in scenario SCN3 leads to the highest increase among all scenarios of concentrations of PM_{10}. The NMB is 11 % for the Paris suburbs, 18 % for Paris city and 29 % at the local scale. Due to the higher fraction of coarse particles of emissions in the SCN3 scenario than in the reference (Table 3.7), $PM_{2.5}$ concentrations are less influenced, and they increase by only 11 % at the local scale. OM concentrations are however strongly impacted with an increase of 40 % at the local scale. BC is the most impacted component of particles, because not only is the tire emission factor of PM_{10} increased, but also the fraction of BC in PM_{10} at emission (from 0.153 to 0.25). The increase in BC concentration is as high as 98 % in average at the local scale (Figure 3.4b). However, despite this high increase, BC concentrations are still underestimated compared to the measurements performed in one of the streets. These results differ from those of Lugon et al. (2021b) in which increasing tire emission factors led to a good modeling of observed BC concentrations. Lugon et al. (2021b) approximated (and probably overestimated) the traffic flow in a number of streets in the network. Here, detailed information of the traffic flow (from the traffic model Symuvia) enabled more accurate calculations of emission factors for each segment of the network. However, discrepancies between simulations and observations remain for BC concentrations and need to be assessed. They could be linked to other emission sources not yet considered, or to uncertainties in the measurements (Malik et al. 2021).

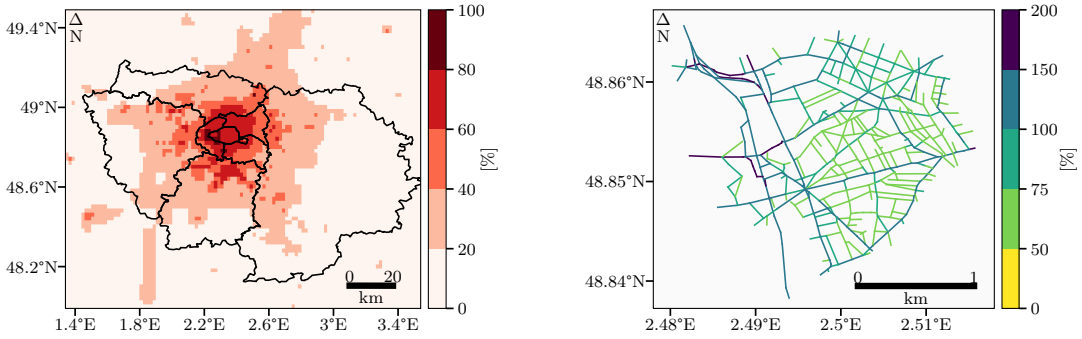

(a) **(b)**

Figure 3.4: Relative differences in concentrations of BC between the SCN3 scenario and the reference at the regional scale (a) and the local scale (b). For information, the annual mean concentrations for the reference are available in Appendix 3.E.

In scenario SCN4, concentrations of OM are higher than in the reference SCN0, as road asphalt emissions in IVOCs, SVOCs and LVOCs have been taken into account. At the regional scale, the increase is larger than 6 % over the Paris suburbs. The average increase reaches 15 % over Paris city. PM_{10} and $PM_{2.5}$ concentrations increase by 5 % over Paris city. At the local scale, the influence is

greater because of the proximity of roads and because of higher regional background concentrations above the streets. The OM concentrations increase by almost 60 % on average. This leads to an increase in PM_{10} and $PM_{2.5}$ concentrations by about 18 %. Note that despite this large increase, PM_{10} and $PM_{2.5}$ still satisfy the less strict criteria compared to observations. Several streets in the network have low traffic emissions. Adding road asphalt emissions thus significantly increases OM concentrations for these streets by up to about 75 % (Figure 3.5b). The concentrations simulated in this scenario are plausible and confirm the conclusions in Khare et al. (2020) that road asphalt could possibly be a major missing source of SOA precursor emissions. However, uncertainties as to the emission factors remain high and the significance of this source after years or decades of use needs to be assessed.

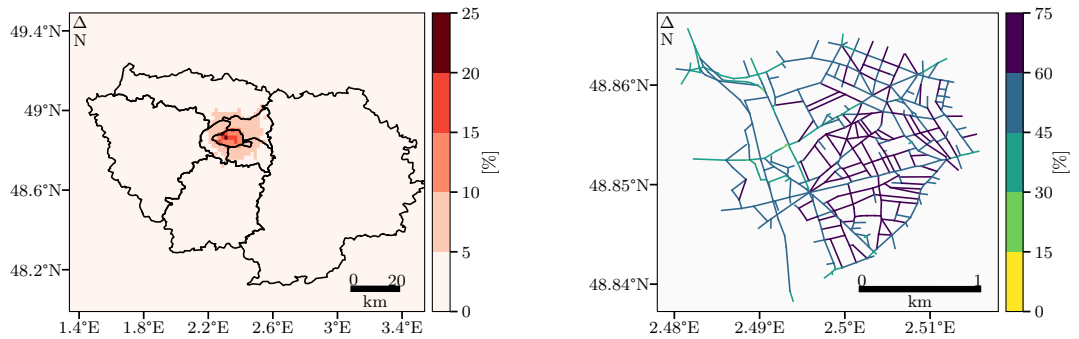

(a) **(b)**

Figure 3.5: Relative differences in concentrations of OM in scenario SCN4 at regional scale (a) and local scale (b). For information, the annual mean concentrations for the reference are available in Appendix 3.E.

3.2.4.1 Impacts of the scenarios on particulate size distribution and on gas-phase I/S/LVOC concentrations

Figure 3.6 presents the annual mean size distribution of PM for the scenarios at both the regional (for the Paris suburbs area) and local scales. For the reference simulation SCN0, about 80% of the mass of PM is in PM_1, followed by $PM_{2.5\text{-}1}$ and finally coarser particles, $PM_{10\text{-}2.5}$. The first two scenarios, SCN1 and SCN2, present similar size distributions as they only impact the OM concentrations, at both the regional and local scales. However, they display smaller total mass compared to the reference.

The higher tire wear emissions of PM in scenario SCN3 induce higher total mass in both scales. Because the emissions of coarse particles by tire wear are higher in this scenario (see Table 3.7), the size distribution of the concentrations demonstrates a higher fraction of coarse particles, $PM_{10\text{-}2.5}$. At the local scale, this results in 20 % of the PM present in the coarse fraction. Finally, for scenario SCN4, which considers road asphalt emissions of SOA precursors, the total mass of PM is also higher than in the reference. However, the impact on the size distributions is limited, because condensation of the SOA precursors mostly modifies the mass of fine particles.

The concentrations of I/S/LVOCs in the gas phase are impacted by the sensitivity scenarios, as can be seen in Figure 3.7. For the reference simulation, in the Paris suburbs area, the IVOC fraction is at 58 %, followed by SVOCs at 40 % and LVOCs at 2 %. At the local scale, the IVOC fraction is lower but still has a majority at 52 %, with SVOCs at 45 % and LVOCs at 3 %. The first scenario SCN1 with recent VOC speciations presents lower total mass of I/S/LVOCs at both scales while

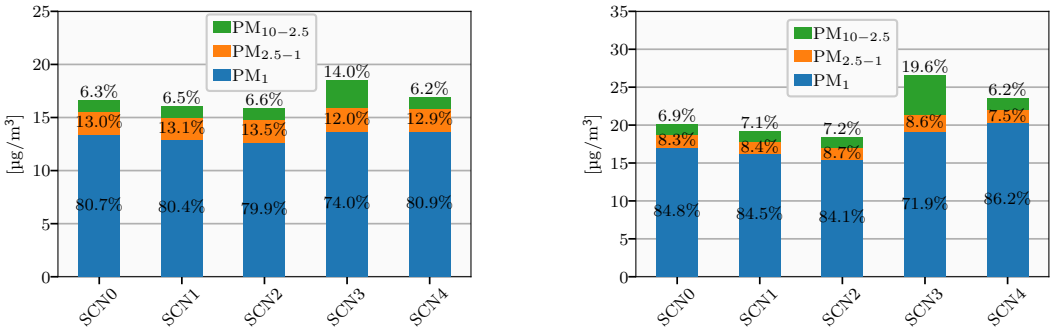

(a) (b)

Figure 3.6: Annual mean size distribution of PM for the reference SCN0 and the sensitivity scenarios at the regional scale for the Paris suburbs area (a) and the local scale (b). The total is expressed in µg m^{-3}.

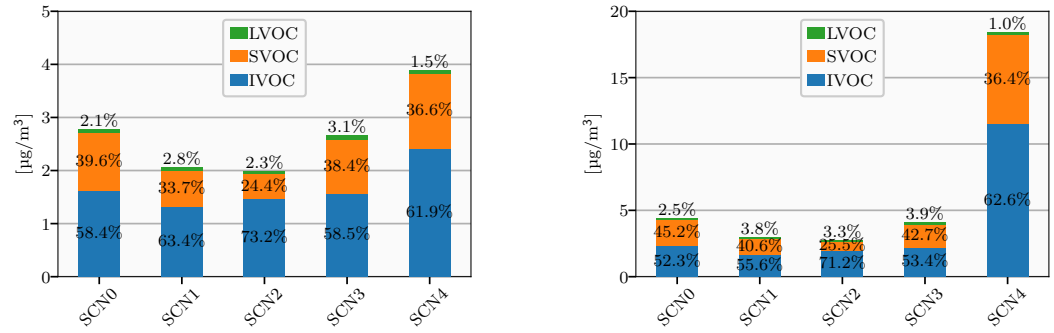

(a) (b)

Figure 3.7: Annual mean fractions of gas-phase I/S/LVOCs for the reference SCN0 and sensitivity scenarios at the regional scale for the Paris suburbs area (a) and the local scale (b). The total is expressed in µg m^{-3}.

having a limited impact on the fractions. IVOC and LVOC fractions are slightly higher while the SVOC fraction is lower. For the second scenario SCN2, the totals are also lower than the reference but at the local scale, the IVOC fraction is higher at 71 % and the SVOC fraction lower at 26 %.

Despite higher tire wear emissions in the third scenario SCN3, thus higher emissions of LVOCs in the particle phase, the totals of gas-phase I/S/LVOCs are lower than the reference at both scales. However, the fractions of LVOCs are slightly higher at both scales. Finally, scenario SCN4 with road asphalt emissions of SOA precursors in the gas phase presents a total mass that is far greater than the other simulations. The impact is less significant at the regional scale where other sources are also considered. At the local scale, the total mass of I/S/LVOCs is more than three times higher than the reference's total. The fractions are also modified at both scales according to this new emission source. The IVOC fraction is higher while fractions of SVOCs and LVOCs are reduced.

3.2.5 Conclusions

Four sensitivity scenarios have been defined to investigate specific sensitivities related to the representation of traffic and road asphalt emissions in the modeling. For exhaust emissions, replacing the outdated NMVOC speciation profiles of the COPERT methodology by recent speciations from

Euro 5 and Euro 6 vehicles leads to a reduction in the modeled concentrations of OM by up to 10 % on average. In particular, different estimations of exhaust I/S/LVOC emissions lead to differences in OM concentrations reaching 30 % on average. These results highlight the necessity of accurately representing the speciation of NMVOC emissions, in particular the fractions of I/S/LVOCs. At the local scale, the simulated BC concentrations remain strongly underestimated compared to observations even when using higher tire wear emissions as suggested in the literature. Further work is needed to assess the discrepancies between modeled and observed BC. This could be linked to missing sources, uncertainties in the measurements, or specific modeling assumptions. Note that although the sensitivity study was performed for 2014 emissions, which is somewhat dated, it still holds for more recent years. Indeed, in chemistry-transport models, the representation of the uncertain sources studied here is not updated as often as in technology and fleet evolutions: VOC speciations are generally based on measurements performed on old vehicles and applied to all vehicles, old or recent. For example, in the COPERT methodology, VOC speciations are based on measurements performed before the year 2000 and applied to all vehicles. Tire wear emission factors are also rarely updated, even with the penetration of electric vehicles in the fleet.

Currently, not considered in emission inventories, emissions of organic aerosol precursors from road asphalt could be several orders of magnitude higher than emissions from traffic. Impacts on concentrations of OM are yet limited to a 60 % increase in average, leading to realistic PM concentrations. However, uncertainties on asphalt emissions are high and need further assessment.

Other sources of sensitivities linked to traffic emissions may be relevant, such as the influence of the fraction of vehicles running under cold-transient conditions (it could be lower for recent vehicles than the value of 30 % considered here), as well as the influence of the traffic emission model (Badin et al. 2017; Borge et al. 2012).

Acknowledgments

This work was partially funded by the MAESTRO (Modeling / Characterization of Gaseous Precursors and Secondary Aerosols in Road Transport) project of the ADEME program CORTEA, and by the POLEMICS project of the ANR program (grant ANR-18-CE22-0011).

Appendices

3.A Traffic information

Diesel is the predominant fuel in the fleet with more than 65 % of PCs being diesel-fueled. Out of the remaining, 30.7 % of PCs are fueled with petrol, followed by petrol hybrid, LPG and electric (2.6 %, 0.6 % and 0.8 % respectively). 97.5 % of LCVs run on diesel, 2.2 % use petrol and the remaining 0.3 % are electric. Most HDTs are diesel-fueled (99.5 %), with only 0.5 % electric. Buses are also mostly diesel-fueled (99 %) with 1 % running on CNG. Lcat all run on petrol.

Two days, the 25th and 30th March 2014, were chosen to represent typical traffic conditions for the weekdays and the weekend and holidays respectively. The morning and evening rush hours for weekdays are respectively around 08:00 and 18:00 local time, with up to 1,400 vehicles per hour in the morning. The peak of vehicles is much lower during the weekend day, around 200 vehicles per hour at 11:00 and 17:00 local time. To apply these profiles for each month of the year, the monthly temporal factors introduced with EMEP gridded emissions are used (Guevara et al. 2021). Mean speed profiles of the weekday and weekend day are similar with higher speeds during the night and morning, 32 km h^{-1} at 03:00 for the weekday and 31 km h^{-1} at 07:00 for the weekend day. Throughout the whole day, speeds remain between 24 km h^{-1} and 32 km h^{-1}.

3.B Size distribution of non-exhaust emissions for the six size sections

Table 3.B.1: Fractions of the size distributions of non-exhaust PM emissions from tire, road and brake wear for the six size section used in this work.

Source		Tire		Brake	Road
Scenario		All except SCN3	SCN3	All	All
Size distribution	[0.01 – 0.0398 µm]	0	0	0	0
	[0.0398 – 0.1585 µm]	0	0	0	0
	[0.1585 – 0.4 µm]	0	0	0	0
	[0.4 – 1 µm]	0.1	0.014	0.1	0
	[1 – 2.5119 µm]	0.6	0.086	0.3	0.54
	[2.5119 – 10 µm]	0.3	0.9	0.6	0.46

3.C Processing of the NMVOC speciations for SCN1

Two Euro 5 petrol passenger cars and one Euro 6 diesel light commercial vehicle (recorded as DIEveh) were tested using the Artemis cold urban cycle. The petrol vehicles differed mainly by the method of injection, one using PFI and the other DI. They are respectively referred to as PFIveh and DIveh hereafter. NMVOC speciations for the three vehicles were obtained using GC-MS and PTR-ToF-MS. GC-MS enabled the measurement of alkanes, cycloalkanes, monoaromatics C6-C10 and naphthalene. PTR-ToF-MS facilitated the measurement of all the other compounds. However, these two techniques were not able to speciate parts of the emissions; approximately 15, 22 and 27 % for PFIveh, DIveh and DIEveh respectively. These unspeciated parts are composed of small saturated and unsaturated compounds C≤6. For the petrol vehicles, Saliba et al. (2017) is used to reconstitute these missing parts. For the diesel vehicle, the COPERT speciation is applied.

Some species were detected (molecular formula known) but not identified between the several isomers. The unidentified parts represent 0.3, 0.4 and 0.2 % of the total masses of NMVOCs for

PFIveh, DIveh and DIEveh respectively. As a result, it was decided to not take into account these unidentified species.

As the limit between IVOCs and SVOCs is somewhat blurry, it was decided to compute saturation concentrations for compounds 15≤C≤22. The online tool UManSysProp [6] allows the $\log_{10}$ of the vapor pressure for a given compound at a given temperature to be calculated. The calculations are based on group contribution methods. This website proposes three different methods to calculate vapor pressure (Nannoolal et al. 2008; Myrdal et al. 1997; Compernolle et al. 2011) and three different methods to calculate the boiling point (Joback et al. 1987; Stein et al. 1994; Nannoolal et al. 2004); all these methods are reviewed in Barley et al. (2010) and O'Meara et al. (2014). Vapor pressures can be calculated using nine configurations to highlight variability and to obtain a better determination of the limit between IVOCs and SVOCs. Once calculated, vapor pressures are converted to saturation concentrations (C*) using the following formula:

$$C^* = \frac{P^{vap}.M_w}{R_{gas}.T} \tag{3.C.1}$$

with P^{vap} the vapor pressure, M_w the molecular mass, R_{gas} the gas constant and T the temperature set to 298 K.

According to the literature (Chrit et al. 2018; Majdi et al. 2019), IVOCs have a $\log_{10}$(C*) between 4 and 6, and SVOCs have a $\log_{10}$(C*) inferior to 4. Linking this information to Table 3.C.1, compounds containing 18 or more carbons are considered to be SVOCs.

Table 3.C.1: Averages over the nine configurations of the $\log_{10}$ of the saturation concentrations µg m^{-3} for compounds C≥15, at a temperature of 25°C.

Species	Number of Carbons	$\log_{10}$(C*) [µg m^{-3}]
Pentadecane	15	4.93
Nonylcyclohexane	15	4.87
Hexadecane	16	4.47
Heptadecane	17	4
Octadecane	18	3.53
Nonadecane	19	3.05
Eicosane	20	2.57
Heneicosane	21	2.09
Docosane	22	1.6

[6] http://umansysprop.seaes.manchester.ac.uk/tool/vapour_pressure (last visited 2023-04-21)

3.D Impacts of sensitivity scenarios on concentrations

Table 3.D.1: Impacts of the sensitivity scenarios on the PM_{10} concentrations over the Paris suburbs and Paris city and at the local scale. Average concentrations are expressed in µg m^{-3} and NMB in %.

PM_{10}		SCN0	SCN1	SCN2	SCN3	SCN4
Polair3D	Average	16.6	16.1	15.8	18.5	16.9
Paris suburbs	NMB	-	-3.0	-4.4	11.0	1.8
Polair3D	Average	19.8	18.7	18.2	23.4	20.7
Paris city	NMB	-	-5.7	-8.1	18.2	4.6
MUNICH	Average	20.1	19.2	18.4	26.6	23.5
	NMB	-	-4.2	-8.0	29.4	17.3

Table 3.D.2: Impacts of the sensitivity scenarios on the $PM_{2.5}$ concentrations over the Paris suburbs and Paris city and at the local scale. Average concentrations are expressed in µg m^{-3} and NMB in %.

$PM_{2.5}$		SCN0	SCN1	SCN2	SCN3	SCN4
Polair3D	Average	15.5	15.0	14.8	15.7	15.8
Paris suburbs	NMB	-	-3.2	-4.7	1.2	2.0
Polair3D	Average	18.1	17.0	16.5	18.5	19.0
Paris city	NMB	-	-6.2	-8.8	2.1	5.0
MUNICH	Average	18.7	17.9	17.1	20.8	22.1
	NMB	-	-4.4	-8.3	10.9	18.3

3.E Annual mean concentrations of BC and OM for SCN0

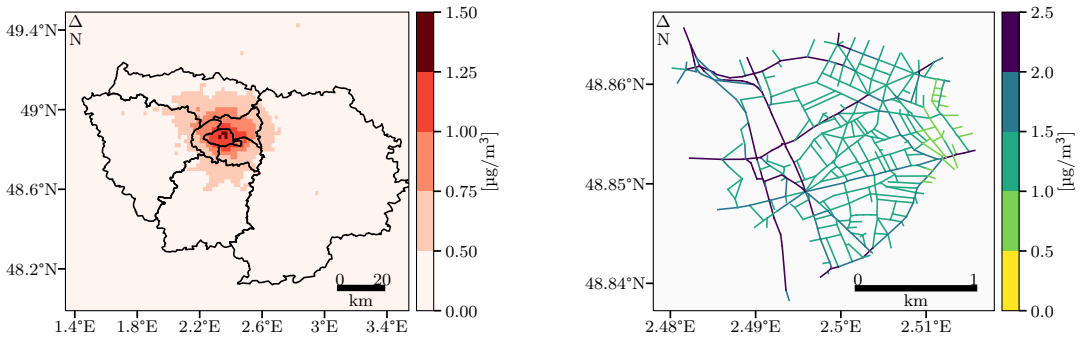

(a) (b)

Figure 3.E.1: Annual mean concentrations of BC for the reference SCN0 at the regional scale (a) and the local scale (b) in µg m^{-3}.

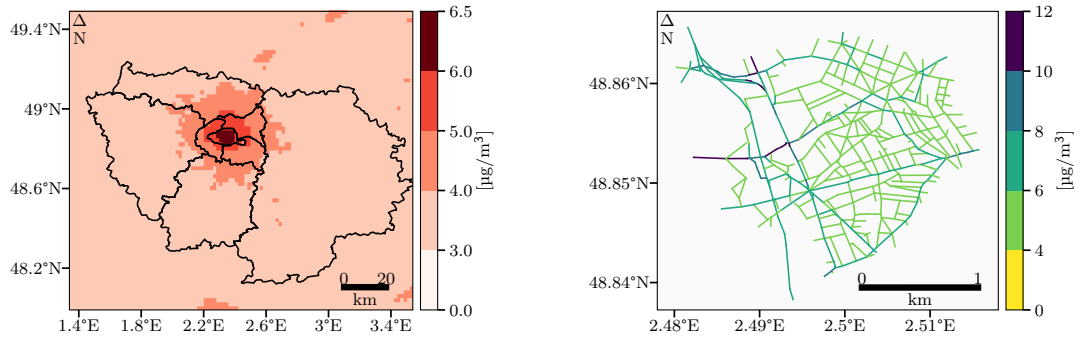

(a) (b)

Figure 3.E.2: Annual mean concentrations of OM for the reference SCN0 at the regional scale (a) and the local scale (b) in µg m^{-3}.

3.F Seasonal variations of emissions and concentrations

This appendix presents seasonal variations in emissions and concentrations. The first 3 sensitivity scenarios, from SCN1 to SCN3, are not presented as they follow the same trends as the reference simulation SCN0. On the contrary, the seasonal variations for the sensitivity scenario SCN4, which considers road asphalt emissions depending mainly on temperature and incident solar flux, are high. Table 3.F.1 displays the average emissions for the four quarters of the year 2014, referred to as Q1 to Q4.

For the Paris suburbs area, emissions of BC and the organics and their precursors are mainly driven by the traffic sector but also by residential heating. Emissions of $I/SVOCs_{gas}$ and $LVOCs_{part}$ are more important during Q2 and Q3, which is consistent with the monthly temporal factors of EMEP for traffic emissions. BC emissions are more uniform throughout the year, as levels of residential heating are higher during Q1 and Q4. In scenario SCN4, road asphalt emissions of $I/SVOCs_{gas}$ drive seasonal variations. Emissions are significantly higher during the summer period (Q2 and Q3) with warmer conditions and more sunlight hours. At the local scale, emissions for Q1 are the lowest in the year due to less traffic during this period. Higher traffic during Q2 and Q3 induces higher emissions. With the same level of traffic as for Q2 and Q3, and lower temperatures, thus higher levels of cold-start emissions, Q4 presents the highest emissions. As for the regional scale, road asphalt emissions in scenario SCN4 drive emissions with higher emissions during Q2 and Q3.

Table 3.F.1: Average emissions per quarter for the reference simulation SCN0 and scenario SCN4 for $I/SVOCs_{gas}$ expressed in ng m^{-2} s^{-1} for the Paris suburbs area and in µg s^{-1} for the local scale.

Average emissions			Q1	Q2	Q3	Q4
$I/SVOCs_{gas}$	POLAIR3D	SCN0	51.7	54.3	53.1	53.4
		SCN4	90.2	111.1	105.7	88.1
	MUNICH	SCN0	192.2	189.0	181.3	207.0
		SCN4	2580	3652	3434	2354
$LVOCs_{part}$	POLAIR3D	SCN0	10.4	11.9	12.2	11.6
	MUNICH	SCN0	109.2	117.3	118.8	120.1
BC	POLAIR3D	SCN0	9.2	9.4	9.0	9.3
	MUNICH	SCN0	84.9	90.4	91.4	93.2

Concentrations of pollutants also present seasonal variations as shown in Table 3.F.2. However, relations with emissions are more difficult to establish as chemical reactions, meteorological conditions, initial conditions and background concentrations all impact on their measurement. For the Paris suburbs area, OM concentrations are higher during the second part of the year and especially during Q3. At the local scale, OM concentrations are higher during the colder periods, i.e., Q1 and Q4. In scenario SCN4 with road asphalt emissions, OM concentrations follows the same trend as the reference at each scale but with higher values. At both scales, BC concentrations are higher during the colder periods, possibly linked to emissions from residential heating. Concentrations of PM_{10} and $PM_{2.5}$ are also higher during Q1 and Q4 at the local scale, but at the regional scale, concentrations are higher during the first half of the year.

Table 3.F.2: Average concentrations per quarter for the reference simulation SCN0 and scenario SCN4 for OM expressed in µg m^{-3} for the Paris suburbs area and at the local scale.

Average concentrations			Q1	Q2	Q3	Q4
OM	POLAIR3D	SCN0	4.1	4.0	5.6	4.8
		SCN4	4.4	4.2	5.9	5.3
	MUNICH	SCN0	5.8	4.6	6.2	7.1
		SCN4	10.8	6.7	7.9	12.3
BC	POLAIR3D	SCN0	0.8	0.6	0.6	0.9
	MUNICH	SCN0	1.6	1.2	1.3	1.8
PM_{10}	POLAIR3D	SCN0	17.9	16.9	15.6	16.1
	MUNICH	SCN0	22.7	18.6	17.7	21.8
$PM_{2.5}$	POLAIR3D	SCN0	16.8	15.8	14.6	15.0
	MUNICH	SCN0	21.4	17.1	16.2	20.6

Chapter 4

Simulation of air quality in 2030 with the introduction of very-low-emission vehicles

Contents

Despite efforts by the authorities to mitigate air pollution, populations are still exposed to high concentrations of pollutants, especially in urban areas. In 2020, among the 75 % of the European population living in urban areas, 89 % are exposed to NO_2 concentrations above the 2021 WHO guidelines, reaching 96 % for $PM_{2.5}$ (EEA 2023). Exposure to these high concentrations of both gas and particle pollutants causes detrimental health effects, ranging from coughing and eye irritation to chronic diseases, e.g. chronic bronchitis and lung cancer (Section 1.1.2.2) (Li et al. 2022a).

Numerous studies investigated the impacts of road traffic on urban air pollution, and ways to reduce its emissions (Roustan et al. 2011; Xia et al. 2015; Tang et al. 2019; André et al. 2020; Zhang et al. 2020; Holnicki et al. 2021; Lugon et al. 2022). Promoting alternative transport (cycling and public transport) in Adelaide, South Australia could reduce concentrations of $PM_{2.5}$ by 25 % (Xia et al. 2015). Although not justified in terms of road safety, raising speed limits in urban areas from

30 km h^{-1} to 50 km h^{-1} could also reduce NO_2 and PM_{10} concentrations by 3 % and 2 % respectively (Tang et al. 2019). The use of recent vehicles appears to be an effective measure to reduce NO_2 and BC concentrations. For example, modernizing the fleet in Warsaw, Poland, to the most recent European emission standards would reduce the population's exposure to NO_x by almost 50 % (Holnicki et al. 2021). Lugon et al. (2022) modeled several scenarios of fleet renewal and evolution (business as usual and promotion of petrol and electric vehicles) from 2014 to 2024 over Paris, France, and observed reductions in concentrations of NO_2 and BC by up to 50 % and of PM_{10} and $PM_{2.5}$ by 20 %. Despite these large reductions of concentrations due to fleet renewal, more than 20 % of the Paris population would still be exposed to NO_2 and $PM_{2.5}$ concentrations exceeding the air quality guidelines. However, this exposure may be overestimated, because the decrease of emissions from sectors other than traffic is not taken into account.

The estimation of the population exposure to outdoor concentrations is strongly linked to the modeling scale. The high concentrations observed in streets are not represented by regional-scale modeling, which provides estimation of the background concentrations. Although traffic emissions do affect those background concentrations, their influence is larger at the local scale (Lugon et al. 2022).

This study aims to evaluate the impact of introducing very-low-emission vehicles in the traffic fleet on the concentrations of pollutants, taking into account the evolution of emissions from the different activity sectors. The exhaust emission factors of these very-low-emission vehicles go further than those proposed for the European emission standard Euro 7. The impact is estimated for the year 2030 on the Paris region and in the streets of a district in the eastern suburb of Paris. The concentrations are compared with those simulated for the year 2014.

Section 4.1 introduces the emission factors related to the very-low-emission vehicles, as well as the two prospective scenarios and their impacts on fleet composition. The evolution of emissions related to the different activity sectors and to the two scenarios are presented in Section 4.2. Finally, the impacts of the scenarios on concentrations are discussed in Section 4.3.

4.1 Road-traffic evolution

The baseline simulation for year 2014, named 2014b, corresponds to the reference simulation, SCN0, from Section 3.2. It uses the COPERT methodology, described in the EMEP/EEA air pollutant emission inventory guidebook (EMEP/EEA 2019) to calculate traffic emissions in streets. The emission factors and fleet evolution are presented below, following the nomenclature of the methodology for vehicles categories and European emission standards.

4.1.1 Emissions from very-low-emission vehicles

Table 4.1 presents the emission factors at exhaust for the very-low-emission vehicles used in this study. For PCs and LCVs, the emission factors for CO, NMVOCs and NH_3 are set to 50 % of the limit values proposed for the European emission standard Euro 7 (Table 2.1). NO_x emission factors go even further, 10 mg km^{-1} against 60 mg km^{-1} for PCs. They are based on the improvement and addition of after-treatment devices, such as afterburners, to reduce cold-start emissions in particular (Gao et al. 2019; Clenci et al. 2022). These emissions factors take into account both hot and cold emissions.

For HDVs and Lcat, the emission factors of CO, NO_x, NMVOCs and NH_3 of the very-low-emission vehicles are set to 50 % of the most recent European emission standards (Euro VI for HDVs and Euro 5 for Lcat). These values are also based on the improvement and addition of after-treatment devices.

Concerning PM, emission factors for the very-low-emission vehicles are identical to the emission factors of the most recent emission standards for the corresponding vehicle category.

Table 4.1: Emission factors at exhaust for very-low-emission vehicles.

	PCs	LCVs	HDVs	Lcat
CO	250 mg km^{-1}[a]	250 mg km^{-1}[a]	50 % Euro VI	50 % Euro 5
NO_x	10 mg km^{-1}	20 mg km^{-1}	50 % Euro VI	50 % Euro 5
NMVOCs	34 mg km^{-1}[a]	34 mg km^{-1}[a]	50 % Euro VI	50 % Euro 5
NH_3	10 mg km^{-1}[a]	10 mg km^{-1}[a]	50 % Euro VI	50 % Euro 5
PM	100 % Euro 6	100 % Euro 6	100 % Euro VI	100 % Euro 5

[a] 50 % of the European emission standard Euro 7 proposal.

Emissions factors from non-exhaust sources (tire and brake wear, and road abrasion) are computed using the values provided by the COPERT methodology. Despite their high uncertainties (Section 3.2) (Lawrence et al. 2013; Jeong et al. 2019; Lugon et al. 2021b), non-exhaust emissions are not expected to change much compared to current emission levels, unless mobility changes. Concerning the speciation of the emissions of NO_x, NMVOCs and PM, in the absence of information specific to future vehicles, information provided by the COPERT methodology for the most recent emission standards are used.

4.1.2 Prospective scenarios and fleet evolution

Two scenarios of the fleet evolution are considered, one with a realistic evolution of the fleet (2030r with r for "realistic fleet") and one with a theoretical fleet made of only very-low-emission and electric vehicles (2030t with t for "theoretical fleet"). The second scenario is introduced to assess the maximum emission and concentration reduction.

The scenario 2030r is representative of a gradual evolution of the fleet, assuming a replacement of the oldest vehicles by newer vehicles, also considering electric vehicles. This fleet evolution is modeled using SIBYL baseline[1]. It is a projection tool for estimating vehicle fleet for 37 European countries based on historical data. In this study, the penetration rates of new vehicles are corrected for years 2021 and 2022 using information from the European automobile manufacturers' association (ACEA) (ACEA 2022b,a). In the scenario 2030t, the fleet is only composed of the most recent vehicles with very low emissions, and electric vehicles.

Table 4.1 presents the distribution of PCs and LCVs in the three fleets of this study according to European emission standards and for electric vehicles. For the other vehicle categories, the distributions are available in Appendix 4.A. The fleet for the baseline simulation 2014b is representative of the year 2014, thus Euro 6 a/b/c is the most recent emission standard for PCs, but only with 2 % of the category. More than 4 % are pre-Euro and Euro 1, and the majority falls into Euro 4 and Euro 5 standards, at 28 % and 42 % respectively. Electric vehicles represent less than 1 % of the PCs. Concerning LCVs, a similar trend is observed, with about 4 % of the vehicles being pre-Euro and Euro 1. The majority also falls into Euro 4 and Euro 5 standards, but with more Euro 4 than Euro 5, at 41 % and 33 % respectively.

The fleet evolution modeled in scenario 2030r leads to the disappearance of pre-Euro and Euro 1 PCs and negligible levels for LCVs. Other emission standards already present in fleet 2014b are less

[1] https://www.emisia.com/utilities/sibyl-baseline/ (last visited 2023-04-21)

represented, e.g. Euro 5 goes from 42 % to 17 % for PCs. Euro 6 d standard becomes preponderant for PCs, at 23 %, while it is Euro 6 a/b/c standard at 19 % for LCVs. The very-low-emission vehicles represent 12 % of the two categories and electric vehicles a higher portion for PCs, at 13 %. In fleet 2030t, it is considered that all non-electric vehicles are very-low-emission vehicles, while keeping the portion of electric vehicles similar to scenario 2030r.

Table 4.1: Distribution of PCs and LCVs in fleets according to European emission standards and for electric vehicles, in %.

		2014b	2030r	2030t
PCs	Pre-Euro	1.3	-	-
	Euro 1	2.9	-	-
	Euro 2	7.2	0.6	-
	Euro 3	15.9	1.1	-
	Euro 4	28.1	8.3	-
	Euro 5	41.6	16.9	-
	Euro 6 a/b/c	2.1	18.3	-
	Euro 6 d-temp	-	6.2	-
	Euro 6 d	-	23.0	-
	VLEV[a]	-	12.3	86.8
	Electric	0.9	13.2	13.2
	Total	100	100	100
LCVs	Pre-Euro	2.1	2.1×10^{-6}	-
	Euro 1	2.1	4.7×10^{-4}	-
	Euro 2	5.2	0.3	-
	Euro 3	17.1	5.4	-
	Euro 4	40.8	12.6	-
	Euro 5	32.5	16.3	-
	Euro 6 a/b/c	-	19.3	-
	Euro 6 d-temp	-	5.0	-
	Euro 6 d	-	17.0	-
	VLEV[a]	-	12.0	87.9
	Electric	0.3	12.1	12.1
	Total	100	100	100

[a] VLEV = Very-low-emission vehicles.

4.2 Evolution of emissions

At the regional scale, the domain is centered on the Île-de-France region, and a district in the eastern suburbs of Paris is defined at the local scale. Biogenic emissions are taken from Sartelet et al. (2018). Their evolution is not considered to have a consistency with the meteorological conditions for 2014. Anthropogenic emissions at the regional scale are computed using the EMEP gridded emission inventory for 2014[2]. Below are presented the reductions applied to anthropogenic emissions to be

[2] https://www.ceip.at/the-emep-grid/gridded-emissions (last visited 2023-04-21)

representative of the year 2030, given the prospective scenarios. Impacts on total emissions are also discussed.

4.2.1 Non-traffic sectors

In order to model background concentrations consistent with year 2030, emission reductions of the non-traffic sectors are taken into account. Table 4.1 presents the emission ratios between 2030 and 2014 used. The majority of the ratios are taken from Allemand et al. (2021) following scenario AME. This scenario, developed in 2021, projects anthropogenic emissions by activity sector in 2030, taking into account the regulations in place until December 31, 2019. For CO and NH_3, some ratios are calculated using the average from the other pollutants, except SO_2. For the emissions of NH_3 and PM from the solvent industry, ratios are extrapolation from year 2014 using information specific to Île-de-France region, provided by the Parisian air quality monitoring association[3]. As no information was available for the emissions (except SO_2) from the sector "Other Stationary Combustion", it was decided to not modify these emissions.

Overall, emissions are reduced from 2014 to 2030, except for NH_3 emissions from the waste and public power sectors, for which they increase by 78 % and 69 % respectively. In the case of the waste sector, it is related to the quantity of waste entering the composting facilities and the degradation of livestock manure. For the public power sector, it is due to the incomplete combustion of the different energies sources, coupled with an increase in the combustion capacity. Offroad, shipping and aviation transport sectors present large reductions in emissions, especially for NO_x (70 %) and PM (62 %). Emission reductions for the agricultural sectors are limited, with up to 15 % for CO. In the other sectors, mainly related to the industry, emissions of NO_x are PM are largely reduced, while emissions of NMVOCs and NH_3 present a lower decrease.

Table 4.1: Emission ratios for the non-traffic sectors between 2030 and 2014.

Sector	CO	NO_x	NMVOCs	NH_3	PM	SO_2
Offroad	0.52[a]	0.30	0.58	0.81	0.38	0.65
Shipping	0.52[a]	0.30	0.58	0.81	0.38	0.65
Aviation	0.52[a]	0.30	0.58	0.81	0.38	0.65
Waste	0.83	0.94	0.83	1.78	0.92	0.75
Agri Livestock	0.85	0.94	0.98	0.95	0.93	1.00
Agri Other	0.85	0.94	0.98	0.95	0.93	1.00
Fugitive	0.68[a]	0.47	0.66	0.68[a]	0.91	0.43
Other Stationary Combustion	1.00[b]	1.00[b]	1.00[b]	1.00[b]	1.00[b]	0.11
Solvents	0.59[a]	0.73	0.92	0.18[c]	0.54[c]	0.84
Industry	0.59	0.60	0.70	0.66	0.38	0.52
Public Power	0.91	0.38	0.77	1.69	0.36	0.18
Other	0.62	0.39	0.47	0.84	0.46	0.41

[a] Average of other pollutants (except SO_2).
[b] No information found.
[c] Extrapolation from the Parisian air quality monitoring association[3].
Other ratios are taken from the AME scenario in Allemand et al. (2021).

[3] https://www.airparif.asso.fr/surveiller-la-pollution/les-emissions (last visited 2023-04-21)

4.2.2 Traffic sector

Traffic emissions are first calculated at the local scale. Emissions in the streets of the network are computed for both prospective scenarios using Pollemission (Section 2.4). However, it is updated to take into account emission factors of very-low-emission vehicles. In the absence of a reliable method to estimate future traffic conditions (vehicle speed and number), these are identical to the baseline simulation. They correspond to a typical urban fleet for the Île-de-France region for 2014 (André et al. 2019).

Then, the influence of the prospective scenarios on reductions of traffic emissions at regional scale is defined. The reductions observed at the local scale over the simulation period are averaged and presented in Table 4.1. As Pollemission does not compute SO_2 emission factors, the emission ratio of 65 % is taken from Allemand et al. (2021) following scenario AME. Emissions present large reductions for both scenarios. They are particularly important for NO_x and NH_3, for which scenario 2030t induces even larger reductions, at 97 % and 96 % respectively. For PM, the decreases are limited to less than 40 % as the majority of the emissions come from non-exhaust sources, left identical in this study. Emissions of NO_x, VOCs and PM are speciated similarly to the local scale, i.e., taking into account the fraction of each vehicle type in the fleet.

Table 4.1: Emission ratios for the traffic sector for the two prospective scenarios between 2030 and 2014.

Scenario	CO	NO_x	NMVOCs	NH_3	PM	SO_2
2030r	0.48	0.35	0.40	0.77	0.66	0.65
2030t	0.33	0.03	0.33	0.04	0.61	0.65

4.2.3 Impacts on total emissions

Following the work presented in Section 3.2, a subset of the regional domain, corresponding to the city of Paris and its outlying suburbs, named Paris suburbs, is extracted to study the prospective scenarios' impacts on emissions where urbanization and transportation are most prominent.

Table 4.1 presents the reductions in total emissions induced by scenarios 2030r and 2030t at regional scale. Both scenarios lead to significant emission reductions. Emissions of NO and BC are reduced by around 58 %. Gas-phase I/SVOCs and NO_2 emissions are the most reduced, at 75 % and 80 % respectively. The further reductions in traffic emissions from scenario 2030t induce larger reductions in total emissions compared to scenario 2030r. The additional reduction for BC is only 5 % as traffic is not the preponderant emitting sector at this scale and PM emission factors are not reduced for very-low-emission vehicles (Table 4.1). For gas-phase I/SVOCs, the additional reduction is around 10 %. Nitrogen oxides present the largest additional reductions. It is at almost 20 % for NO_2, 25 % for NO_x and 30 % for NO. The total reductions are at 87 %, 89 % and 96 % for NO, NO_x and NO_2 respectively.

Table 4.2 presents the reductions in traffic emissions induced by scenarios 2030r and 2030t at local scale. As at the regional scale, both scenarios lead to significant emission reductions. Overall, reductions are larger at the local scale, except in scenario 2030r for NO_2 and gas-phase IVOCs. Reductions in NO_2 emissions are at 80 % against 68 %, for gas-phase I/SVOCs, it is 75 % against 62 %. This is due to the emission reductions applied to all activity sectors at the regional scale. For other pollutants, the reductions are around 65 %, except for BC, which presents a larger reduction at 72 %. Reductions observed in scenario 2030r are only due to the replacement of the oldest vehicles

Table 4.1: Reductions in total emissions for the two prospective scenarios compared to the baseline simulation for the Paris suburbs area. Average emissions are expressed in ng m^{-2} s^{-1}, and the relative differences in %.

	Average	Relative difference	
	2014r	2030r	2030f
NO	380.1	-57.4	-87.1
NO_2	184.9	-79.6	-96.2
NO_x	767.8	-62.7	-89.2
BC	9.2	-58.3	-63.1
$I/SVOCs_{gas}$	53.1	-74.6	-82.2

by new ones, with lower emissions. Reductions from scenario 2030t are larger than the ones from scenario 2030r. This is expected as only the most recent vehicles, i.e. with the lowest emissions, are considered. The additional reductions induced by scenario 2030t are limited to about 10 % for BC and gas-phase I/SVOC emissions. For the nitrogen oxides, the additional reductions are superior to 30 %, with total reductions at 97 %, 98 % to 99.5 % for NO, NO_x and NO_2 respectively.

Table 4.2: Reductions in traffic emissions for the two prospective scenarios compared to the baseline simulation at local scale. Average emissions are expressed in µg s^{-1}, and the relative differences in %.

	Average	Relative difference	
	2014r	2030r	2030t
NO	2727.7	-62.9	-96.5
NO_2	2067.3	-67.7	-99.5
NO_x	6249.8	-64.6	-97.5
BC	90.1	-71.6	-79.0
$I/SVOCs_{gas}$	192.3	-62.3	-71.1

The absolute differences in emissions of NO_2 and BC over the whole simulation domain for scenario 2030r are presented in Figure 4.1. For scenario 2030t, absolute differences present similar behaviors, with larger values. They are available in Appendix 4.B. Absolute differences are used here instead of relative differences because emissions in rural areas of the domain are extremely low, resulting in an explosion of the relative differences in these areas. Urban areas of the domain, i.e. the city of Paris and its outlying suburbs, are the most affected, with reductions up to 0.4 µg m^{-2} s^{-1} and 0.015 µg m^{-2} s^{-1} for NO_2 and BC emissions. In scenario 2030t, emissions of NO_2 and BC are reduced by up to 0.45 µg m^{-2} s^{-1} and 0.015 µg m^{-2} s^{-1} respectively.

Figure 4.2 presents the relative differences in emissions of NO_2 and BC over the street network for scenario 2030r. For scenario 2030t, relative differences present similar behaviors, with larger values. They are available in Appendix 4.B. Emissions in the streets with high traffic circulation are greatly reduced. NO_2 and BC emissions are reduced up by to 70 % and 75 % respectively. In scenario 2030t, emissions of NO_2 and BC are reduced up by to 90 % and 85 % respectively. On the contrary, streets with no traffic circulation are not affected.

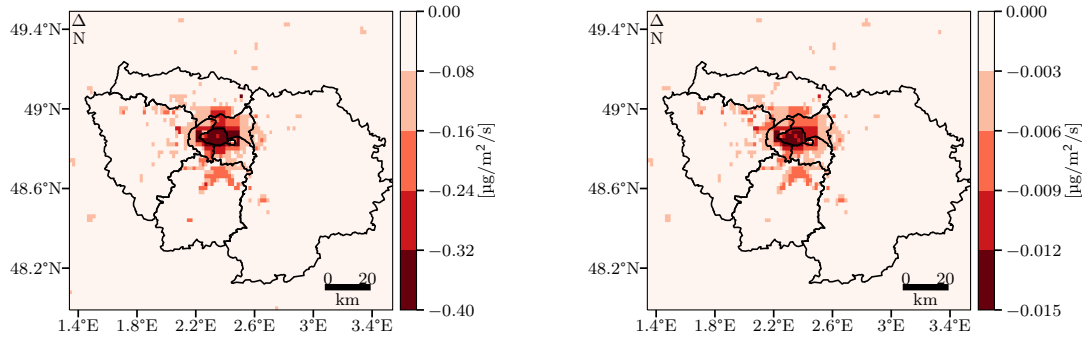

(a) **(b)**

Figure 4.1: Absolute differences (in $\mu g\,m^{-2}\,s^{-1}$) in emissions of NO_2 (a) and BC (b) at the regional scale for scenario 2030r. For information, the annual mean emissions for the baseline simulation are available in Appendix 4.B.

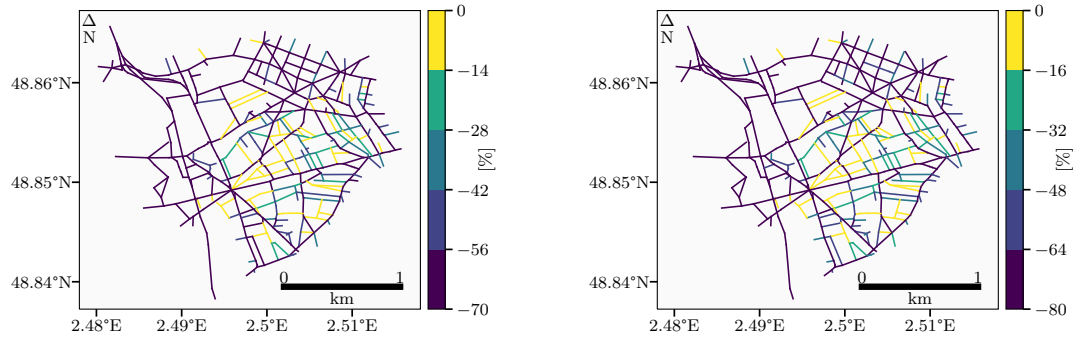

(a) **(b)**

Figure 4.2: Relative differences (in %) in emissions of NO_2 (a) and BC (b) at the local scale for scenario 2030r. For information, the annual mean emissions for the baseline simulation are available in Appendix 4.B.

4.3 Impacts on concentrations

This section presents the impacts of the scenarios on concentrations at both the regional and local scales. Evaluation of the multiscale modeling chain against observations for the baseline simulation, 2014b, is available in Section 3.2.2.3. As for emissions and the work presented in Section 3.2, impacts at the regional scale are studied on a subset of the domain corresponding to Paris city and its suburbs, and also to Paris city alone for the impacts on dense traffic areas. Furthermore, the concentrations presented at the regional scale are surface concentrations, i.e., they correspond to those simulated in the first vertical level of the domain (from 0 m to 30 m).

4.3.1 Modelling tools

Polair3D is used to simulate background concentrations on the regional domain with a horizontal resolution of 0.02°x0.02°. Concentrations in the streets of the network are simulated with MUNICH. The simulation periods are from 8 January to 27 December 2014 for the regional scale, and 10 January to 27 December 2014 for the local scale. Both models are coupled to SSH-aerosol to take into account gas-phase chemistry and aerosol dynamics.

Boundary and initial conditions are taken from Sartelet et al. (2018). Meteorological conditions are modeled using the WRF model (version 3.9.1.1), as detailed in Lugon et al. (2020). Boundary, initial conditions and meteorology are kept the same in the reference and in the prospective scenarios.

4.3.2 Regulated pollutants

This section presents the concentration levels of NO_2, PM_{10} and $PM_{2.5}$. The concentration levels of these pollutants are regulated by the European air quality directives (Table 1.1). The annual average limits are 40 µg m^{-3} for NO_2 and PM_{10}, and 25 µg m^{-3} for $PM_{2.5}$. In its air quality guidelines, WHO proposes more stringent annual average limits, 10 µg m^{-3} for NO_2, 15 µg m^{-3} for PM_{10} and 5 µg m^{-3} for $PM_{2.5}$.

Table 4.1 presents the average concentrations and relative differences for the two prospective scenarios compared to the baseline simulation for NO_2, PM_{10} and $PM_{2.5}$. The emission reductions induced by the two prospective scenarios are reflected in the concentrations at both regional and local scales. For the three pollutants, but particularly NO_2, the average concentrations are lower when considering the Paris suburbs area than with the Paris city area and the local scale (28 µg m^{-3} against 46 µg m^{-3} and 50 µg m^{-3} respectively). This is due to the Paris suburbs area including districts less urbanized than the city itself, and its larger footprint on the domain increases the influence of the other activity sectors, with emissions not as reduced as traffic emissions (Tables 4.1 and 4.1).

Table 4.1: Impacts of the prospective scenarios on regulated pollutant concentrations over the Paris suburbs and Paris city areas, and at the local scale. Average concentrations are expressed in µg m^{-3} and relative differences in %.

NO_2		2014b	2030r	2030t
Polair3D Paris suburbs	Average	28.2	14.3	7.7
	Relative difference	-	-49.8	-72.6
Polair3D Paris city	Average	45.8	24.6	13.7
	Relative difference	-	-46.5	-70.2
MUNICH	Average	49.9	23.4	9.6
	Relative difference	-	-52.5	-79.4
PM_{10}		2014b	2030r	2030t
Polair3D Paris suburbs	Average	16.6	14.6	14.3
	Relative difference	-	-11.4	-13.7
Polair3D Paris city	Average	19.8	16.3	15.7
	Relative difference	-	-17.8	-20.5
MUNICH	Average	20.1	16.3	15.7
	Relative difference	-	-17.9	-20.9
$PM_{2.5}$		2014b	2030r	2030t
Polair3D Paris suburbs	Average	15.5	13.7	13.3
	Relative difference	-	-11.6	-14.0
Polair3D Paris city	Average	18.1	14.8	14.2
	Relative difference	-	-18.4	-21.3
MUNICH	Average	18.7	15.1	14.4
	Relative difference	-	-18.6	-21.9

For NO_2, the emission reductions of 80 % and 96 % observed for scenarios 2030r and 2030t

respectively for the Paris suburbs area lead to reductions in concentrations by 50 % and 73 %. Paris city area presents slightly lower reductions, at 47 % and 70 % respectively, but with higher absolute concentrations, e.g. 25 µg m^{-3} versus 14 µg m^{-3} for scenario 2030r. At the local scale, concentration reductions are more important at 53 % and 79 % for scenarios 2030r and 2030t respectively, thanks to the predominance of the traffic and larger emission reductions for both scenarios, at 68 % and 99.5 %. When these concentrations for year 2030 are compared to the WHO guideline of 10 µg m^{-3} for NO_2, only scenario 2030t presents an annual average concentration slightly lower at the local scale, of 9.6 µg m^{-3}. The average concentration of 7.7 µg m^{-3} observed for the Paris suburbs area is also lower than the guideline, but this is due to the inability of regional-scale simulations to represent the higher concentrations observed in streets. However, the less strict limit value of 40 µg m^{-3} imposed by the European air quality directives is respected in the two prospective scenarios.

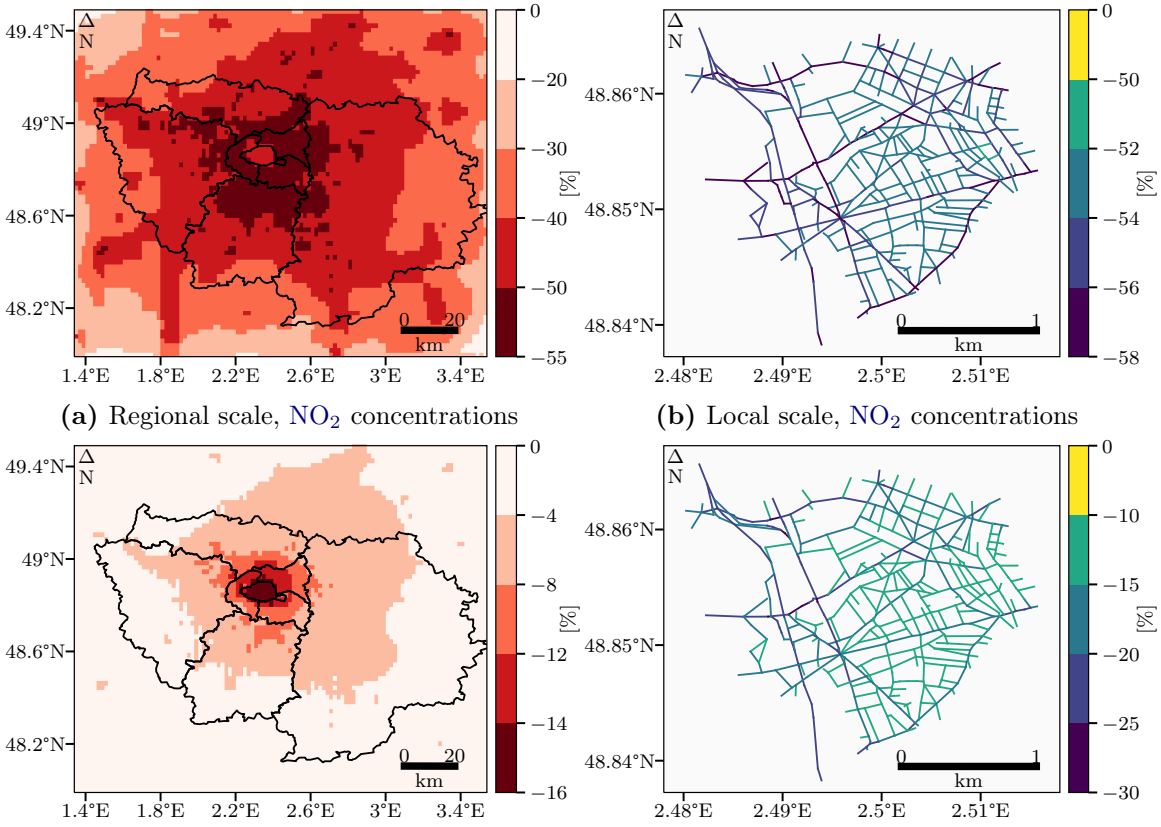

(a) Regional scale, NO_2 concentrations

(b) Local scale, NO_2 concentrations

(c) Regional scale, PM_{10} concentrations

(d) Local scale, PM_{10} concentrations

Figure 4.1: Relative differences in concentrations of NO_2 (top panels) and PM_{10} (bottom panels) for scenario 2030r at the regional scale (left panel) and local scale (right panel). For information, the relative differences for scenario 2030t and the annual average concentrations for the baseline simulation are available in Appendix 4.C.

As expected since PM emissions are less reduced, concentrations of PM_{10} and $PM_{2.5}$ are much less impacted than NO_2 concentrations. The Paris suburbs area presents reductions of PM_{10} concentrations of 11 % and 14 % for the scenarios 2030r and 2030t respectively, while reductions are at 18 % and 21 % for the Paris city area and the local scale. $PM_{2.5}$ concentrations are slightly more important, reaching 19 % and 22 % at local scale. Concentrations of PM_{10} at the local scale for both scenarios are just above the WHO guideline of 15 µg m^{-3}, at 16 µg m^{-3} for both scenarios.

For $PM_{2.5}$, concentrations remain superior to the WHO guideline of $5\,\mu g\,m^{-3}$, at $15.1\,\mu g\,m^{-3}$ and $14.4\,\mu g\,m^{-3}$ respectively. When considering the limit values imposed by the European air quality directives for PM_{10} ($40\,\mu g\,m^{-3}$) and $PM_{2.5}$ ($25\,\mu g\,m^{-3}$), concentrations of the baseline simulation 2014b are already in accordance, at $20\,\mu g\,m^{-3}$ and $19\,\mu g\,m^{-3}$ respectively. With exhaust emissions of PM already well regulated and controlled, the focus should be to better understand and reduce non-exhaust emissions from tire and brake wear, and road abrasion to respect the more stringent WHO guidelines.

The impacts of the scenario 2030r on the concentrations of NO_2 and PM_{10} on the regional domain and the street network are presented in Figure 4.1. The impacts are similar in the scenario 2030t with more extreme values. They are available in Appendix 4.C. The figure for NO_2 at the regional scale displays important concentration reductions throughout the domain, with the highest reductions for the most urbanized areas. PM_{10} concentration reductions are much more limited outside the city of Paris and its suburbs. The reductions go up to 55 % and 16 % for NO_2 and PM_{10} respectively. At the local scale, concentrations reductions are larger than at the regional scale, particularly for streets with high traffic circulation. These reductions reach 58 % and 30 % for NO_2 and PM_{10} respectively.

Scenario 2030r can also be compared to scenario 2-BAU from Lugon et al. (2022). This scenario "business-as-usual" simulates concentrations for 2024 with fleet evolution (promotion of Euro 5 and Euro 6 diesel vehicles) from 2014 to 2024. The introduction of the very-low-emission vehicles in the fleet in scenario 2030r induces a larger reduction of the concentrations of NO_2 compared to scenario 2-BAU, 53 % to 38 %. However, for PM_{10}, the reduction is slightly more important in scenario 2-BAU, 22 % against 18 %. Reductions for $PM_{2.5}$ as very similar, at 19 %, in both scenarios. These differences on PM could be due to the different street networks considered. In scenario 2-BAU, MUNICH represents the concentrations over the city of Paris, while, in this study, it represents a district in the eastern suburbs of Paris. The city of Paris is much more urbanized and the influence of traffic is thus greater.

4.3.3 Non-regulated pollutants

As presented in Section 1.1.2.2, BC and OM are known to have negative effects on the human health. The impacts of the prospective scenarios on BC and OM concentrations are thus presented in Table 4.1. The reductions for these two pollutants are larger than the ones for PM_{10} and $PM_{2.5}$. The BC emission reduction of 58 % at the regional scale for scenario 2030r induces reductions of BC concentrations by 30 % and 35 % for the Paris suburbs and Paris city areas. For the scenario 2030t, the emission reduction of 63 % induces slightly larger concentration reductions, by 32 % and 38 % respectively. At the local scale, reductions in BC concentrations reach 42 % and 45 % for the scenarios 2030r and 2030t. Concerning the OM concentrations, the differences in reduction between the two scenarios are limited to 2 % maximum. On the Paris suburbs area, reductions are around 17.5 %, while they are almost the double for the Paris city area, around 31 %. At the local scale, concentration levels and reductions are very similar to the Paris city area, with $4\,\mu g\,m^{-3}$ and around 31 % of reduction.

Impacts of the scenario 2030r on the concentrations of BC and OM on the regional domain and the street network are presented in Figure 4.1. The impacts of the scenario 2030t are similar with more extreme values. They are available in Appendix 4.C. BC and OM concentrations at the regional scale display similar behaviors to BC emissions (Figure 4.1). The most significant reductions take place on the most urbanized areas while rural areas are less impacted. As for NO_2, the impact of keeping the boundary conditions identical are visible on the limits of the domain. The reductions reach 35 % and 25 % for BC and OM respectively. At the local scale, concentration reductions are

Table 4.1: Impacts of the prospective scenarios on non-regulated pollutant concentrations over the Paris suburbs and Paris city areas, and at the local scale. Average concentrations are expressed in $\mu g\,m^{-3}$ and relative differences in %.

	BC	2014b	2030r	2030t
Polair3D	Average	0.7	0.5	0.5
Paris suburbs	Relative difference	-	-29.9	-32.1
Polair3D	Average	1.1	0.7	0.7
Paris city	Relative difference	-	-35.0	-37.7
MUNICH	Average	1.5	0.8	0.7
	Relative difference	-	-41.5	-45.2
	OM	2014b	2030r	2030t
Polair3D	Average	4.6	3.8	3.8
Paris suburbs	Relative difference	-	-17.1	-17.7
Polair3D	Average	5.9	4.1	4.0
Paris city	Relative difference	-	-30.1	-31.5
MUNICH	Average	5.9	4.1	3.9
	Relative difference	-	-30.1	-32.1

overall larger than at the regional scale, except for streets with low to no traffic circulation. On the opposite, streets with high traffic circulation present the highest reductions, up to 60 % for BC and 40 % for OM.

When compared to scenario 2-BAU from Lugon et al. (2022), the reduction of the BC concentrations in scenario 2030r is lower, at 42 % against 48 %. As for PM, this difference can be linked to the different street networks and greater influence of traffic in scenario 2-BAU, but also to the higher tire-wear emissions considered in Lugon et al. (2022). The influence of the background concentrations, with emission reductions from all the activity sectors, on OM concentrations in scenario 2030r leads to a larger reduction than in scenario 2-BAU, at 30 % against 24 %.

4.4 Conclusions

Air quality for the year 2030 has been modeled with two prospective scenarios, taking into account the introduction of very-low-emission vehicles in the fleet. Emission factors for these vehicles were defined based on the development of technologies, such as afterburners, to reduce cold-start emissions in particular, and they are lower than those postulated for the forthcoming European emission standard Euro 7. The evolution of the fleet composition was modeled to replace the older vehicles by more recent, and less polluting, vehicles. Reductions of the emissions for all activity sectors were considered to generate background concentrations consistent with the simulated year.

In the first scenario, representative of a gradual evolution of the fleet, NO_2 emissions are reduced by 80 % and 68 % at the regional and local scales respectively. However, the impacts on the concentrations are limited to 53 % at the local scale. Concentrations of PM_{10} and $PM_{2.5}$ are reduced only by 18 % at both scales, as traffic exhaust emissions are not the main source of PM. When looking into the concentrations of BC and OM, reductions are larger, up to 42 % and 30 % respectively on average at the local scale. Despite these reductions, concentration levels are still superior to the WHO guidelines, particularly for $PM_{2.5}$, while satisfying the less stringent European air quality directives.

The second scenario, composed only of very-low-emission and electric vehicles, presents larger

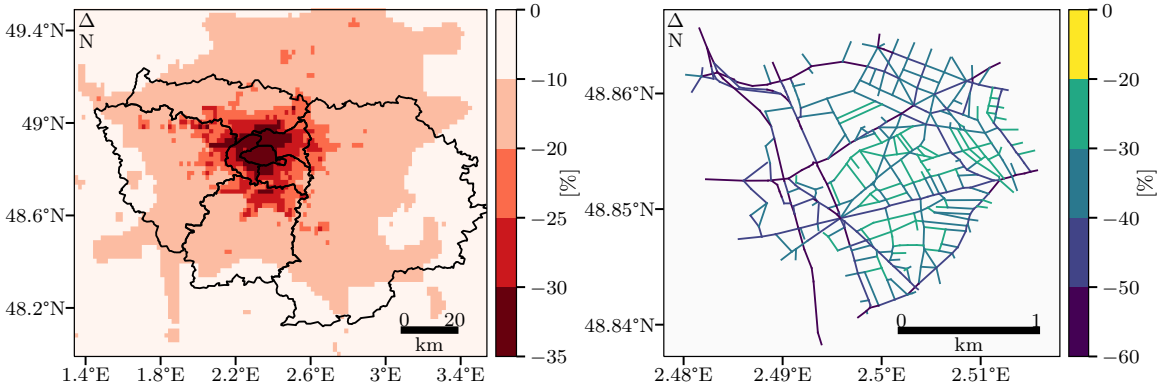

(a) Regional scale, BC concentrations

(b) Local scale, BC concentrations

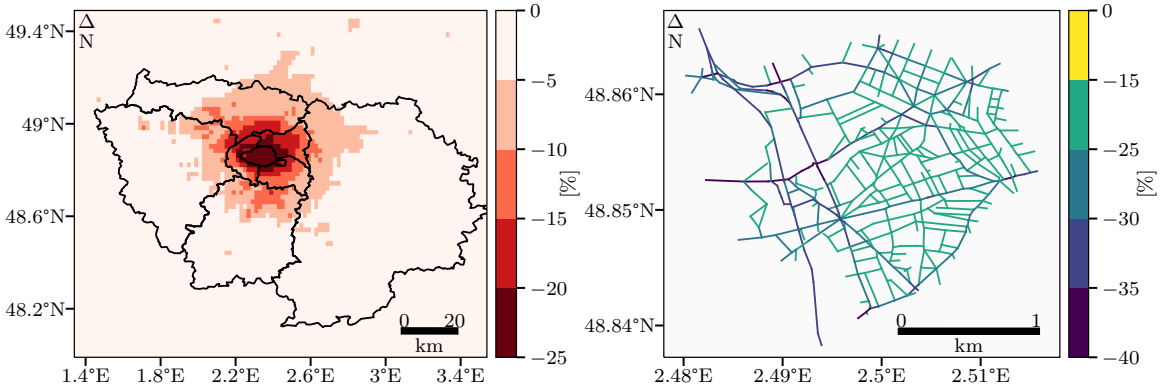

(c) Regional scale, OM concentrations

(d) Local scale, OM concentrations

Figure 4.1: Relative differences in concentrations of BC (top panels) and OM (bottom panels) for the scenario 2030r at the regional scale (left panel) and local scale (right panel). For more information, the relative differences for the scenario 2030t and the annual average concentrations for the baseline simulation are available in Appendix 4.C.

reductions than the first scenario for all pollutants. NO_2 and BC emissions are reduced by up to 99.5 % and 79 %. The NO_2 concentrations at the local-scale thus decrease by almost 80 %, allowing the WHO guidelines to be met (9.6 µg m^{-3} for 10 µg m^{-3}). However, concentrations of PM_{10} and $PM_{2.5}$ are less impacted (-22 % at the local scale) and do not meet the guidelines. BC and OM concentrations are slightly more impacted than PM, with a reduction of 45 % and 32 % respectively.

This study shows that the development of new vehicles, with more efficient technologies to reduce exhaust emissions, is important for improving air quality in streets. Considering only the evolution of the exhaust emissions in this study induced large reductions of the concentrations of NO_2 while having a limited impact on PM concentrations. The focus should now be to study the importance of the non-exhaust emissions (tire and brake wear, and road abrasion) to reduce PM emissions from traffic.

Appendices

4.A Fleet evolution with prospective scenarios

Table 4.A.1: Distribution of HDTs, buses and Lcat in fleets according to European emission standards and for electric vehicles, in %.

		2014b	2030r	2030t
HDTs	Pre-Euro	0.2	-	-
	Euro II	10.9	-	-
	Euro III	26.0	1.2	-
	Euro IV	21.9	4.3	-
	Euro V	34.8	10.1	-
	Euro VI A/B/C	5.8	21.1	-
	Euro VI D/E	-	28.3	-
	VLEV[a]	-	26.7	91.7
	Electric	0.5	8.3	8.3
	Total	100	100	100
Bus	Pre-Euro	0.5	-	-
	Euro I	1.2	-	-
	Euro II	11.8	-	-
	Euro III	21.8	2.0	-
	Euro IV	15.4	6.3	-
	Euro V	40.8	11.8	-
	Euro VI A/B/C	7.8	19.4	-
	Euro VI D/E	-	27.0	-
	VLEV[a]	-	25.2	91.9
	EEV (CNG)	0.8	-	-
	Electric	0.0	8.1	8.1
	Total	100	100	100
Lcat	Pre-Euro	6.1	-	-
	Euro 1	7.5	-	-
	Euro 2	25.0	-	-
	Euro 3	61.4	0.1	-
	Euro 4	-	5.4	-
	Euro 5	-	46.8	-
	VLEV[a]	-	34.0	86.3
	Electric	-	13.7	13.7
	Total	100	100	100

[a] VLEV = Very-low-emission vehicles.

4.B Impacts of prospective scenarios on emissions

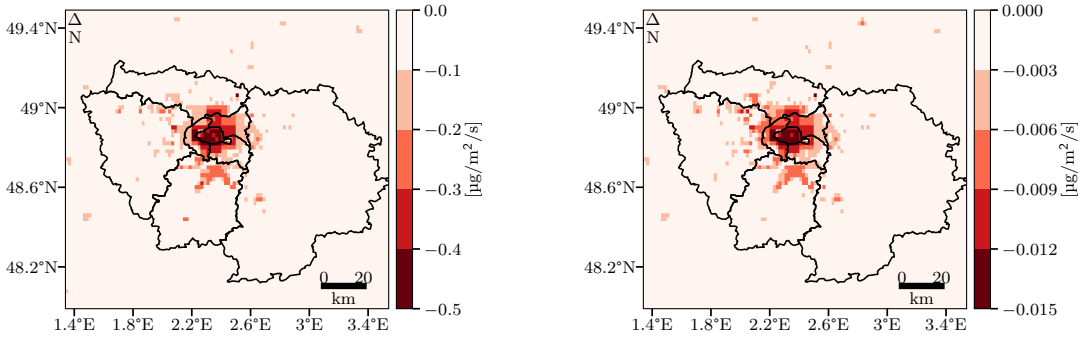

(a) **(b)**

Figure 4.B.1: Absolute differences (in $\mu g\,m^{-2}\,s^{-1}$) in emissions of NO_2 (a) and BC (b) at the regional scale for scenario 2030t.

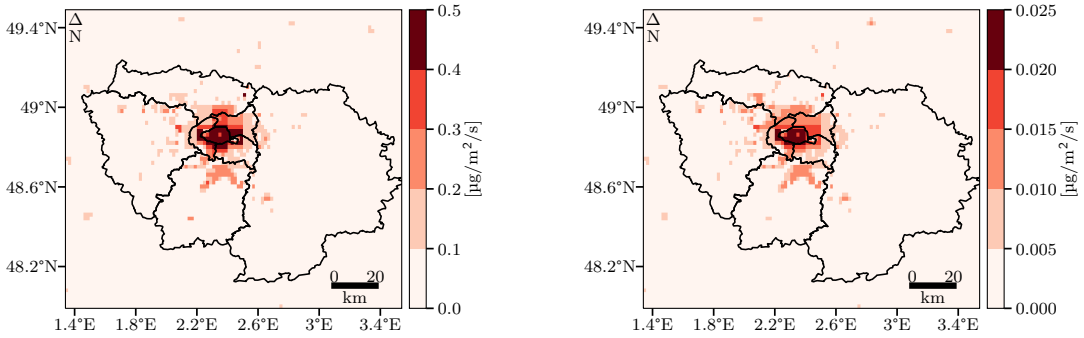

(a) **(b)**

Figure 4.B.2: Annual mean emissions (in $\mu g\,m^{-2}\,s^{-1}$) of NO_2 (a) and BC (b) at the regional scale for the baseline simulation 2014r.

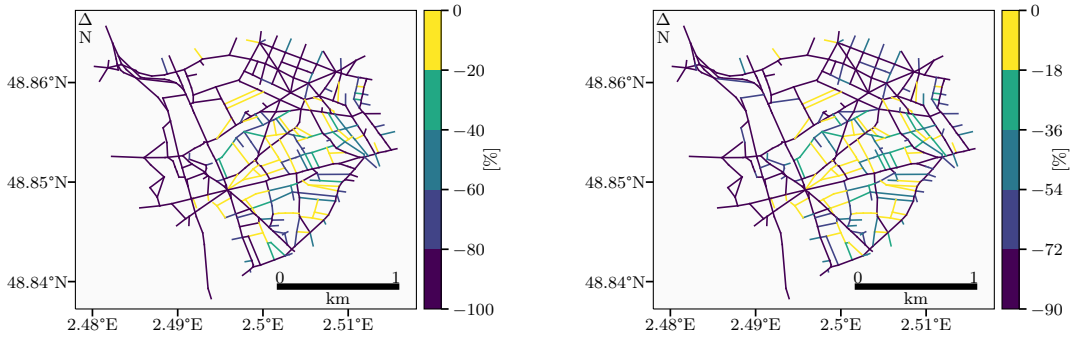

(a) **(b)**

Figure 4.B.3: Relative differences (in %) in emissions of NO_2 (a) and BC (b) at the local scale for scenario 2030t.

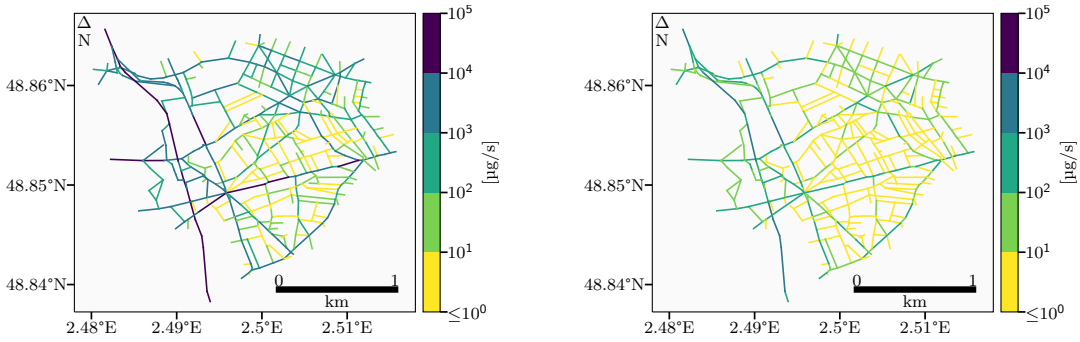

(a) **(b)**

Figure 4.B.4: Annual mean emissions (in $\mu g\,s^{-1}$) of NO_2 (a) and BC (b) at the local scale for the baseline simulation 2014r.

4.C Impacts of prospective scenarios on concentrations

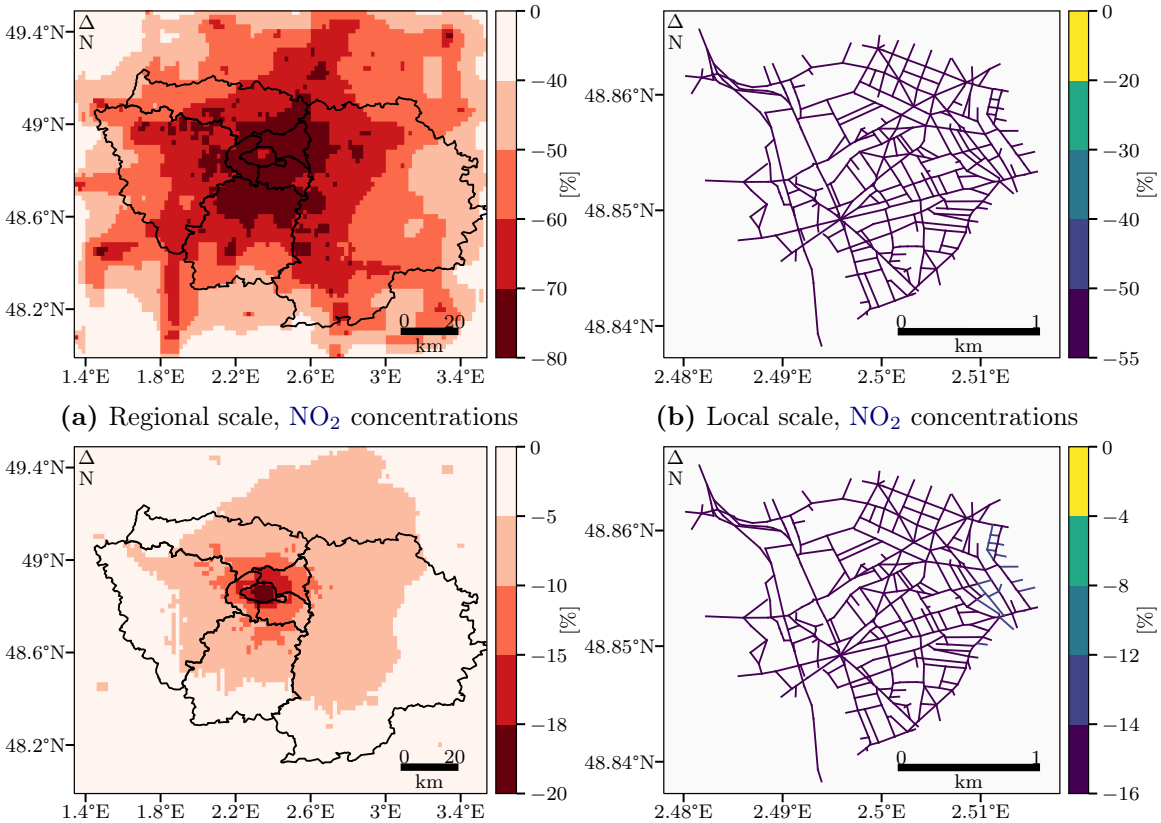

(a) Regional scale, NO_2 concentrations

(b) Local scale, NO_2 concentrations

(c) Regional scale, PM_{10} concentrations

(d) Local scale, PM_{10} concentrations

Figure 4.C.1: Relative differences in concentrations of NO_2 (top panels) and PM_{10} (bottom panels) for scenario 2030t at the regional scale (left panel) and local scale (right panel).

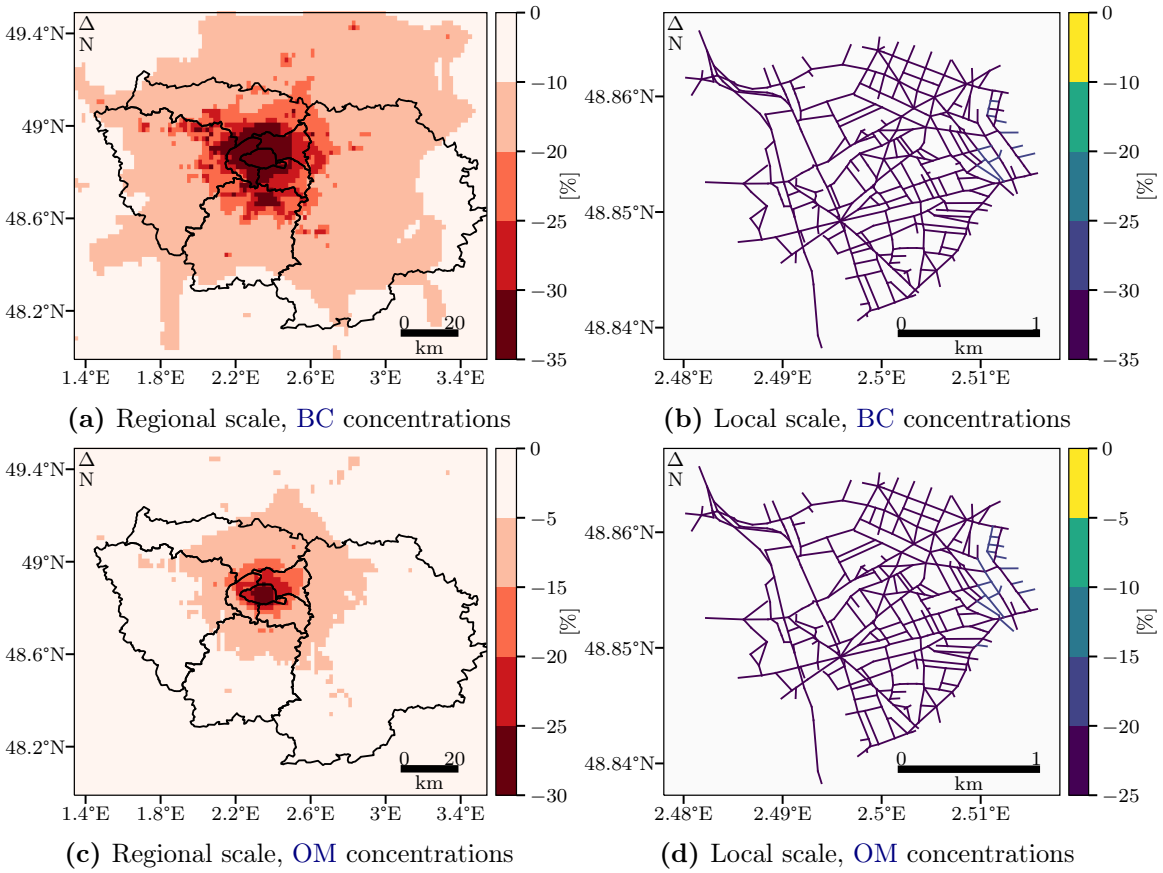

(a) Regional scale, BC concentrations

(b) Local scale, BC concentrations

(c) Regional scale, OM concentrations

(d) Local scale, OM concentrations

Figure 4.C.2: Relative differences in concentrations of BC (top panels) and OM (bottom panels) for scenario 2030t at the regional scale (left panel) and local scale (right panel).

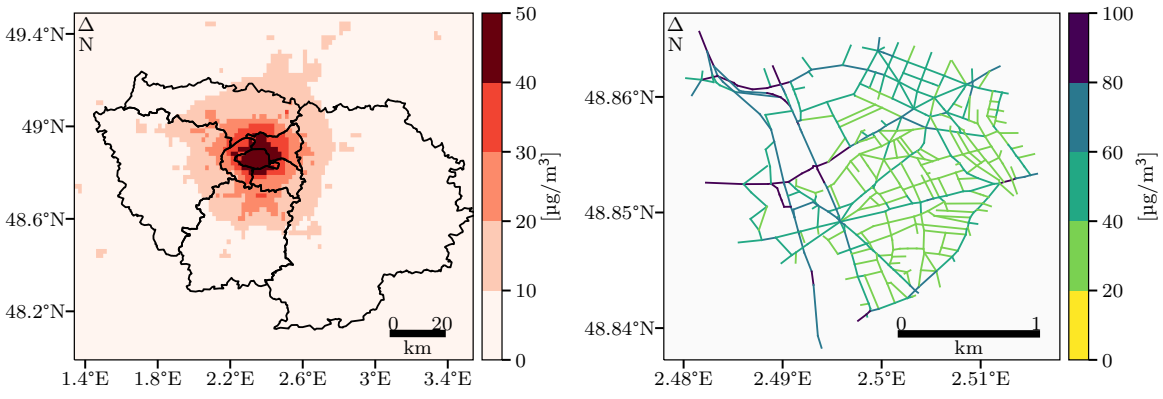

(a) 2014b, regional scale

(b) 2014b, local scale

Figure 4.C.3: Annual average concentrations of NO_2 for the baseline simulation 2014b at the regional scale (left panel) and local scale (right panel) in $\mu g\,m^{-3}$.

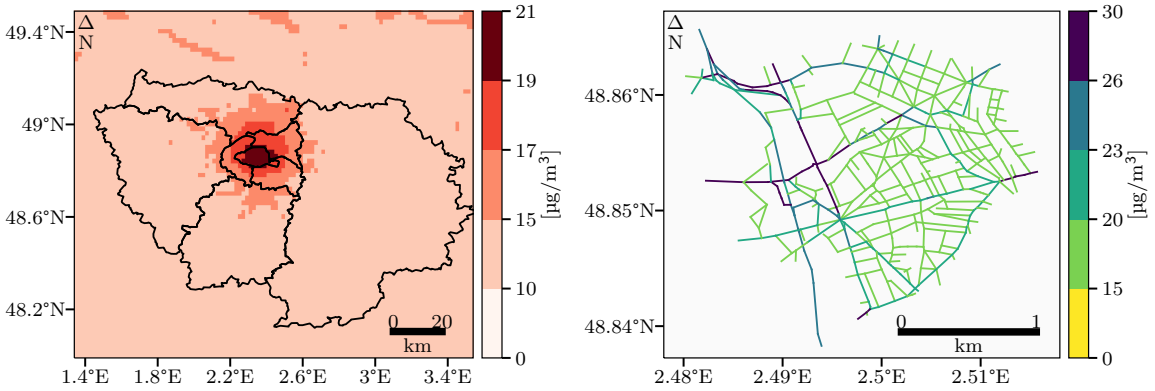

(a) 2014b, regional scale **(b)** 2014b, local scale

Figure 4.C.4: Annual average concentrations of PM_{10} for the baseline simulation 2014b at the regional scale (left panel) and local scale (right panel) in $\mu g\,m^{-3}$.

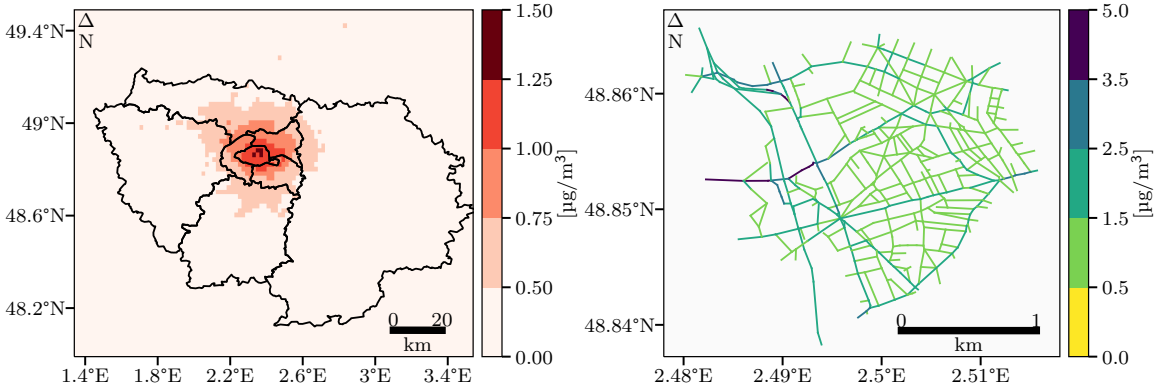

(a) 2014b, regional scale **(b)** 2014b, local scale

Figure 4.C.5: Annual average concentrations of BC for the baseline simulation 2014b at the regional scale (left panel) and local scale (right panel) in $\mu g\,m^{-3}$.

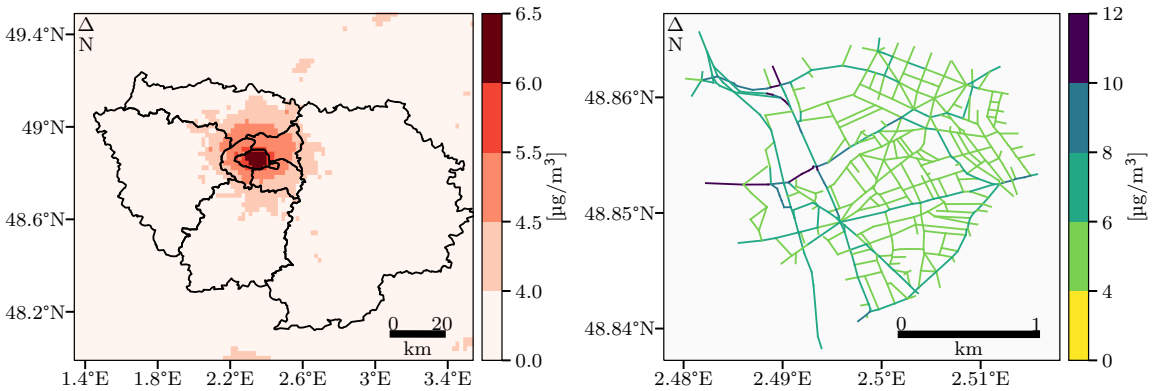

(a) 2014b, regional scale **(b)** 2014b, local scale

Figure 4.C.6: Annual average concentrations of OM for the baseline simulation 2014b at the regional scale (left panel) and local scale (right panel) in $\mu g\,m^{-3}$.

Chapter 5

Modelling concentration heterogeneities in streets using the street-network model MUNICH

Contents

Populations in urban areas are exposed to high local concentrations of pollutants, such as nitrogen dioxide and particulate matter, because of unfavorable dispersion conditions and the proximity to traffic. To simulate these concentrations over cities, models like the street-network model MUNICH rely on parameterizations to represent the air flow and the concentrations of pollutants in streets. In the current version MUNICH v2.0, concentrations are assumed to be homogeneous in each street segment. A new version of MUNICH where the street volume is discretized is developed to represent the street gradients and better estimate people exposure. Three vertical levels are defined in each street segment. A horizontal discretization is also introduced under specific conditions by considering

two zones with a parameterization taken from OSPM. Simulations are performed over two districts of Copenhagen, Denmark, and one district of Greater Paris, France. Results show an improvement of the comparison to observations with higher concentrations at the bottom of the street, closer to traffic, of pollutants emitted by traffic (NO_x, BC, OM). These increases reach up to 60 % for NO_2 and 30 % for PM_{10} comparatively to MUNICH v2.0. The aspect ratio (ratio between building height and street width) influences the extent of the increase of the first-level concentrations compared to the average of the street. The increase is higher for wide streets (low aspect ratio and often higher traffic), by up to 53 % for NO_x and 18 % for PM_{10}. Finally, a sensitivity analysis to the influence of the street network highlights the importance to use the model MUNICH with a network rather than with a single street.

This article is currently under review for publication in the special issue *Air quality research at street level – Part II* from the journal *Geoscientific Model Development* (Sarica et al. 2023a).

5.1 Introduction

Pollution is estimated to be responsible for approximately 9 million premature deaths in 2015 (Landrigan et al. 2018). This figure remains valid in 2019 despite an improvement of the types of pollution associated with extreme poverty (e.g., household air pollution and water pollution) (Fuller et al. 2022). This is partly due to an increase in the number of premature deaths attributable to ambient air pollution. The consequences of air pollution are particularly substantial in urban areas, where individuals are exposed to local high concentrations of air pollutants due to unfavorable dispersion conditions and proximity to traffic. As more than half of the world's population already lives in urban areas, rising to 68 % by 2050 (United Nations 2019), it is crucial to estimate as accurately as possible the exposure of population to atmospheric pollutant concentrations in urban areas. For many years, various modelling approaches have been developed to contribute to the understanding of the phenomena that drive the concentrations of pollutants in the atmosphere and to provide decision support tools (Collett et al. 1997; Vardoulakis et al. 2003; El-Harbawi 2013; Conti et al. 2017; Khan et al. 2021).

Regional-scale chemistry-transport models, such as Polair3D (Mallet et al. 2007; Sartelet et al. 2018), CHIMERE (Menut et al. 2021; Falasca et al. 2018), CMAQ (Wong et al. 2012; Paz et al. 2015), represent the urban background concentrations by solving the chemistry-transport equation for spatial resolutions down to 1 km^2. However, they can not represent street concentrations, which are often higher than background concentrations for pollutants such as NO_2 and particles (Lugon et al. 2020). To represent these concentrations, local-scale models are thus developed with different approaches of variable complexity and computational cost. Models based on CFD, such as code_saturne (Archambeau et al. 2004; Gao et al. 2018), OpenFoam (Lin et al. 2022) and PALM (Wolf et al. 2020), are able to represent the dispersion of pollutants and the physicochemical processes taking place in urban districts and streets with a fine spatial resolution by solving the Navier-Stokes equations and mass conservation equations for pollutants. However, they suffer from high computational cost, as they use fine meshes to describe the morphology of buildings and streets. Other models use approaches that are less accurate than CFD but run faster. They are typically based on a Gaussian or an Eulerian approach (Vardoulakis et al. 2003; Liang et al. 2023). Among these, can be mentioned ADMS-Urban (McHugh et al. 1997; Hood et al. 2021), SIRANE (Soulhac et al. 2011, 2023), AERMOD (Cimorelli et al. 2004; Rood 2014), EPISODE (Karl et al. 2019) and CALIOPE-Urban (Benavides et al. 2019). They either consider each street independently of the others with exchanges between the street and the background concentrations above the street (Berkowicz 2000b), or a street network

with incoming/outcoming flows between streets at intersections (Soulhac et al. 2009; Kim et al. 2022). OSPM couples a Gaussian-plume model for traffic emissions and a box model for the recirculation in the street (Berkowicz 2000b). It is thus able to represent concentration heterogeneities in the street, but cannot include complex chemistry. MUNICH uses solely an Eulerian box-model approach (Lugon et al. 2020). As MUNICH is coupled with the SSH-aerosol model (Sartelet et al. 2020), the formation and aging of primary and secondary gas and particles in streets are represented. In the current version of MUNICH (v2.0) (Kim et al. 2022), concentrations are considered homogeneous in each street segment. However, as shown by several on-site and modelling studies, the concentrations are very heterogeneous in streets with traffic emissions (Xie et al. 2003; Vardoulakis et al. 2011; Lateb et al. 2016; Sanchez et al. 2016; Amato et al. 2019; Lin et al. 2022). They are higher near the ground than at the top of the street, especially for primary pollutants.

A "heterogeneous" version of MUNICH is developed in this study aiming to represent the concentration heterogeneities in the street, while keeping the Eulerian approach of MUNICH to retain the ability to accurately model chemistry and aerosol dynamics. The street volume is discretized vertically in three subvolumes. Traffic emissions are not instantaneously diluted in the whole street volume as in MUNICH v2.0, but only in the first subvolume, i.e. the one closest to the ground. With this discretization we do not aim to reproduce finely the vertical profile of concentrations. The main objective is to improve the representation of concentrations close to the ground by avoiding the excessive dilution associated with the homogeneity assumption. To represent the street horizontal heterogeneities, a recirculation zone of the shape of a trapeze is defined, based on a parameterization of OSPM. It depends on the meteorological conditions and the street morphology, and it is applied under specific conditions in MUNICH that are described later.

A description of the differences between the homogeneous version of MUNICH (v2.0) and the new heterogeneous version is presented in Section 5.2. The applications to two street networks in Copenhagen, Denmark, with comparisons to observations of NO_2 and CO, and to concentrations simulated by OSPM are discussed in Section 5.3. MUNICH is applied in Section 5.4 to the street network near Paris, France, used to validate MUNICH v2.0 (Kim et al. 2022), and the impacts of the heterogeneous version on concentrations of NO_2 and particles are studied. To estimate the impact of the modelling hypothesis on the transport of pollutants between streets in the new version of MUNICH, a sensitivity analysis to the presence of a street network is performed in Section 5.5.

5.2 Model description

The homogeneous version of MUNICH (v2.0) and the new heterogeneous version (see Figure 5.1) are briefly described in this section, focusing on the differences between the two versions. The heterogeneous version was developed from MUNICH v2.0. In the following, the homogeneous and heterogeneous versions of MUNICH are referred to as MUNICH-homo and MUNICH-hete respectively. For a complete description of MUNICH, please refer to Section 1.2.2 and Kim et al. (2018, 2022); Lugon et al. (2020, 2021a).

In order to solve the evolution equation of the street concentrations C_{str}, a first-order operator splitting between transport and chemistry is performed:

$$\frac{\mathrm{d}C_{\text{str}}}{\mathrm{d}t} = \left.\frac{\mathrm{d}C_{\text{str}}}{\mathrm{d}t}\right|_{\text{tr}} + \left.\frac{\mathrm{d}C_{\text{str}}}{\mathrm{d}t}\right|_{\text{ch}} \tag{5.1}$$

The transport term includes advection from one street to another and vertical transport between the street and the background above it. The chemistry includes gas-phase chemistry, as well as aerosol dynamics (coagulation, condensation/evaporation). As deposition and resuspension processes

have minor effects compared to transport and chemistry (Lugon et al. 2021b; Kim et al. 2022), they are omitted in the rest of this study.

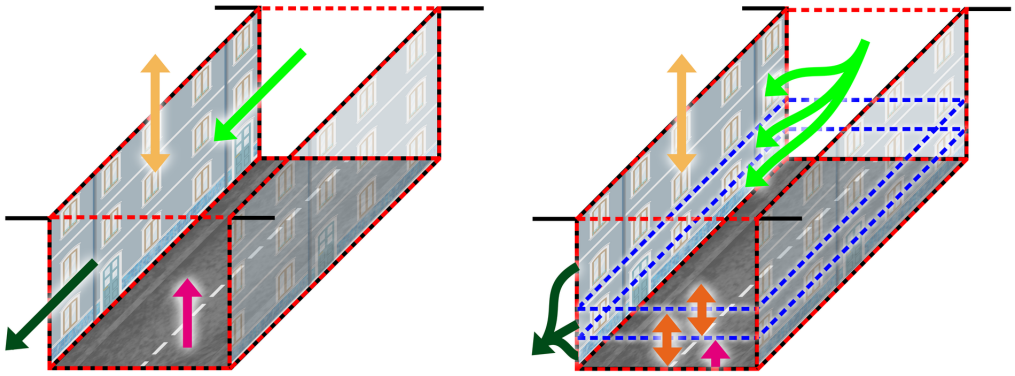

Figure 5.1: Representation of the processes in the homogeneous version (a) and the heterogeneous version (b) of MUNICH. The red dotted lines represent the street volume. In (a), the street canopy is represented by a single volume, whereas in (b), it is divided into 3 subvolumes delimited by the blue dotted lines. The rose arrows represent the traffic emissions (including brake, tyre and road wear), the light green arrows the fluxes entering the street via the upwind intersection and the dark green arrows the fluxes leaving the street via the downwind intersection. The yellow arrows symbolize the vertical turbulent exchanges with the background and, in (b), the orange arrows the vertical exchanges among the subvolumes.

5.2.1 Homogeneous approach

Using a box-model approach, the concentrations are assumed to be homogeneous in the whole street volume and the effect of the processes on the concentrations are represented by the equation:

$$\left.\frac{\mathrm{d}C_{\mathrm{str}}}{\mathrm{d}t}\right|_{\mathrm{tr}} = \frac{1}{V}\left(Q_{\mathrm{em}} + Q_{\mathrm{inflow}} + Q_{\mathrm{outflow}} + Q_{\mathrm{vert}}\right) \tag{5.1}$$

with V the volume of the rectangular cuboid street, Q_{em} the traffic emission flux, Q_{inflow} the flux entering the street via the upwind intersection, Q_{outflow} the flux leaving the street via the downwind intersection and Q_{vert} the vertical turbulent flux between the background and the street.

The street volume is defined as $V = HWL$, with H the average building height over the street segment, W the mean street width and L its length. MUNICH considers that buildings on each side of the street are continuous, thus not representing inflow/outflow that could be induced by gaps in the buildings. The inflow term Q_{inflow} is obtained from the computation of the fluxes at the upwind intersection (Kim et al. 2018; Soulhac et al. 2009) (see Section 5.5 for a brief description). The outflow term Q_{outflow} is expressed as :

$$Q_{\mathrm{outflow}} = HWu_{\mathrm{str}}C_{\mathrm{str}} \tag{5.2}$$

with u_{str} the mean horizontal wind speed in the street.

The vertical turbulent flux Q_{vert} between the street and the overlying atmosphere is:

$$Q_{\mathrm{vert}} = q_{\mathrm{vert}}WL\frac{(C_{\mathrm{str}} - C_{\mathrm{bkgd}})}{H} \tag{5.3}$$

with q_{vert} the vertical transfer coefficient and C_{bkgd} the background concentration.

The vertical transfer coefficient and the horizontal wind speed are the key parameters representing the dispersion of concentrations. As their formulation differs between the homogeneous and the heterogeneous versions of MUNICH, they are now detailed.

5.2.1.1 Vertical transfer coefficient for turbulent flux

Three parameterizations are implemented in MUNICH to determine the vertical transfer coefficient, q_{vert}, between the street and the overlying atmosphere (Maison et al. 2022). However, currently only the parameterization adapted from Wang (2014) is designed to provide vertical profiles for both wind speed and mixing length within the street. We therefore limit our analysis to the latter.

In MUNICH-homo, the vertical transfer coefficient at the roof level is expressed as:

$$q_{\text{vert}} = \sigma_{\text{w}} l_{\text{m}}(z = H) \quad \text{with} \quad l_{\text{m}}(z) = \frac{\kappa z \, l_{\text{c}}}{l_{\text{c}} + \kappa z} \tag{5.4}$$

where σ_{w} is the standard deviation of the vertical wind velocity at roof level, l_{m} is the mixing length defined as a harmonic mean between two length scales (Coceal et al. 2004) i) κz, with the Von Kármán constant ($\kappa = 0.42$) and ii) l_{c} a characteristic length of the street chosen equals to $0.5W$ (Maison et al. 2022).

5.2.1.2 Mean horizontal wind speed in the street

As for the calculation of the vertical transfer coefficient, three parameterizations are proposed in MUNICH to determine the mean horizontal wind speed in the street (Maison et al. 2022). In the *Wang* parameterization, the mean horizontal wind speed in the street u_{str} is equal to:

$$u_{\text{str}} = \frac{1}{H - z_{0s}} \int_{z_{0s}}^{H} u_Y(z) \, \mathrm{d}z = \frac{u_H |cos(\varphi)|}{(H - z_{0s})} \int_{z_{0s}}^{H} \left[J_1 I_0(g(z)) + J_2 K_0(g(z)) \right] \mathrm{d}z \tag{5.5}$$

with $u_H|cos(\varphi)|$ the wind speed at roof level in the direction of the street and z_{0s} the wall and ground roughness length in the street (fixed to 0.01 m). I_0 and K_0 are the first and second kind modified Bessel function of order 0. J_1 and J_2 are integration coefficients equal to:

$$J_1 = \frac{1}{I_0(g(H)) - I_0(g(z_{0s}))K_0(g(H))/K_0(g(z_{0s}))} \text{ and } J_2 = -\frac{J_1 I_0(g(z_{0s}))}{K_0(g(z_{0s}))} \tag{5.6}$$

The function $g(z)$ is calculated as:

$$g(z) = 2\sqrt{C_B a_r \frac{z}{l_{\text{m}}(H)}} \tag{5.7}$$

with $a_r = H/W$ the aspect ratio of the street and C_B a coefficient dependent on the wind angle with the street and the aspect ratio (Maison et al. 2022).

5.2.2 Heterogeneous approach

In MUNICH-hete, the street is divided into 3 vertical levels to limit the artificial dilution of the traffic emissions and the concentrations in the whole street volume (see Figure 5.1(b) and Figure 5.1). Levels are ordered from the ground to the top of the street. The first level (i=1) contains the traffic emissions. The thickness h_1 is taken as 2 m, which correspond to a zone where the traffic producing

turbulence mixes and dilutes traffic emissions (Solazzo et al. 2008). This traffic-induced turbulence is not explicitly considered in the model. The second level (i=2) thickness h_2 is also of 2 m. It acts as a buffer zone between the first level where traffic emissions are and the third level where exchanges with the background take place. Starting at 4 m, the third level (i=3) goes to the roof level ($h_3 = (H - 4)$ m). The minimum street height considered in the model is set at 6 m. The three levels of the heterogeneous version are referred to as munich-hete-l1, munich-hete-l2 and munich-hete-l3 respectively. Each level i is thus associated to a specific volume, V_i, and the evolution equations may be written as:

$$\left.\frac{\mathrm{d}C^i_{\mathrm{str}}}{\mathrm{d}t}\right|_{\mathrm{tr}} = \frac{1}{V_i}\left(Q^i_{\mathrm{em}} + Q^i_{\mathrm{inflow}} + Q^i_{\mathrm{outflow}} + Q^{i,i+1}_{\mathrm{vert}} + Q^{i-1,i}_{\mathrm{vert}}\right) \tag{5.1}$$

with Q^i_{em} the traffic emission flux (only in the first level (i=1)), Q^i_{inflow} the flux entering the level via the upwind intersection, Q^i_{outflow} the flux leaving the level via the downwind intersection, $Q^{i,i+1}_{\mathrm{vert}}$ the vertical turbulent flux between the levels i and i+1 (for i=3, it exchanges with the background) and $Q^{i-1,i}_{\mathrm{vert}}$ the vertical turbulent flux between the levels i-1 and i (equals to zero if i=1).

Note that more than three vertical levels could be defined in MUNICH-hete, as the vertical variations within the streets of winds and mixing lengths are parameterized when discretizing the streets. However, the first vertical level at the bottom of the street should not be too thin because of mixing due to traffic turbulence. A minimum height for the first layer of 1.5 m seems reasonable.

In OSPM, the flow developing into a vortex in the street between buildings is represented by a recirculation zone. It occupies the whole street volume for narrow streets, and it has the shape of a trapeze for wider streets (Berkowicz et al. 1997; Berkowicz 2000b; Ottosen et al. 2015). When the recirculation zone does not occupy the whole street volume, there is a ventilation zone (see Figure 5.1) where concentrations of pollutants emitted by traffic are usually lower than in the recirculation zone. In MUNICH-homo, the recirculation zone is not explicited, whatever the street ratio H/W is. In MUNICH-hete, the volume of the recirculation zone is computed as in OSPM, as detailed in Appendix 5.A. For now, concentrations in the ventilation zone are considered homogeneous and equal to the background concentrations, i.e. concentrations above the street. The ventilation zone is thus taken into account when it is not affected by traffic emissions. In practice, this means that the width of the trapeze base can only be equal to or larger than the width W of the street (see Appendix 5.A). The width W_i of the level i can thus be inferior to the width W of the street, reducing the level volume (see Figure 5.1). Appendix 5.A presents the algorithm implemented in MUNICH-hete to consider the volume reduction of the ventilation zone. Further work is needed to differentiate the two zones for cases where the ventilation zone develops further into the street.

To quantify mass transfer through intersection, the fluxes are assumed to be vertically homogeneous and remain determined as proposed by Soulhac et al. (2009), as the shape of intersections may differ from one to another and turbulence is not quantified. The flux Q_{inflow} entering the street is assumed to be the same for each vertical level. The flux Q_{outflow} leaving a street is a surface-weighted average of the fluxes leaving each vertical level of the street:

$$Q_{\mathrm{outflow}} = \sum_{i=1}^{i=3} Q^i_{\mathrm{outflow}} = \sum_{i=1}^{i=3} S^v_i u_i C^i_{\mathrm{str}} \tag{5.2}$$

with S^v_i the vertical surface of the level i as presented in Appendix 5.A and u_i the mean horizontal wind speed of the level i (see Section 5.2.2.2).

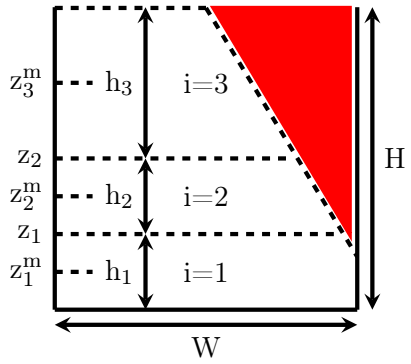

Figure 5.1: Schematic of the discretization in MUNICH-hete. The red triangle represent the ventilation zone that is present under specific conditions, and the white trapeze represents the recirculation zone. z_i^m is the middle height of level i.

5.2.2.1 Vertical turbulent fluxes

To compute the vertical turbulent transfer $Q_{\text{vert}}^{i,i+1}$ at the interface of the vertical levels i and i+1, Equation (5.3) is modified to represent the vertical exchanges between the levels i and i+1:

$$Q_{\text{vert}}^{i,i+1} = q_{\text{vert}}^{i} W_i L \frac{(C_i - C_{i+1})}{\Delta z_i^m} \tag{5.3}$$

with C_i and C_{i+1} the concentrations in the levels i and i+1 respectively, W_i the width of the level i that is inferior or equal to the width W of the street and Δz_i^m the difference in altitude between the middles of the levels i+1 and i, which are noted z_1^m, z_2^m and z_3^m (see Figure 5.1). For i=3, i.e. the highest level, z_{i+1}^m is taken as the symmetric of z_3^m to the roof level, and noted z_{bkgd}^m. It gives an approximation of the volume that effectively exchanges with the third level.

Among the three parameterizations implemented in MUNICH to determine the vertical transfer coefficient q_{vert}, only the *Wang* parameterization is adapted to the discretization. It is thanks to its explicit vertical dependency and validity for a wide range of street-canyon and wind characteristics (Maison et al. 2022). To compute the vertical turbulent transfer $Q_{\text{vert}}^{i,i+1}$, the vertical transfer coefficient is taken at the height of the interface between the two vertical levels considered, and Equation (5.4) is now written as:

$$q_{\text{vert}}^{i} = \sigma_w \kappa z_i \frac{l_c}{l_c + \kappa z_i} \tag{5.4}$$

with z_i the height of the interface between levels i and i+1. The influence of the atmospheric stability on vertical mixing is taken into account by modifying the standard deviation of the vertical wind velocity at roof level and thus the vertical transfer rate depending on the length of Monin-Obukhov, as in MUNICH-homo.

By combining Equation (5.3) and Equation (5.4), the vertical turbulent transfer $Q_{i,i+1}$ can be

written for each level as:

$$Q_{\text{vert}}^{1,2} = \sigma_{\text{w}} \kappa z_1 \frac{l_{\text{c}}}{l_{\text{c}} + \kappa z_1} W_i L \frac{C_1 - C_2}{z_2^m - z_1^m} \tag{5.5}$$

$$Q_{\text{vert}}^{2,3} = \sigma_{\text{w}} \kappa z_2 \frac{l_{\text{c}}}{l_{\text{c}} + \kappa z_2} W_i L \frac{C_2 - C_3}{z_3^m - z_2^m} \tag{5.6}$$

$$Q_{\text{vert}}^{3,\text{bkgd}} = \sigma_{\text{w}} \kappa H \frac{l_{\text{c}}}{l_{\text{c}} + \kappa H} W_i L \frac{C_3 - C_{\text{bkgd}}}{z_{\text{bkgd}}^{\text{m}} - z_3^{\text{m}}} \tag{5.7}$$

with C_1, C_2, C_3 and C_{bkgd} the concentrations of the three levels and the background respectively.

5.2.2.2 Mean horizontal wind speed in the street

As for the vertical turbulent flux, the *Wang* parameterization is preferred among the three parameterizations available in MUNICH to compute the mean horizontal wind speeds in the street. It is thanks to its explicit vertical dependency and the no-slip condition at the ground that is always satisfied ($u(z = 0) = 0$) (Maison et al. 2022). Therefore, the mean horizontal wind speed can be computed at each level in the street, by modifying Equation (5.5) to integrate vertically between the level heights:

$$u_1 = \frac{1}{z_1 - z_{0s}} \int_{z_{0s}}^{z_1} u_Y(z)\,\mathrm{d}z \tag{5.8}$$

$$u_2 = \frac{1}{z_2 - z_1} \int_{z_1}^{z_2} u_Y(z)\,\mathrm{d}z \tag{5.9}$$

$$u_3 = \frac{1}{H - z_2} \int_{z_2}^{H} u_Y(z)\,\mathrm{d}z. \tag{5.10}$$

with z_1 and z_2 the limits of the first two levels as presented in Figure 5.1.

5.3 Application to street networks in Copenhagen with comparison to OSPM

This section presents two applications of MUNICH-hete to assess its capabilities compared to MUNICH-homo and OSPM. Simulations are performed over the year 2019 to generate hourly concentrations for two street networks in Copenhagen, Denmark. The first street network is centered around the H. C. Andersens Boulevard and the second around the Jagtvej street. They are named HCAB and JGTV respectively in the following. They have been selected as observational data of CO, NO_2, NO_x and O_3 are available for the HCAB and, NO_2 and NO_x for JGTV over the whole year. OSPM simulations were also performed to compare model performances. As OSPM does not represent air fluxes at intersections, OSPM simulations are performed only for the streets where there are observations. Thanks to its coupled approach between a Gaussian plume model and a box model, OSPM is able to calculate concentrations on the two sides of the street (Berkowicz et al. 1997; Berkowicz 2000b; Ottosen et al. 2015). Two receptors are used to compare with the observed concentrations on each side of the street: OSPM-R1 and OSPM-R2. The height of the receptors is taken as 2 m to correspond roughly to the height at which observations were performed. They are compared to the concentrations simulated at the first two levels of MUNICH-hete, which are representative of the concentrations at 1 m and 3 m.

MUNICH and OSPM use the same input data to estimate the street concentrations. The meteorological parameters originate from simulations performed with the Weather Research and

Forecasting model (WRF) (Skamarock et al. 2008). The background concentrations are simulated using the Urban Background Model (UBM) (Berkowicz 2000a), which is "a multiple source model that applies a Gaussian approach for horizontal dispersion and a linear approach for vertical dispersion up to the boundary layer" (Jensen et al. 2016). Traffic emissions are generated using the procedure implemented in the local-scale Gaussian air pollution model OML-Highway (Olesen et al. 2015) allowing for precise information for each street segment. Traffic data (average daily traffic, travel speed, and share of heavy-duty vehicles) are used to generate emissions by use of the European emission model COPERT IV. Traffic emissions include exhaust emissions of gases and particles, and non-exhaust emissions of particles. Non-exhaust emissions consist of brake, tyre and road wear. The street parameters (building height and street width) used in MUNICH originate from the OSPM setups.

OSPM represents NO_2 and O_3 chemical transformations using a system of 2 reactions (Berkowicz et al. 1997; Berkowicz 2000b). The first one describes the production of NO_2 due to reaction of NO with O_3, and the second one the photodissociation of NO_2 leading to reproduction of NO and O_3. For a fair comparison, MUNICH is configured to run with a simple chemistry scheme, the Leighton photostationary state for O_3 (Leighton 1961; Kim et al. 2018):

$$NO_2 + h\nu \longrightarrow NO + O(^3P) \quad \text{(R1)}$$

$$O(^3P) + O_2 + M \longrightarrow O_3 + M \quad \text{(R2)}$$

$$NO + O_3 \longrightarrow NO_2 + O_2 \quad \text{(R3)}$$

5.3.1 H. C. Andersens Boulevard

H. C. Andersens Boulevard is a wide, densely-trafficked boulevard, with an aspect ratio $a_r = H/W$ of about 0.2 ($H = 9.9\,\text{m}$, $W = 50\,\text{m}$). It is open on one side with trees instead of buildings. This configuration can be represented in OSPM. However, in MUNICH, a mean building height is defined for each street. Here, it is estimated by averaging the building and the tree heights. The simulated street network is composed of 86 street segments centered around the street where the observation station is located (see brown cross on Figure 5.2). Figure 5.1 presents the monthly-averaged concentrations of CO and NO_2 from the OSPM and MUNICH simulations compared to observations. Appendix 5.B contains monthly-averaged concentrations of NO_x and O_3, and statistical indicators of the comparison for all four pollutants.

OSPM-R1 is the receptor that is close to the measurement station, thus better suited to be compared to observations. Differences in concentrations between OSPM-R1 and OSPM-R2 highlight the importance to take into account horizontal heterogeneities in the street. Observations lies between the concentrations simulated at the two receptors, except for CO for which OSPM slightly underestimates concentrations in the first half of the year. This underestimation could be linked to underestimation of sources other than traffic, e.g. biomass burning, at the regional scale; but also to the absence of volatile organic compounds in the simulation. Overall, the concentrations are well estimated with OSPM with errors between 26% and 33% for CO, and between 34% and 46% for NO_2.

For CO, NO_2 and NO_x, which are emitted by traffic in the bottom of the street, the concentrations are higher in the first level MUNICH-hete-l1 near the bottom and lower in the third level near the roof level. For O_3, the opposite behavior is observed as it is mainly imported by the atmosphere above the street, and it is titrated by NO near the ground. The first two levels munich-hete-l1 and munich-hete-l2 have higher concentrations of CO, NO_2 and NO_x than munich-homo, thus improving the comparison to observations and OSPM concentrations. For CO, the error is improved from 36% in

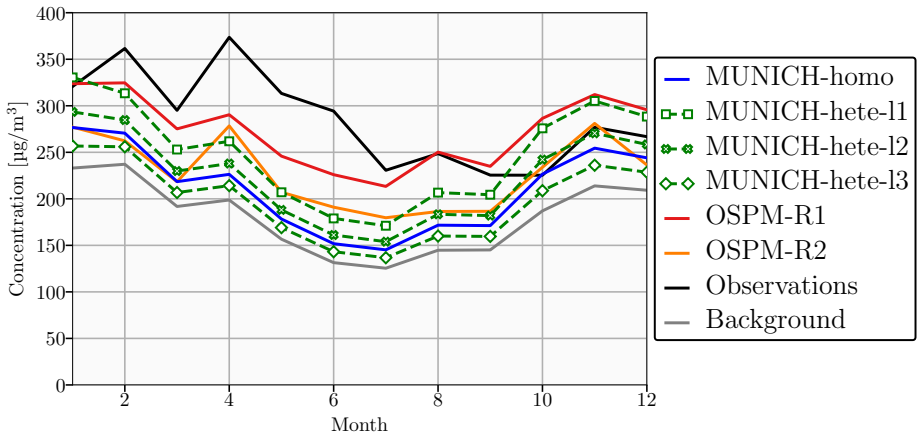

(a) CO

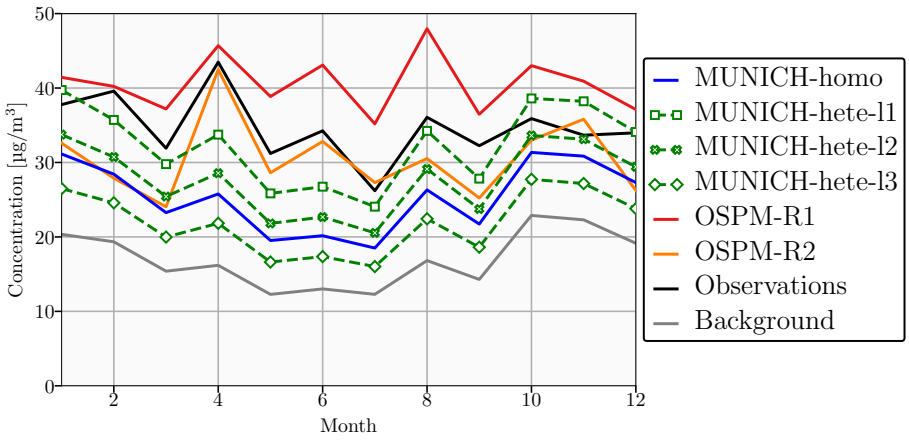

(b) NO_2

Figure 5.1: Monthly-average concentrations (in $\mu g\,m^{-3}$) of CO (a) and NO_2 (b) at HCAB monitoring station. The solid blue line represents the homogeneous version of MUNICH. The three green dashed lines represents the three levels of the heterogeneous version of MUNICH, the lowest level (l1) with square markers, the intermediate level (l2) with cross markers and the top level (l3) with diamond markers. The solid red line represents the OSPM receptor that is close to the measurement station and the solid orange line the second OSPM receptor located on the other side of the street. The observations are in solid black and the background concentrations in solid grey.

MUNICH-homo to 28% in MUNICH-hete-l1, and for NO_2, it is improved from 48% in MUNICH-homo to 35% in MUNICH-hete-l1. Although the concentrations of NO_2 and CO are underestimated in MUNICH-homo compared to observations, they are well modelled in the first level MUNICH-hete-l1 with low errors and biases (see Appendix 5.B). For CO, the concentrations simulated in the first level MUNICH-hete-l1 lies between the two OSPM receptors for most of the year. This is the case for NO_2 as well, except between April and August, when NO_2 concentrations are underestimated in MUNICH-hete compared to observations and OSPM concentrations. The formation of NO_2 in the lower levels (see Reaction (R3)) could be limited with the current model setup, because volatile

organic compounds are not taken into account in the Danish cases. However, they may participate in O_3 and NO_2 formation through HO_2 and RO_2 radicals (Atkinson 2000; Kwak et al. 2012; Zhong et al. 2017; Dai et al. 2021). Furthermore, the vertical discretization is coarse, limiting O_3 transport deep into the street.

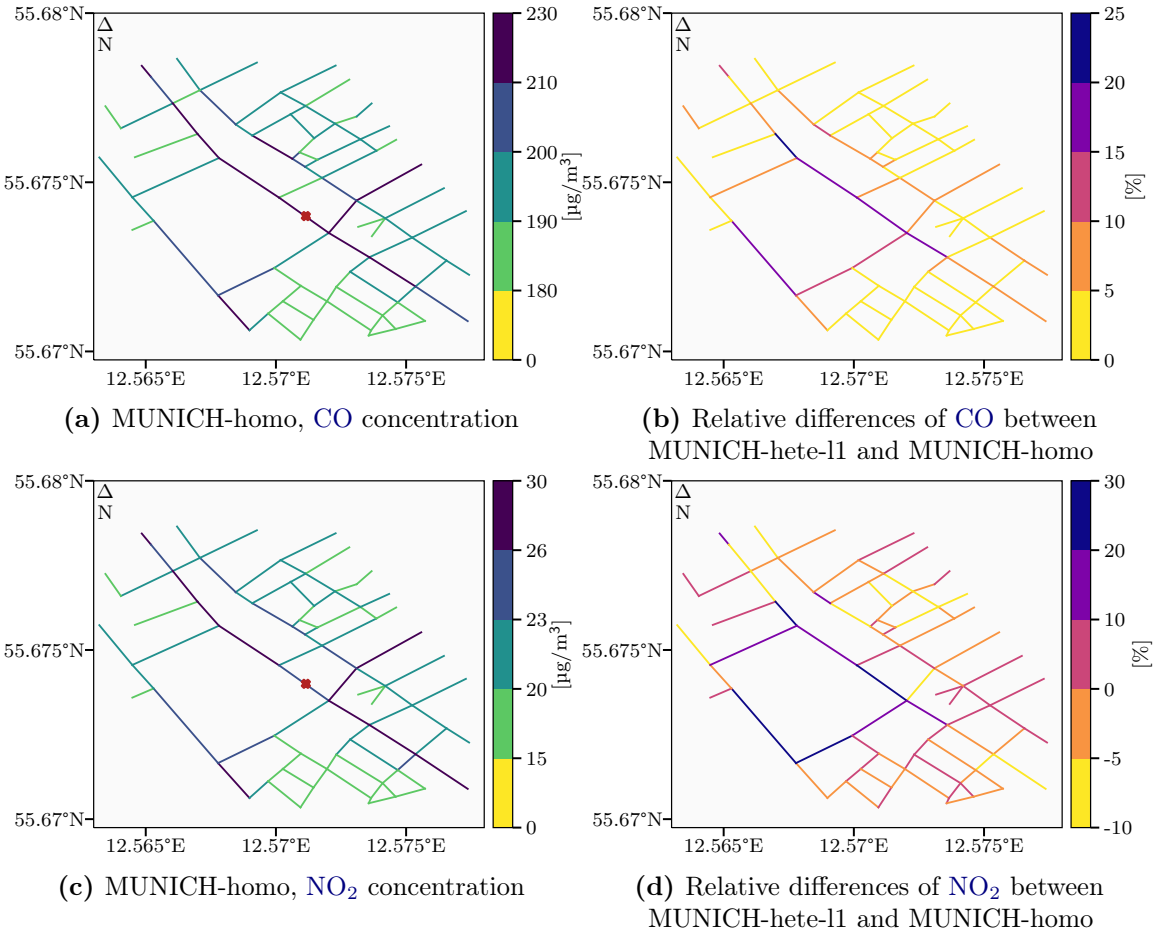

(a) MUNICH-homo, CO concentration

(b) Relative differences of CO between MUNICH-hete-l1 and MUNICH-homo

(c) MUNICH-homo, NO_2 concentration

(d) Relative differences of NO_2 between MUNICH-hete-l1 and MUNICH-homo

Figure 5.2: CO and NO_2 time-averaged concentrations (in $\mu g\,m^{-3}$) for MUNICH-homo on the upper and lower left panels respectively for the HCAB street network. Relative differences (in %) between the first level of MUNICH-hete and MUNICH-homo for CO and NO_2 on the upper and lower right panels respectively for the HCAB street network. A positive relative difference indicates higher concentrations for MUNICH-hete. The brown cross on panels (a) and (c) represents the position of the measurement station.

Over the whole street network, as presented in Figure 5.2, the differences between the concentrations simulated in the first vertical level of MUNICH-hete compared to those simulated in MUNICH-homo vary. For wide streets and avenue with dense traffic, the concentrations are higher in MUNICH-hete-l1 than in MUNICH-homo, with an increase by up to 23 % for CO and 30 % for NO_2. This increase is lower in more narrow and less frequented streets. Although the concentrations in MUNICH-hete-l1 are always higher than those in MUNICH-homo for CO, for NO_2, in narrow streets, the concentrations are lower in MUNICH-hete-l1. These lower NO_2 concentrations are probably related to the limited transport of O_3 from the background to the bottom of the street, limiting the titration of NO.

5.3.2 Jagtvej

Jagtvej is a conventional street canyon with an aspect ratio of about 0.8 ($H = 20.3\,\mathrm{m}$, $W = 26.2\,\mathrm{m}$). The simulated street network is composed of 265 street segments centered around the street where the observation station is located (see brown cross on Figure 5.2). The monthly-averaged concentrations of CO and NO_2 from the OSPM and MUNICH simulations compared to observations, for NO_2 only, are presented in Figure 5.1. Appendix 5.C contains monthly-averaged concentrations of NO_x and O_3, and statistical indicators of the comparison for NO_2 and NO_x.

OSPM-R2 is the receptor that is close to the measurement station, thus better suited to be compared to observations. The differences between the concentration of the two OSPM receptors are lower in JGTV than in HCAB (see Figure 5.1). JGTV is narrower with higher buildings on both sides, thus limiting the ventilation zone and the penetration in the street of background concentrations that would reduce the concentrations at the downwind receptor. OSPM tends to slightly overestimate NO_2 and NO_x concentrations (with errors between 41% and 53% and between 42% and 63% respectively).

Concentrations from the homogeneous version of MUNICH are close to OSPM concentrations for CO. They are lower than OSPM concentrations for NO_2, but they compare well to observations with a bias of -3%, and an error of 46%. These lower NO_2 concentrations are linked to lower NO_x concentrations (with a bias of -19% compared to observations and an error of 53%). As for HCAB, the MUNICH-hete concentrations decrease from the bottom to the top of the street. For CO and NO_x, only the first level have concentrations higher than MUNICH-homo while for NO_2, all three levels have concentrations lower than MUNICH-homo. O_3 concentrations are also higher for the three levels (see Figure 5.C.1). The NO_x concentrations of MUNICH-hete-l1 compare slightly better to observations than MUNICH-homo, while MUNICH-homo is slightly better for NO_2. However, the statistics of the two models are quite close (Appendix 5.C).

Conclusions are similar for the whole street network (see Figure 5.2). The CO concentrations are slightly higher in the first level of MUNICH-hete than in MUNICH-homo. However, NO_2 concentrations at the bottom of the street in the first level of MUNICH-hete tend to be lower than in MUNICH-homo. In some specific street segments of the network, the differences of concentrations for both CO and NO_2 are higher in MUNICH-hete-l1 than in MUNICH-homo. This is due to a mix of different traffic emissions and street morphologies which favor the transport of pollutants.

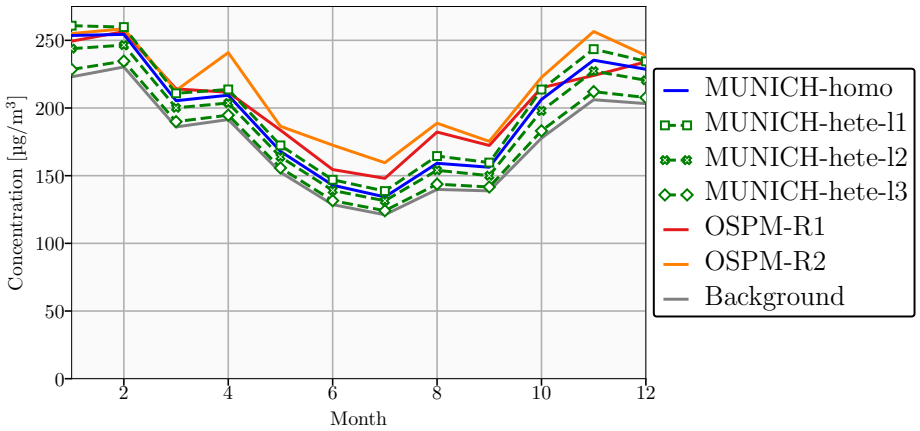

(a) CO

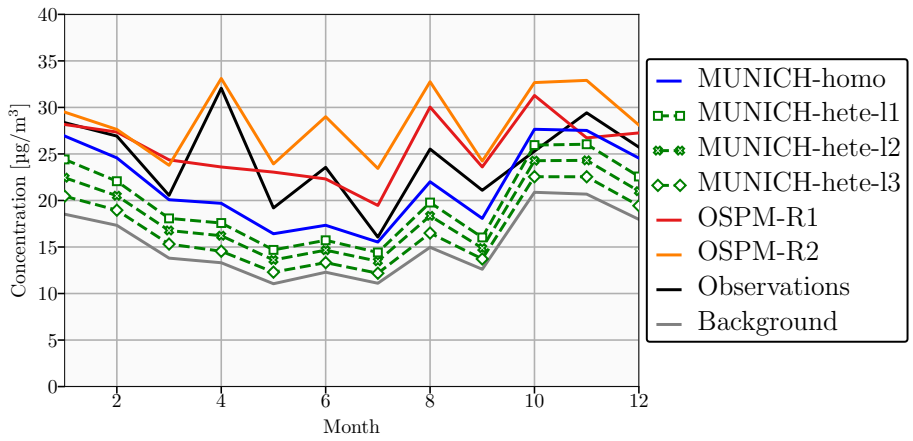

(b) NO_2

Figure 5.1: Monthly-average concentrations (in $\mu g\, m^{-3}$) of CO (a) and NO_2 (b) at JGTV monitoring station. The solid blue line represents the homogeneous version of MUNICH. The three green dashed lines represents the three levels of the heterogeneous version of MUNICH, the lowest level (l1) with square markers, the intermediate level (l2) with cross markers and the top level (l3) with diamond markers. The solid orange line represents the OSPM receptor that is close to the measurement station and the solid red line the second OSPM receptor located on the other side of the street. The observations (only available for NO_2) are in solid black and the background concentrations in solid grey

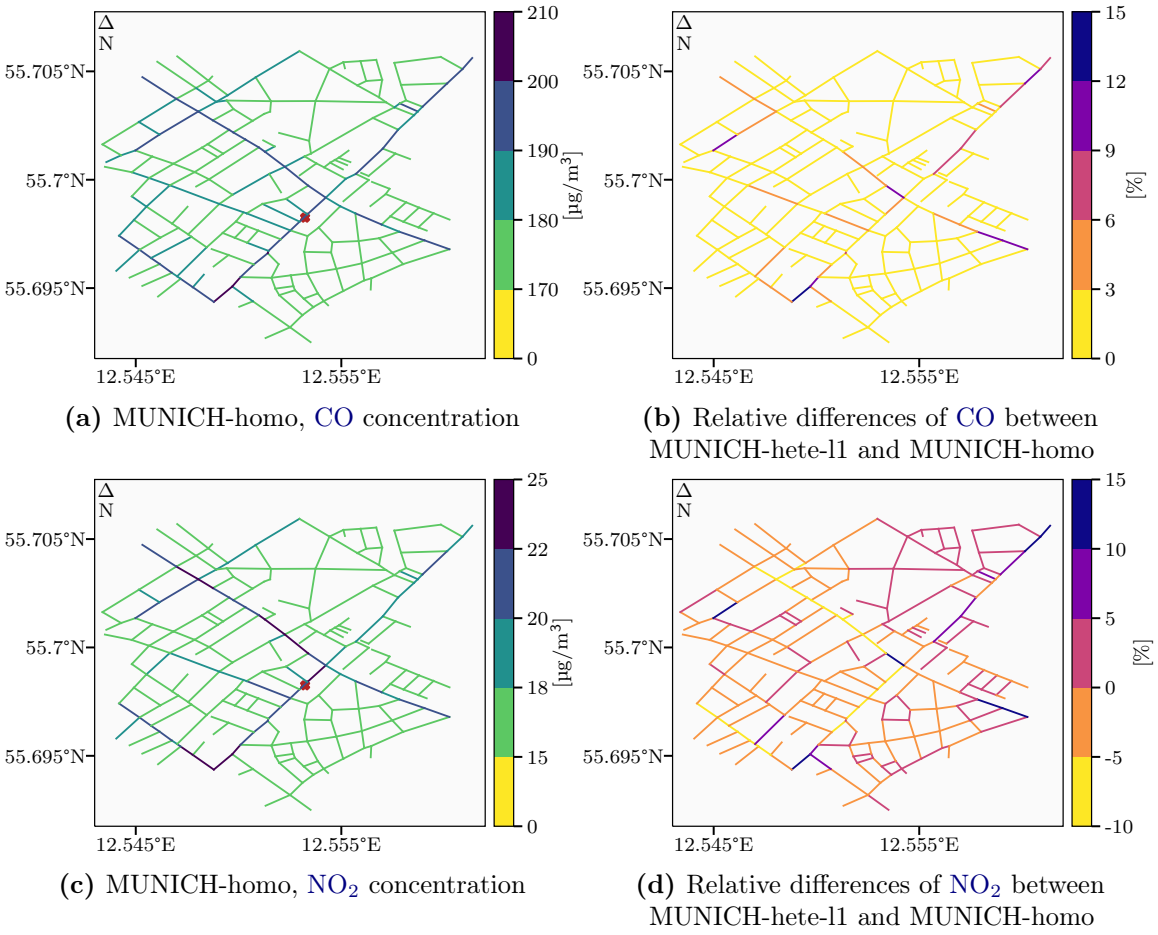

(a) MUNICH-homo, CO concentration

(b) Relative differences of CO between MUNICH-hete-l1 and MUNICH-homo

(c) MUNICH-homo, NO_2 concentration

(d) Relative differences of NO_2 between MUNICH-hete-l1 and MUNICH-homo

Figure 5.2: CO and NO_2 time-averaged concentrations (in $\mu g\,m^{-3}$) for MUNICH-homo in the upper and lower left panels respectively for the JGTV street network. Relative differences (in %) between the first level of MUNICH-hete and MUNICH-homo for CO and NO_2 in the upper and lower right panels respectively for JGTV. A positive relative difference indicates higher concentrations for MUNICH-hete. The brown cross on panels (a) and (c) represents the position of the measurement station.

5.4 Application to a street network in Greater Paris

The impacts of the discretization on gas and particle concentrations is evaluated over the street network near Paris, France, which was used to validate MUNICH v2.0 (Kim et al. 2022) and in several sensitivity studies (Lugon et al. 2021b; Sarica et al. 2022, 2023c). The street network represents a district of Le Perreux-sur-Marne, a suburb 13 km east of Paris, France. It is composed of 577 street segments (see Figure 5.2). The street parameters (building height and street width) were obtained from the BD TOPO database (https://geoservices.ign.fr/bdtopo).Simulations are performed from 22 March to 15 June 2014 to generate hourly concentrations with input data (emissions, including exhaust emissions and brake, tyre and road wear, meteorological parameters and background concentrations) from the reference simulation SCN0 of Sarica et al. (2023c). For this case, MUNICH is coupled to SSH-aerosol (Sartelet et al. 2020) to represent gas-phase chemistry and aerosol dynamics. Observational data are available for the whole simulation period for NO_2, NO_x, $PM_{2.5}$, PM_{10} and BC at a segment of Boulevard d'Alsace Lorraine (see brown cross on Figure 5.2). They were performed at a height of about 2 m and they are thus to be compared to the concentrations of the first two levels (i=1 and i=2) of MUNICH-hete. The segment has an aspect ratio of about 0.3 ($H = 8.6$ m, $W = 26$ m).

The average daily profiles of NO_x and PM_{10} concentrations are shown in Figure 5.1, and for NO, NO_2 and the statistical indicators in Appendix 5.D.1. As in the Danish streets, for pollutants emitted by traffic, the concentrations are higher in MUNICH-hete at the bottom of the street decreasing to the roof level. The concentrations of PM_{10}, NO_2, NO_x and BC are higher on average by 12 %, 21 %, 40 % and 30 % respectively in MUNICH-hete-l1 than in MUNICH-homo. The lower concentration difference for PM_{10} than for the other compounds reflects that non-traffic sources are more important for PM_{10}, and inversely they are small for BC. Despite the higher concentrations in MUNICH-hete-l1, BC concentrations remain strongly underestimated compared to observations, in agreement with the CFD simulations of Lin et al. (2022). For PM_{10}, NO_2 and NO_x, the concentrations compare well to observations, e.g. the error is 33% for NO_2 and 37% for PM_{10}, with slightly better statistics using MUNICH-hete-l1 than MUNICH-homo. For all pollutants, the concentrations of the intermediate level (i=2) are very close to the concentrations of MUNICH-homo. This is due to a mixture of different parameters such as street morphology and dispersion conditions over the simulated period.

In streets, both BC and OM exhibit higher concentrations than in the background (Lugon et al. 2021a). OM consists of primary and secondary aerosols that are formed from the oxidation of VOCs and/or the condensation of semi-volatile organic compounds. Concentrations of both BC and OM simulated in MUNICH-homo and in the first level of MUNICH-hete are compared in Figure 5.2 (see Figure 5.D.2 for NO_2 and PM_{10}). The concentrations simulated in MUNICH-hete-l1 are always higher than in MUNICH-homo. In most streets of the network that are narrow and with limited traffic, the increase in concentrations is limited. It is more important for more open and frequented streets, such as the Boulevard d'Alsace Lorraine.

BC being a primary inert pollutant emitted by traffic, its concentrations are strongly influenced by the discretization as emissions are no longer artificially diluted in the whole street volume. They are now constraint at the bottom of the street inducing an average increase of 30 % compared to the homogeneous version. For OM and PM_{10}, the increase is lower (16 % and 12 % respectively), because of the stronger influence of non-traffic sources.

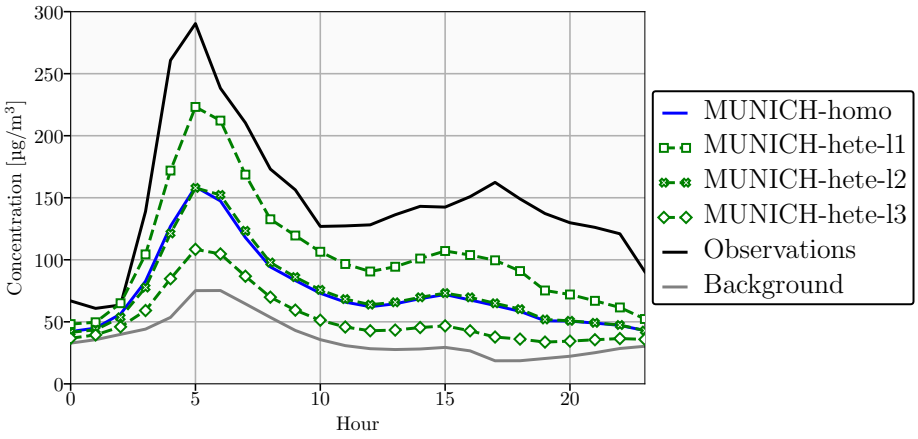

(a) NO_x

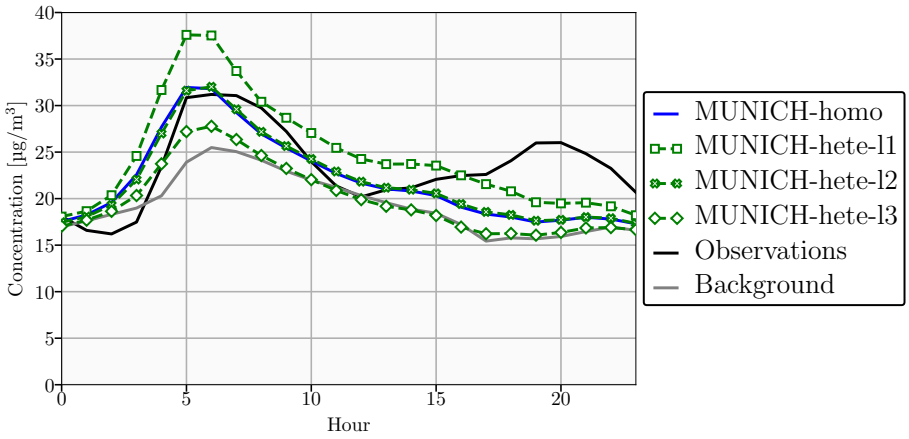

(b) PM_{10}

Figure 5.1: Average daily profile of the concentrations of NO_x (a) and PM_{10} (b) over the simulation period at the Boulevard d'Alsace Lorraine monitoring station. The solid blue line represents the homogeneous version of MUNICH. The three green dashed lines represents the three levels of the heterogeneous version of MUNICH, the lowest level (l1) with square markers, the intermediate level (l2) with cross markers and the top level (l3) with diamond markers. The observations are in solid black and the background concentrations in solid gray.

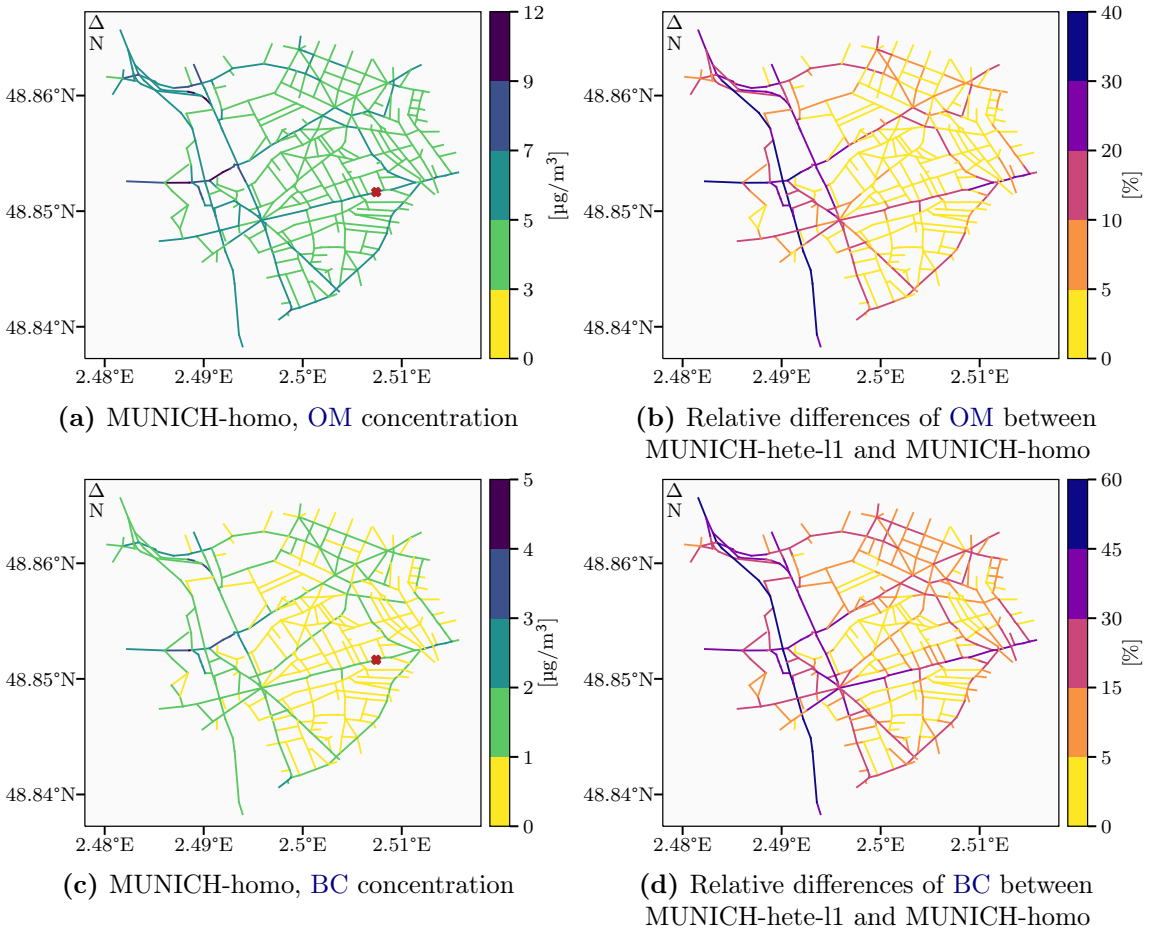

(a) MUNICH-homo, OM concentration

(b) Relative differences of OM between MUNICH-hete-l1 and MUNICH-homo

(c) MUNICH-homo, BC concentration

(d) Relative differences of BC between MUNICH-hete-l1 and MUNICH-homo

Figure 5.2: OM and BC time-averaged concentrations (in $\mu g\,m^{-3}$) for MUNICH-homo in the upper and lower left panels respectively for the district of Le Perreux-sur-Marne. Relative differences (in %) between the first level of MUNICH-hete and MUNICH-homo for OM and BC in the upper and lower right panels respectively for the district of Le Perreux-sur-Marne. A positive relative difference indicates higher concentrations for MUNICH-hete. The brown cross on panels (a) and (c) represents the position of the measurement station.

5.5 Sensitivity analysis

In this section, the influence of the aspect ratio a_r on the concentrations in the heterogeneous version of MUNICH is studied. The sensitivity of the heterogeneous version of MUNICH to the presence of a street network, which influences the concentrations entering the street via the upwind intersection, is also estimated.

5.5.1 Influence of the aspect ratio

The aspect ratio a_r, defined as the ratio between building height H and street width W, is used to determine general behaviors of streets with similar geometries. When a_r is small, i.e. W larger than H, the street is wide, such as a boulevard or an avenue. On the contrary, when a_r is large, i.e. H is larger than W, the street is narrow and closer to a typical street canyon. In the three cases presented in this study in Greater Paris and Copenhagen, streets with small a_r are associated with higher traffic emissions.

Table 5.1 and Appendix 5.E present the influence of the aspect ratio on concentrations in the first vertical level of the heterogeneous version of MUNICH, MUNICH-hete-l1, compared to the homogeneous version. It is quantified using the normalized mean bias (NMB). The homogeneous version of MUNICH presents higher concentrations of pollutants in wide streets (interval [0, 0.5[) in Greater Paris, due to higher traffic emissions compared to narrower streets. The increase in concentration in the first level from using the heterogeneous version of the model is more important for wide streets, up to 53 % for NO_x. Concerning particles, PM_{10} concentrations are increased by up to 18 %, while the increase is about 42 % and 23 % for BC and OM respectively. In streets with larger a_r (interval [1, 1.5[), NO_x concentrations are only 12 % higher than in the homogeneous version, and the PM_{10} concentrations 2.5 %.

Concerning the two cases in Copenhagen, CO and NO_x concentrations present similar behavior than for the Greater Paris case. For the JGTV street network, the increase is limited compared to the HCAB network, 3 % against 11.5 % respectively for CO. Wide streets (interval [0, 0.5[) have higher concentrations of NO_2 compared to the homogenous version of MUNICH, whereas for the other intervals of a_r, they are lower. Thus, O_3 concentrations are lower for wide streets and larger for the other intervals. This could be linked to the lack of volatile organic compounds in these 2 Copenhagen cases.

5.5.2 Sensitivity to the street network

The computation of inflow and outflow fluxes at intersections is performed by estimating the balance of fluxes entering and leaving the intersection from the different street segments attached to it. If this balance is not perfect, there are exchanges with the atmosphere above the intersection. When the total flux entering the intersection is higher than the one leaving it, the flow overload is directed to the atmosphere. When the total flux leaving the intersection is higher, a flux from the atmosphere to the intersection is considered. Further explanation is available in Kim et al. (2018, 2022).

Without a street network around the street segment of interest, the pollutant mass fluxes entering the street are determined from the background concentration. The contribution of the neighboring streets is thus not taken into account and concentrations of pollutants emitted in streets are expected to be lower than when there is a street network.

Table 5.1 and Appendix 5.F present the influence of the neighboring streets for the three cases of the study. It is quantified using the normalized mean error (NME) and NMB between the simulations without and with the neighboring streets. As expected, without the street network, the concentrations

Table 5.1: Statistical indicators of the influence of the aspect ratio on concentrations in MUNICH-hete-l1 for the street network in Greater Paris. Indicators are presented in Appendix A2.

		Mean concentration [µg m^{-3}]	NMB [%]
Pollutant	a_r	MUNICH-homo	MUNICH-hete-l1
NO_2	[0, 0.5[	54.92	33.99
	[0.5, 1[	41.13	11.95
	[1, 1.5[	34.26	6.27
	≥ 1.5	-	-
NO_x	[0, 0.5[	84.31	53.06
	[0.5, 1[	59.85	22.90
	[1, 1.5[	43.71	12.02
	≥ 1.5	-	-
PM_{10}	[0, 0.5[	23.06	18.01
	[0.5, 1[	20.59	6.09
	[1, 1.5[	19.13	2.63
	≥ 1.5	-	-
$PM_{2.5}$	[0, 0.5[	21.10	16.01
	[0.5, 1[	19.01	5.32
	[1, 1.5[	17.91	2.50
	≥ 1.5	-	-
BC	[0, 0.5[	1.56	41.84
	[0.5, 1[	1.19	16.28
	[1, 1.5[	0.96	7.78
	≥ 1.5	-	-
OM	[0, 0.5[	5.60	22.58
	[0.5, 1[	4.91	7.98
	[1, 1.5[	4.46	3.27
	≥ 1.5	-	-

are lower. The bias is between 12% and 21% for NO_2, 18% and 27% for NO_x and 14% for BC. Biases are lower for OM and PM (2 %), because of stronger influence of background concentrations for those compounds.

Table 5.1: Statistical indicators of the influence of the street network on concentrations simulated at each level with MUNICH-hete for the street segment of the Boulevard d'Alsace Lorraine with the monitoring station. Average concentrations are expressed in µg m^{-3}. NME and NMB, expressed in %, are presented in Appendix A2.

Level			NO_2	NO_x	PM_{10}	$PM_{2.5}$	BC	OM
l1	With network	Average	58.92	104.74	24.58	22.18	1.84	6.13
	Without network	Average	51.50	85.46	24.15	21.97	1.58	5.98
		NME	23.25	23.63	17.26	17.28	20.95	20.29
		NMB	-12.58	-18.41	-1.75	-0.98	-14.02	-2.37
l2	With network	Average	47.81	75.36	21.94	20.08	1.42	5.30
	Without network	Average	42.67	62.34	21.77	20.04	1.25	5.25
		NME	20.97	23.11	14.55	14.46	19.37	17.11
		NMB	-10.74	-17.28	-0.75	-0.20	-12.15	-0.96
l3	With network	Average	37.97	52.63	19.91	18.41	1.09	4.69
	Without network	Average	35.65	47.01	19.89	18.44	1.02	4.69
		NME	12.83	15.21	8.11	8.05	11.78	9.47
		NMB	-6.10	-10.67	-0.08	0.15	-6.70	-0.12

5.6 Conclusions

The street-network model MUNICH v2.0 has been modified to introduce concentration heterogeneities in the street, and to better represent population exposure. To model the vertical gradients frequently observed, the streets were discretized with three levels, thus limiting the artificial dilution of emissions and concentrations. Based on a parameterization from OSPM, a ventilation zone is considered under specific conditions to represent horizontal heterogeneities. In order to test these developments, the heterogeneous version of MUNICH (MUNICH-hete) has been applied to two cases in Copenhagen, Denmark, with comparisons to OSPM, and to one case near Paris, France. Overall, MUNICH-hete improves the comparison to observations compared to the homogeneous version. The errors to observations are reduced by up to 20 % for NO_x and 15 % for BC.

As expected, in MUNICH-hete, concentrations of compounds emitted by traffic (CO, NO_2, NO_x, PM_{10}, BC and OM) are higher at the bottom of the street than at the top. These increases can reach up to 60 % and 30 % for NO_2 and PM_{10} respectively. The intermediate level, serving as a buffer, presents concentrations higher or similar to the homogeneous version (MUNICH-homo). Finally, concentrations in the highest level, in direct contact with the atmosphere above the street, are the lowest of the street. For the Danish cases, the low NO_2 concentrations observed in the lower levels could be related to the absence of VOCs in the model setup and the coarse vertical discretization limiting O_3 transport deep into the street.

A sensitivity study of the influence of the street network on concentrations in the streets shows the importance of considering neighboring streets in MUNICH. When no network is considered, concentrations in the street are lower due to the overestimated impact of the atmosphere above. At the bottom of the street, concentrations of NO_2 and BC are reduced by up to 28 % and 14 % respectively without a network. PM and OM are less impacted with a reduction of about 2 % due to a strong influence of non-traffic sources.

For the next step, the ventilation zone will be fully discretized vertically to facilitate the penetration of background concentrations to the bottom of the street. The horizontal exchange fluxes between the two zones will be also be modelled. Deposition and resuspension processes that were not considered in

this development will be added. The fluxes that are currently assumed to be vertically homogeneous will be discretized. Finally, chemistry of volatile organic compounds could be added in the Danish cases if the background concentrations and emissions are available.

Code and data availability. MUNICH-hete is available at Sarica et al. (2023b). The configuration files, the input data and also the scripts to generate the figures and statistics are available at Sarica et al. (2023b).

Appendices

5.A Volumes of the recirculation and ventilation zones

The algorithm used in the heterogeneous version of MUNICH to compute the volumes of the recirculation and ventilation zones is based on the parameterization of OSPM (Berkowicz et al. 1997; Berkowicz 2000b; Ottosen et al. 2015). This algorithm is applied at the beginning of each time step as the size of the recirculation zone is dependent on wind speed and direction. Figure 5.A.1 presents the shape of the recirculation zone and the associated parameters.

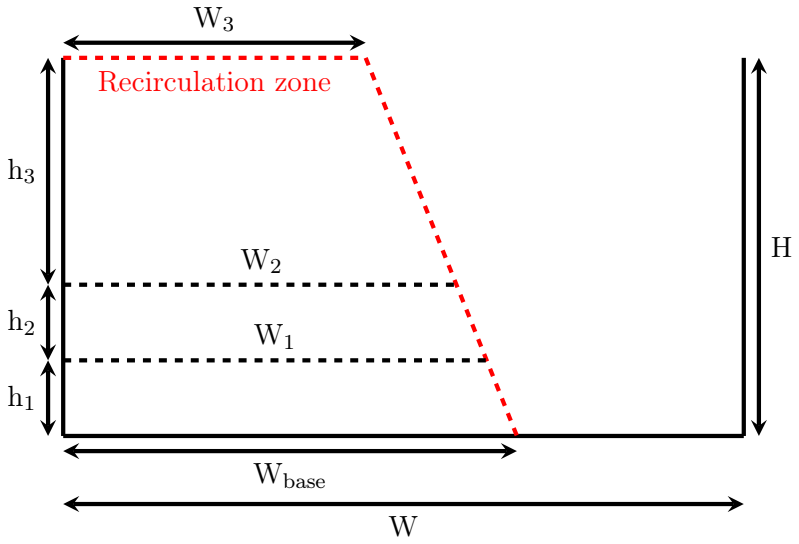

Figure 5.A.1: Representation of the recirculation zone in the heterogeneous version of MUNICH.

The first step is to compute the length of the vortex in the direction of the wind:

$$L_{\text{vortex}} = 2Hf \tag{5.A.1}$$

with H the height of the street and

$$f = \begin{cases} 1 \; if \; u_{\text{roof}} \; \geq \; 2\,ms^{-1} \\ \sqrt{0.5u_{\text{roof}}} \; if \; u_{\text{roof}} \; < \; 2\,ms^{-1} \end{cases} \tag{5.A.2}$$

with u_{roof} the wind speed at roof level.

The width of the trapeze base is the projection of L_{vortex} in the street:

$$W_{base} = L_{\text{vortex}} sin(\theta)) \tag{5.A.3}$$

with θ the angle between the wind direction and the street orientation.

The width of the trapeze top is equal to half of the base:

$$W_3 = \frac{L_{\text{vortex}} sin(\theta)}{2} \tag{5.A.4}$$

Knowing these lengths and using algebraic considerations, the widths W_1 and W_2 can be calculated:

$$\begin{cases} W_1 = W_3 + \dfrac{(h_2 + h_3)\Delta W}{H} \\ W_2 = W_3 + \dfrac{h_3 \Delta W}{H} \end{cases} \tag{5.A.5}$$

with $\Delta W = W_{base} - W_3$

The horizontal surfaces for vertical exchanges between the levels and with the concentrations above the street are calculated as followed:

$$\begin{cases} S_1^h = W_1 L \\ S_2^h = W_2 L \\ S_3^h = W_3 L \end{cases} \tag{5.A.6}$$

with L the street length.

The vertical surfaces for advection via intersections are determined with:

$$\begin{cases} S_1^v = \dfrac{W_1 (h_1)^2 (W_{base} - W_1)}{2} \\ S_2^v = \dfrac{W_2 (h_2)^2 (W_1 - W_2)}{2} \\ S_3^v = \dfrac{W_3 (h_3)^2 (W_2 - W_3)}{2} \end{cases} \tag{5.A.7}$$

Finally, the volumes associated to each level of the recirculation zone are :

$$\begin{cases} V_1 = h_1 L \left(W_1 + \dfrac{(W_{base} - W_1)}{2} \right) \\ V_2 = h_2 L \left(W_2 + \dfrac{(W_1 - W_2)}{2} \right) \\ V_3 = h_3 L \left(W_3 + \dfrac{(W_2 - W_3)}{2} \right) \end{cases} \tag{5.A.8}$$

In the current version of MUNICH-hete, it is assumed that traffic emissions are all affected to the recirculation zone. Therefore, its base W_{base} has to be superior or equal to the street width W. If it is not the case, the recirculation zone is considered to fill the whole street volume.

When considered, the other widths are also limited by the street width:

$$\begin{cases} W_1 = min(W, W_1) \\ W_2 = min(W, W_2) \\ W_3 = min(W, W_3) \end{cases} \tag{5.A.9}$$

5.B Additional information for HCAB

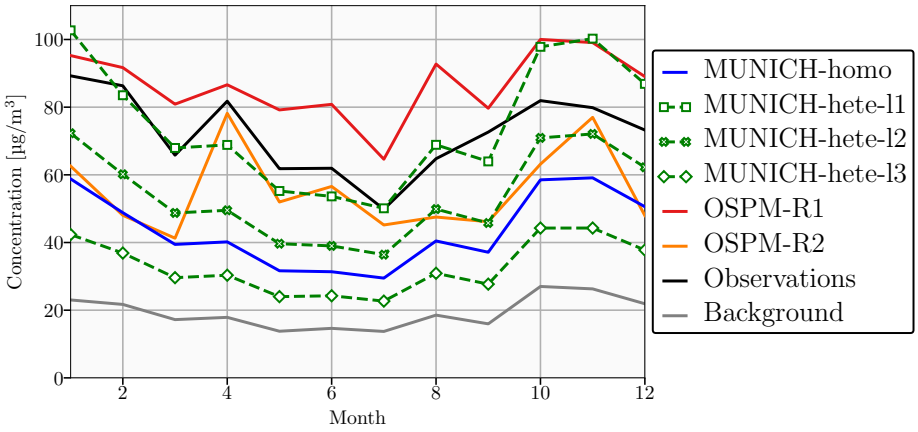

(a) NO_x

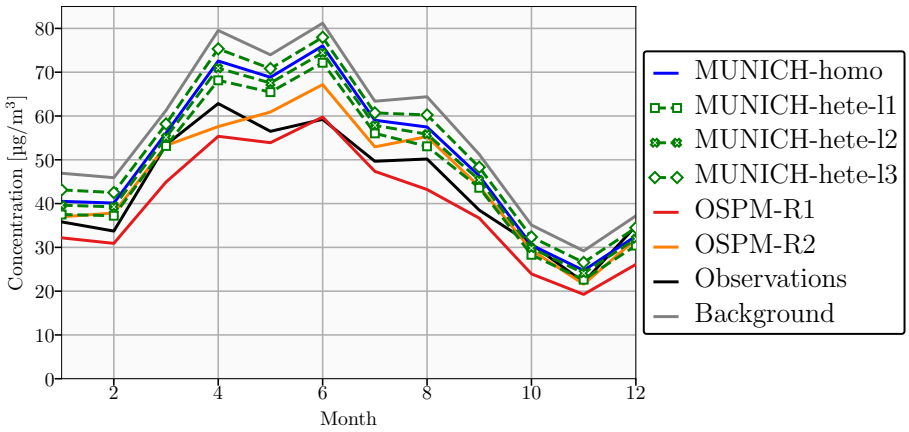

(b) O_3

Figure 5.B.1: Monthly-average concentrations (in $\mu g\,m^{-3}$) of NO_x (a) and O_3 (b) at HCAB monitoring station. The solid blue line represents the homogeneous version of MUNICH. The three green dashed lines represents the three levels of the heterogeneous version of MUNICH, the lowest level (l1) with square markers, the intermediate level (l2) with cross markers and the top level (l3) with diamond markers. The solid red line represents the OSPM receptor that is close to the measurement station and the solid orange line the second OSPM receptor located on the other side of the street. The observations are in solid black and the background concentrations in solid gray.

Table 5.B.1: Statistical indicators of the evaluation of the hourly simulated concentrations to observations at HCAB monitoring station. Average concentrations are expressed in µg m^{-3}. Indicators are presented in Appendix A1.

		CO	NO_2	NO_x	O_3
Observations	Average	285.35	34.64	72.30	44.33
MUNICH-homo	Average	210.88	25.34	43.77	50.44
	MFE	0.36	0.48	0.55	0.38
	MFB	-0.29	-0.29	-0.42	0.14
	FAC2	0.91	0.73	0.63	0.83
MUNICH-hete-l1	Average	249.29	32.37	74.95	47.34
	MFE	0.28	0.35	0.35	0.37
	MFB	-0.14	-0.06	0.05	0.07
	FAC2	0.96	0.87	0.86	0.84
MUNICH-hete-l2	Average	223.39	27.69	53.86	49.36
	MFE	0.32	0.42	0.43	0.37
	MFB	-0.24	-0.21	-0.24	0.12
	FAC2	0.93	0.80	0.78	0.83
MUNICH-hete-l3	Average	197.59	21.87	32.90	52.59
	MFE	0.39	0.57	0.73	0.39
	MFB	-0.34	-0.43	-0.65	0.20
	FAC2	0.88	0.61	0.42	0.82
OSPM-R1	Average	272.86	40.59	86.60	39.50
	MFE	0.26	0.34	0.40	0.35
	MFB	-0.05	0.19	0.21	-0.11
	FAC2	0.96	0.87	0.82	0.86
OSPM-R2	Average	227.84	30.53	55.43	45.77
	MFE	0.33	0.46	0.61	0.36
	MFB	-0.23	-0.16	-0.33	0.05
	FAC2	0.93	0.74	0.61	0.84

5.C Additional information for JGTV

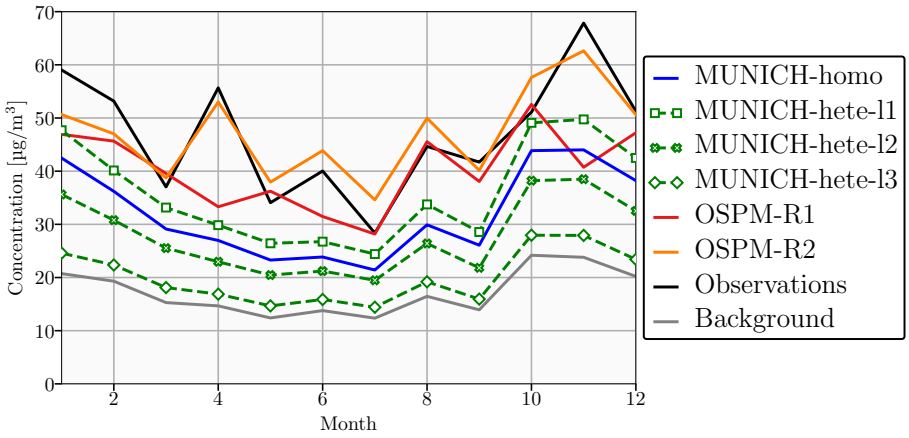

(a) NO_x

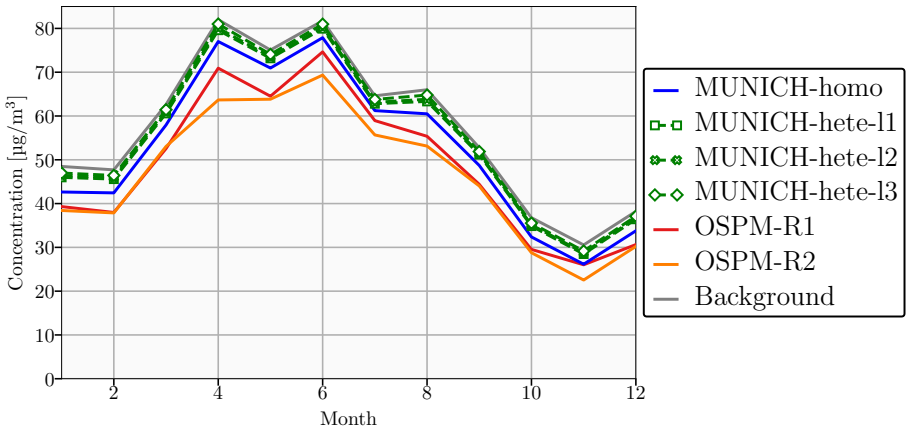

(b) O_3

Figure 5.C.1: Monthly-average concentrations (in $\mu g\,m^{-3}$) of NO_x (a) and O_3 (b) at JGTV monitoring station. The solid blue line represents the homogeneous version of MUNICH. The three green dashed lines represents the three levels of the heterogeneous version of MUNICH, the lowest level (l1) with square markers, the intermediate level (l2) with cross markers and the top level (l3) with diamond markers. The solid orange line represents the OSPM receptor that is close to the measurement station and the solid red line the second OSPM receptor located on the other side of the street. The observations are in solid black and the background concentrations in solid grey

Table 5.C.1: Statistical indicators of the evaluation of the hourly simulated concentrations to observations at JGTV monitoring station. Average concentrations are expressed in µg m^{-3}. Indicators are presented in Appendix A1.

		NO_2	NO_x
Observations	Average	24.50	46.94
MUNICH-homo	Average	21.69	32.10
	MFE	0.46	0.53
	MFB	-0.03	-0.19
	FAC2	0.75	0.66
MUNICH-hete-l1	Average	19.77	35.99
	MFE	0.49	0.51
	MFB	-0.13	-0.11
	FAC2	0.75	0.68
MUNICH-hete-l2	Average	18.37	27.78
	MFE	0.52	0.58
	MFB	-0.20	-0.32
	FAC2	0.71	0.61
MUNICH-hete-l3	Average	16.81	20.10
	MFE	0.57	0.74
	MFB	-0.29	-0.58
	FAC2	0.68	0.46
OSPM-R1	Average	25.60	40.46
	MFE	0.53	0.63
	MFB	0.15	0.03
	FAC2	0.67	0.56
OSPM-R2	Average	28.41	47.21
	MFE	0.41	0.42
	MFB	0.25	0.18
	FAC2	0.80	0.79

5.D Additional information for the district of Le Perreux-sur-Marne

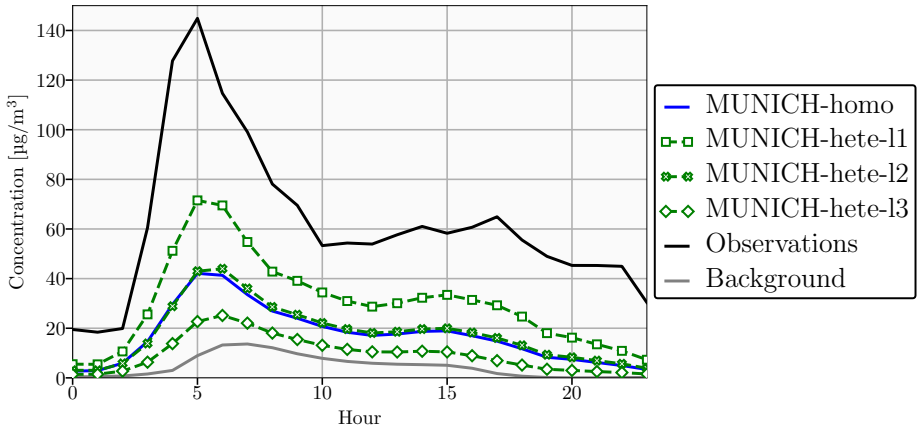

(a) NO

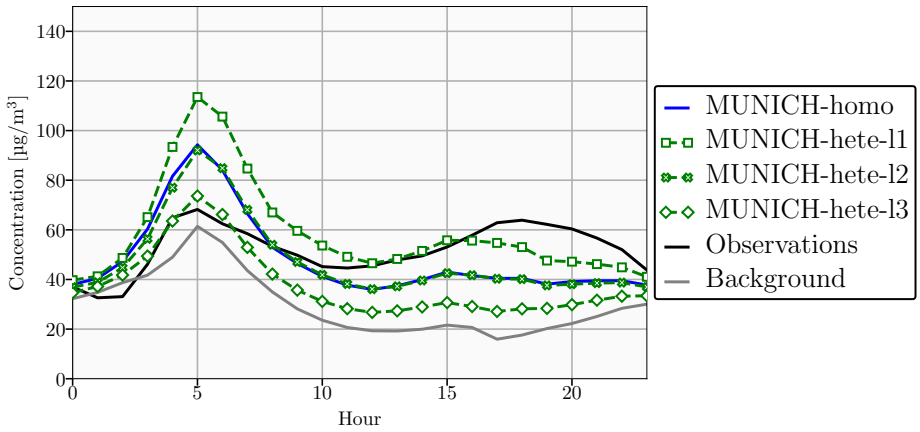

(b) NO_2

Figure 5.D.1: Average daily profile of the concentrations of NO (a) and NO_2 (b) over the simulation period at the Boulevard d'Alsace Lorraine monitoring station. The solid blue line represents the homogeneous version of MUNICH. The three green dashed lines represents the three levels of the heterogeneous version of MUNICH, the lowest level (l1) with square markers, the intermediate level (l2) with cross markers and the top level (l3) with diamond markers. The observations are in solid black and the background concentrations in solid gray.

Table 5.D.1: Statistical indicators of the evaluation of the hourly simulated concentrations to observations at the Boulevard d'Alsace Lorraine monitoring station. Average concentrations are expressed in µg m^{-3}. Indicators are presented in Appendix A1.

		NO_2	NO_x	PM_{10}	$PM_{2.5}$	BC
Observations	Average	52.16	147.19	23.42	12.72	6.10
MUNICH-homo	Average	48.49	74.62	21.89	20.06	1.41
	MFE	0.36	0.65	0.38	0.53	1.17
	MFB	-0.11	-0.60	-0.08	0.38	-1.16
	FAC2	0.87	0.52	0.84	0.67	0.09
MUNICH-hete-l1	Average	58.92	104.74	24.58	22.18	1.84
	MFE	0.33	0.41	0.37	0.57	1.01
	MFB	0.08	-0.30	0.03	0.47	-1.00
	FAC2	0.91	0.80	0.86	0.61	0.16
MUNICH-hete-l2	Average	47.81	75.36	21.94	20.08	1.42
	MFE	0.36	0.64	0.38	0.53	1.17
	MFB	-0.12	-0.59	-0.08	0.38	-1.16
	FAC2	0.86	0.53	0.84	0.67	0.08
MUNICH-hete-l3	Average	37.97	52.63	19.91	18.41	1.09
	MFE	0.49	0.90	0.42	0.50	1.30
	MFB	-0.35	-0.88	-0.18	0.30	-1.30
	FAC2	0.71	0.25	0.80	0.70	0.06

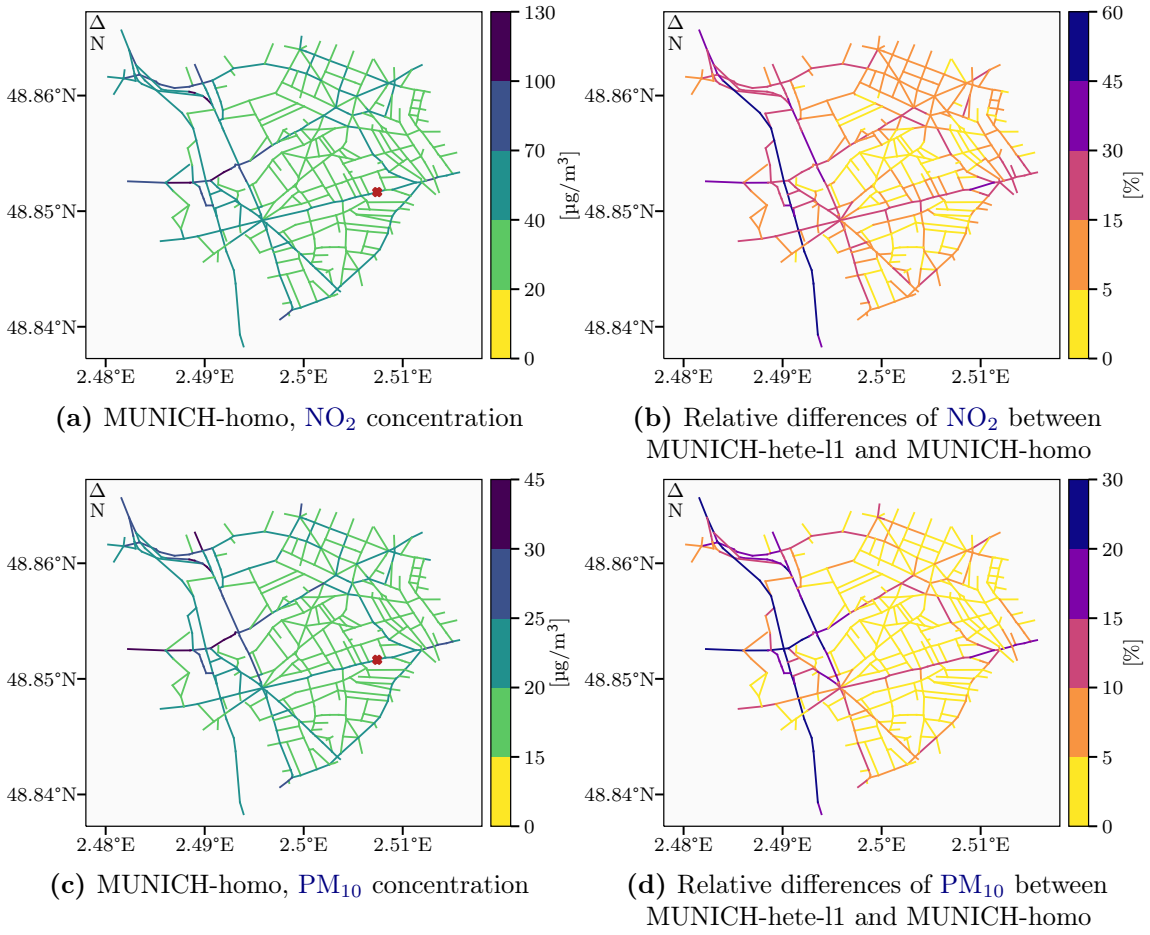

(a) MUNICH-homo, NO_2 concentration

(b) Relative differences of NO_2 between MUNICH-hete-l1 and MUNICH-homo

(c) MUNICH-homo, PM_{10} concentration

(d) Relative differences of PM_{10} between MUNICH-hete-l1 and MUNICH-homo

Figure 5.D.2: NO_2 and PM_{10} time-averaged concentrations (in $\mu g\,m^{-3}$) for MUNICH-homo in the left panel for the district of Le Perreux-sur-Marne. Relative differences (in %) between the first level of MUNICH-hete and MUNICH-homo for PM_{10} in the right panel for the district of Le Perreux-sur-Marne. A positive relative difference indicates higher concentrations for MUNICH-hete. The brown cross on panels (a) and (c) represents the position of the measurement station.

5.E Additional information for the influence of the aspect ratio

Table 5.E.1: Statistical indicators of the influence of the aspect ratio on concentrations in MUNICH-hete-l1 for the street network around HCAB. Indicators are presented in Appendix A2.

		Mean concentration [µg m^{-3}]	NMB [%]
Pollutant	a_r	MUNICH-homo	MUNICH-hete-l1
CO	[0, 0.5[	201.26	11.61
	[0.5, 1[	196.24	4.71
	[1, 1.5[	192.05	3.12
	>= 1.5	193.23	2.12
NO_2	[0, 0.5[	23.18	14.46
	[0.5, 1[	21.69	-0.09
	[1, 1.5[	20.62	-1.24
	>= 1.5	20.56	-3.27
NO_x	[0, 0.5[	34.84	51.16
	[0.5, 1[	29.67	21.34
	[1, 1.5[	26.40	15.84
	>= 1.5	25.87	9.29
O_3	[0, 0.5[	51.48	-2.08
	[0.5, 1[	52.33	1.68
	[1, 1.5[	53.01	1.57
	>= 1.5	53.00	1.94

Table 5.E.2: Statistical indicators of the influence of the aspect ratio on concentrations in MUNICH-hete-l1 for the street network around JGTV. Indicators are presented in Appendix A2.

		Mean concentration [µg m^{-3}]	NMB [%]
Pollutant	a_r	MUNICH-homo	MUNICH-hete-l1
CO	[0, 0.5[	180.72	2.82
	[0.5, 1[	181.49	2.06
	[1, 1.5[	179.85	1.28
	>= 1.5	176.26	0.26
NO_2	[0, 0.5[	17.06	3.76
	[0.5, 1[	17.62	-0.75
	[1, 1.5[	17.31	-2.23
	>= 1.5	16.14	-1.69
NO_x	[0, 0.5[	21.59	16.75
	[0.5, 1[	22.02	11.23
	[1, 1.5[	20.67	7.64
	>= 1.5	18.30	1.91
O_3	[0, 0.5[	56.06	-0.31
	[0.5, 1[	55.54	0.85
	[1, 1.5[	55.67	1.11
	>= 1.5	56.57	0.58

5.F Additional information for the sensitivity to street network

Table 5.F.1: Statistical indicators of the influence of the street network on concentrations simulated at each level with MUNICH-hete for the street segment HCAB with the monitoring station. Average concentrations are expressed in µg m^{-3}. NME and NMB, expressed in %, are presented in Appendix A2.

Level			CO	NO_2	NO_x	O_3
l1	With network	Average	249.29	32.37	74.95	47.34
	Without network	Average	214.27	23.28	46.69	52.98
		NME	14.05	28.06	37.70	11.90
		NMB	-14.05	-28.06	-37.70	11.90
l2	With network	Average	223.39	27.69	53.86	49.36
	Without network	Average	198.12	20.78	33.47	53.79
		NME	11.32	24.95	37.86	8.99
		NMB	-11.32	-24.95	-37.86	8.99
l3	With network	Average	197.59	21.87	32.90	52.59
	Without network	Average	186.96	18.65	24.33	54.78
		NME	5.38	14.73	26.05	4.17
		NMB	-5.38	-14.73	-26.05	4.17

Table 5.F.2: Statistical indicators of the influence of the street network on concentrations simulated at each level with MUNICH-hete for the street segment JGTV with the monitoring station. Average concentrations are expressed in µg m^{-3}. NME and NMB, expressed in %, are presented in Appendix A2.

Level			CO	NO_2	NO_x	O_3
l1	With network	Average	201.21	19.77	35.99	55.19
	Without network	Average	189.24	17.46	27.56	56.45
		NME	6.09	12.38	23.63	3.13
		NMB	-5.95	-11.70	-23.43	2.29
l2	With network	Average	189.49	18.37	27.78	55.54
	Without network	Average	181.01	16.52	21.80	56.64
		NME	4.71	10.87	21.85	2.85
		NMB	-4.47	-10.03	-21.53	1.99
l3	With network	Average	178.59	16.81	20.10	56.12
	Without network	Average	176.03	15.92	18.30	56.80
		NME	1.84	6.16	9.57	1.83
		NMB	-1.43	-5.30	-8.92	1.21

Chapter 6

Conclusions and perspectives

Contents

6.1 Conclusions

This thesis aimed to improve the understanding of the sources and uncertainties linked to the high concentrations of NO_2, PM, BC and OM observed in urban areas and streets. Different parts of the modeling have been identified as having a poor representation and high uncertainties. To quantify them, numerical simulations are performed, by using a multiscale modeling chain, composed of Polair3D and MUNICH. The models are coupled to SSH-aerosol to have a consistent representation of the gas-phase chemistry and aerosol dynamics at both the regional and local scales. The multiscale modeling chain is described in Chapter 1, alongside the air pollution, its impacts on the environment and the human health, and the existing regulations. Chapter 2 focuses on road transport, one of the main sources of pollutants in urban areas. Its different exhaust and non-exhaust emissions are presented, and the European emission standards are introduced. Finally, the different approaches to model traffic emission are briefly described, and Pollemission, the traffic emission computational tool, is presented.

The studies presented in Chapter 3, which look at the sensitivities of road traffic emissions, suggest the need for more detailed information on I/S/LVOC exhaust emissions and non-exhaust emissions of PM. Moreover, road asphalt appears to be a significant source of organic aerosol precursors, currently missing from emission inventories. The access to recent speciations of NMVOCs at exhaust from laboratory measurements on Euro 5 and Euro 6 vehicles provides a finer description of the I/SVOC fractions. When replacing the outdated speciation profiles from the COPERT methodology by these new speciations, OM concentrations are reduced by up to 10 %. Using different estimations of exhaust I/S/LVOC emissions induces larger differences in OM concentrations, reaching 30 % on average. Despite emission factors of PM from tire wear nine times higher, in accordance with the literature, concentrations of BC remain strongly underestimated compared to observations. Emissions of organic aerosol precursors from road asphalt may be several orders of magnitude higher than traffic emissions, but impacts on OM concentrations are yet reasonable, corresponding to an increase of 60 % on average. This leads to realistic PM concentrations. Modeling the influence of the urban background on street concentrations considerably amplifies the impacts of the road traffic emission sensitivities, by up to 50 %.

Air quality over the Paris region for the year 2030 is modeled in Chapter 4 taking into account the introduction of very-low-emission vehicles in the fleet. Emissions of pollutants are greatly reduced, but the concentrations, which are also greatly affected, remain mostly above the WHO air quality guidelines. Emission factors for these very-low-emission vehicles are defined based on the use of different technologies, such as afterburners, to reduce cold-start emissions in particular. This leads to emissions lower than the Euro 7 standard to come. Both the evolution of the fleet composition and the emission reductions for all activity sectors are modeled to generate emissions and background concentrations consistent with the simulated year. NO_2 emissions are reduced by 68 % at the local scale, which induces a 53 % decrease in the concentrations. The non-exhaust emissions, not modified in this study, contribute to the majority of the PM emissions. It thus limits the reduction of the PM concentrations to 18 %. NO_2 emissions get reduced by 99 % when the fleet is composed only of very-low-emission and electric vehicles. The concentrations, decreased by 80 %, now respect the WHO air quality guideline for NO_2 ($9.6\,\mu g\,m^{-3}$ for $10\,\mu g\,m^{-3}$). Concentrations of PM, still affected by non-exhaust emissions, are reduced by 22 % and do not meet the WHO air quality guidelines.

The development of a new version of MUNICH, able to represent concentration heterogeneities in streets, is presented in Chapter 5. It improves the comparison to observations with higher concentrations of pollutants emitted by traffic at the bottom of the street. The street volume is vertically discretized in three levels to limit the artificial dilution of traffic emissions. Based on the street model OSPM, a ventilation zone is considered under specific conditions to represent horizontal heterogeneities in the street. This new version is applied to street networks in Paris and Copenhagen with comparison to observations and to OSPM in Copenhagen. Concentrations of NO_2 and PM_{10} at the bottom of the street, closer to traffic, are increased by up to 60 % and 30 % respectively. Concentrations then gradually decrease in the two vertical levels above. A sensitivity study highlights the importance of considering neighboring streets in MUNICH. In the absence of a street network, concentration of NO_2 and BC at the bottom of the street are reduced by up to 28 % and 14 % respectively.

6.2 Perspectives

Building on the work presented in this thesis, multiple lines of research can be considered to further improve the understanding of the emission sources, and their uncertainties. They can be classified in two main categories, the lines of research to better represent the emission sources in the models, and the development of the models themselves.

The first step is to continue the sensitivity study presented in this thesis. It should focus on finding more information, especially measurement data, that are recent and representative of the current vehicles and technologies. The description of the speciations of VOCs at exhaust, and the I/SVOC fractions, needs to be more exhaustive. Non-exhaust emission of PM from tire wear is still poorly understood and subject to high uncertainties. The emission factors of organic aerosol precursors from road asphalt used in this study are based on measurement performed using fresh samples (hours to days after paving operations) and representative of the United States. These emissions will be replaced by data collected on used asphalt (several years of use) and representative of France.

Other sources of sensitivities, also related to traffic emissions, could be relevant. The cold-start emissions of the vehicles may be lower than 30 % for recent vehicles, especially with the use of afterburners and such in future very-low-emission vehicles. The influence of the traffic emission model on the emission levels in streets have to be assessed. The COPERT methodology used in this thesis is

not able to represent explicitly the traffic conditions, such as braking sections and traffic congestion. Other models, such as HBEFA, could improve the representation of traffic emissions, especially with the new heterogeneous version of MUNICH.

The sensitivity and prospective studies use simulations for the year 2014 as a reference. It could be interesting to develop a new reference simulation representative of the recent year, 2022 for example.

The prospective study should focus on the non-exhaust emissions to reduce PM emissions from traffic to meet the WHO air quality guidelines.

Concerning the development of the models, the first step is to continue the development of the new heterogeneous version of MUNICH. The deposition and resuspension processes, not considered in this development, will be added. The resuspension processes will then be limited to the first level at the bottom of the street, instead of being artificially diluted like traffic emissions in the homogeneous version. Concentrations in the first level are thus expected to increase when taking into account the resuspension. The ventilation zone, currently considered only under specific conditions, will be vertically discretized into three levels, just like the rest of the street volume. This will facilitate the penetration of the background concentrations to the bottom of the street. Once the recirculation and ventilation zones are discretized, horizontal exchange fluxes between the two zones will be added. This future version of MUNICH will be able to calculate concentration heterogeneities with much more accuracy in streets and would not be limited in the consideration of the ventilation zone. It could be used in other multiscale studies investigating the relationship between outdoor and indoor air pollution.

Finally, a new version of the Street-in-Grid (SinG) model coupled with SSH-aerosol could be developed. In its current version, SinG integrates a two-way dynamic coupling between Polair3D and MUNICH, but only for gas-phase species and inert particles. This new version of the model would then be applied in place of the multiscale modeling chain used in this thesis, which integrates a one-way coupling between Polair3D and MUNICH.

Appendices

A Statistical indicators

A1 Statistical indicators for simulation evaluation

In the following formulae, o and s represent the observed and the simulated concentrations respectively. The overbar represents the average.

- Correlation: $Correlation = \frac{\overline{(o-\overline{o})(s-\overline{s})}}{\sqrt{\overline{(o-\overline{o})^2} \times \overline{(s-\overline{s})^2}}}$
- Fractional bias: $FB = 2 \times \overline{\left(\frac{s-o}{s+o}\right)}$
- Geometric mean bias: $MG = \exp\left(\overline{\ln(o)} - \overline{\ln(s)}\right)$
- Geometric variance: $VG = \exp\left(\overline{(\ln(o) - \ln(s))^2}\right)$
- Normalized absolute difference: $NAD = \frac{\overline{|o-s|}}{(\overline{o+s})}$
- Normalized mean square error: $NMSE = \frac{\overline{(o-s)^2}}{(\overline{o} \times \overline{s})}$
- Mean fractional error: $MFE = 2 \times \overline{\left(\frac{|s-o|}{s+o}\right)}$
- Mean fractional bias: $MFB = 2 \times \overline{\left(\frac{s-o}{s+o}\right)}$
- Factor of 2: fraction of data that satisfy $0.5 \leq \frac{s}{o} \leq 2.0$

A2 Statistical indicators for simulation comparison

In the following formulae, X can represent emissions or concentrations with X_0 for the reference simulation and X_i for one of the four sensitivity scenarios. The overbar represents the average.

- Normalized mean bias:
$$NMB = \frac{\overline{(X_i - X_0)}}{\overline{X_0}}$$
- Normalized mean error:
$$NME = \frac{\overline{|X_i - X_0|}}{\overline{X_0}}$$

Bibliography

Abdallah, C., Afif, C., El Masri, N., Öztürk, F., Keleş, M., and Sartelet, K. (2018). "A first annual assessment of air quality modeling over Lebanon using WRF/Polyphemus". In: *Atmos. Pollut. Res.* 9.4, pp. 643–654. DOI: 10.1016/j.apr.2018.01.003 (cited on p. 24).

ACEA (2022a). *Fuel types of new cars: battery electric 11.9 %, hybrid 22.6 % and petrol 37.8 % market share in Q3 2022*. URL: https://www.acea.auto/fuel-pc/fuel-types-of-new-cars-battery-electric-11-9-hybrid-22-6-and-petrol-37-8-market-share-in-q3-2022/ (visited on 04/21/2023) (cited on p. 71).

— (2022b). *Fuel types of new passenger cars in the EU*. URL: https://www.acea.auto/figure/fuel-types-of-new-passenger-cars-in-eu/ (visited on 04/21/2023) (cited on p. 71).

Agrawal, M (2005). "Effects of air pollution on agriculture : An issue of national concern". In: *National Academy Science Letters - India* 28.3-4, pp. 93–106 (cited on p. 20).

Ali, M. U., Siyi, L., Yousaf, B., Abbas, Q., Hameed, R., Zheng, C., Kuang, X., and Wong, M. H. (2021). "Emission sources and full spectrum of health impacts of black carbon associated polycyclic aromatic hydrocarbons (PAHs) in urban environment: A review". In: *Crit Rev Environ Sci Technol* 51.9, pp. 857–896. DOI: 10.1080/10643389.2020.1738854 (cited on p. 21).

Allemand, N., Andre, J.M., Bongrand, G., Cuniasse, B., Durand, A., Mazin, V., and Vieira da Rocha, T. (2021). *Scénarios prospectifs d'émissions de polluants atmosphériques pour la France de 2020 à 2050 par intervalle de 5 ans selon un scénario AME et un scénario AMS, sur la base du scénario énergie climat AME 2021*. Tech. rep. Centre interprofessionnel technique d'études de la pollution atmosphérique (CITEPA). URL: https://www.consultations-publiques.developpement-durable.gouv.fr/IMG/pdf/rapport-final-ame.pdf (visited on 04/21/2023) (cited on pp. 73, 74).

Alvarez, R., Weilenmann, M., and Novak, P. (2008). "Pollutant emissions from vehicles with regenerating after-treatment systems in regulatory and real-world driving cycles". In: *Sci. Total Environ.* 398.1, pp. 87–95. DOI: 10.1016/j.scitotenv.2008.02.022 (cited on p. 32).

Alves, C. A., Vicente, E. D., Vicente, A. M. P., Casotti Rienda, I., Tomé, M., Querol, X., and Amato, F. (2020). "Loadings, chemical patterns and risks of inhalable road dust particles in an Atlantic city in the north of Portugal". In: *Sci. Total Environ.* 737, p. 139596. DOI: 10.1016/j.scitotenv.2020.139596 (cited on p. 34).

Amato, F., Favez, O., Pandolfi, M., Alastuey, A., Querol, X., Moukhtar, S., B., Bruge; Verlhac, S., Orza, J. A. G., Bonnaire, N., Le Priol, T., Petit, J.-F., and Sciare, J. (2016). "Traffic induced particle resuspension in Paris: Emission factors and source contributions". In: *Atmos. Environ.* 129, pp. 114–124. DOI: 10.1016/j.atmosenv.2016.01.022 (cited on p. 34).

Amato, F., Pérez, N., López, M., Ripoll, A., Alastuey, A., Pandolfi, M., Karanasiou, A., Salmatonidis, A., Padoan, E., Frasca, D., Marcoccia, M., Viana, M., Moreno, T., Reche, C., Martins, V., Brines, M., Minguillón, M. C., Ealo, M., Rivas, I., van Drooge, B.,

Benavides, J., Craviotto, J. M., and Querol, X. (2019). "Vertical and horizontal fall-off of black carbon and NO2 within urban blocks". In: *Sci. Total Environ.* 686, pp. 236–245. DOI: 10.1016/j.scitotenv.2019.05.434 (cited on p. 89).

André, M. et al. (July 2019). *Particules de l'air extérieur - Impact sur la pollution atmosphérique des technologies et de la composition du parc de véhicules automobiles circulant en France*. Tech. rep. ANSES. URL: https://www.anses.fr/fr/system/files/AIR2014SA0156Ra-Emission.pdf (visited on 04/21/2023) (cited on pp. 28, 38, 52, 53, 74).

André, M., Sartelet, K., Moukhtar, S., André, J. M., and Redaelli, M. (2020). "Diesel, petrol or electric vehicles: What choices to improve urban air quality in the Ile-de-France region? A simulation platform and case study". In: *Atmos. Environ.* 241, p. 117752. DOI: 10.1016/j.atmosenv.2020.117752 (cited on pp. 46, 52, 69).

Archambeau, F., Méchitoua, N., and Sakiz, M. (2004). "Code Saturne: A Finite Volume Code for the computation of turbulent incompressible flows - Industrial Applications". In: *International Journal on Finite Volumes* 1.1, http://www.latp.univ–mrs.fr/IJFV/spip.php?article3. URL: https://hal.science/hal-01115371 (cited on pp. 23, 88).

Atkinson, R. (2000). "Atmospheric chemistry of VOCs and NOx". In: *Atmos. Environ.* 34.12, pp. 2063–2101. DOI: 10.1016/S1352-2310(99)00460-4 (cited on p. 97).

Badin, A. L., Clavel, A., Vittoz, T., Sorand, C., Lejri, D., Leclerc, L., and Olny, X. (2017). "Combining microscopic traffic modelling and 3 pollutant emission modellings to assess modifications of traffic supply and demand". In: *Journal of Earth Sciences and Geotechnical Engineering* 7, pp. 175–190 (cited on p. 62).

Baensch-Baltruschat, B., Kocher, B., Stock, F., and Reifferscheid, G. (2020). "Tyre and road wear particles (TRWP) - A review of generation, properties, emissions, human health risk, ecotoxicity, and fate in the environment". In: *Sci. Total Environ.* 733, p. 137823. DOI: 10.1016/j.scitotenv.2020.137823 (cited on p. 33).

Barley, M. H. and McFiggans, G. (2010). "The critical assessment of vapour pressure estimation methods for use in modelling the formation of atmospheric organic aerosol". In: *Atmos. Chem. Phys.* 10.2, pp. 749–767. DOI: 10.5194/acp-10-749-2010 (cited on p. 64).

Benavides, J., Snyder, M., Guevara, M., Soret, A., Pérez García-Pando, C., Amato, F., Querol, X., and Jorba, O. (2019). "CALIOPE-Urban v1.0: coupling R-LINE with a mesoscale air quality modelling system for urban air quality forecasts over Barcelona city (Spain)". In: *Geosci. Model Dev.* 12.7, pp. 2811–2835. DOI: 10.5194/gmd-12-2811-2019 (cited on p. 88).

Berkowicz, R. (2000a). "A simple model for urban background pollution". In: *Environ. Monit. Assess.* 65.1/2, pp. 259–267. DOI: 10.1023/a:1006466025186 (cited on p. 95).

— (2000b). "OSPM - a parameterised street pollution model". In: *Environ. Monit. Assess.* 65, pp. 323–331. DOI: 10.1023/A:1006448321977 (cited on pp. 24, 88, 89, 92, 94, 95, 108).

Berkowicz, R., Hertel, O., Larsen, S., Sørensen, N., and Nielsen, M. (Apr. 1997). "Modelling traffic pollution in streets". In: URL: https://backend.orbit.dtu.dk/ws/portalfiles/portal/128001317/Modelling_traffic_pollution_in_streets.pdf (visited on 04/21/2023) (cited on pp. 92, 94, 95, 108).

Boeglin, M. L., Wessels, D., and Henshel, D. (2006). "An investigation of the relationship between air emissions of volatile organic compounds and the incidence of cancer in Indiana counties". In: *Environ. Res.* 100.2, pp. 242–254. DOI: 10.1016/j.envres.2005.04.004 (cited on p. 21).

Bond, T. C., Doherty, S. J., Fahey, D. W., Forster, P. M., Berntsen, T., DeAngelo, B. J., Flanner, M. G., Ghan, S., Kärcher, B., Koch, D., Kinne, S., Kondo, Y., Quinn, P. K., Sarofim, M. C., Schultz, M. G., Schulz, M., Venkataraman, C., Zhang, H., Zhang, S., Bellouin, N., Guttikunda, S. K., Hopke, P. K., Jacobson, M. Z., Kaiser, J. W., Klimont, Z., Lohmann, U., Schwarz, J. P., Shindell, D., Storelvmo, T., Warren, S. G., and Zender, C. S. (2013). "Bounding the role of black carbon in the climate system: A scientific assessment". In: *J. Geophys. Res. Atmos.* 118.11, pp. 5380–5552. DOI: 10.1002/jgrd.50171 (cited on p. 20).

Borge, R., Miguel, I. de, Paz, D. de la, Lumbreras, J., Pérez, J., and Rodríguez, E. (2012). "Comparison of road traffic emission models in Madrid (Spain)". In: *Atmos. Environ.* 62, pp. 461–471. DOI: 10.1016/j.atmosenv.2012.08.073 (cited on pp. 50, 62).

Borucka, A., Wisniowski, P., Mazurkiewicz, D., and Swiderski, A. (2021). "Laboratory measurements of vehicle exhaust emissions in conditions reproducing real traffic". In: *Measurement* 174. DOI: 10.1016/j.measurement.2021.108998 (cited on p. 31).

Boulter, P. (2005). *A Review of Emission Factors and Models for Road Vehicle Non-Exhaust Particulate Matter*. Tech. rep. PPR065. TRL Limited, Wokingham, UK. URL: https://uk-air.defra.gov.uk/library/reports?report%5C_id=364 (visited on 04/21/2023) (cited on pp. 50, 56).

Boutahar, J., Lacour, S., Mallet, V., Quelo, D., Roustan, Y., and Sportisse, B. (2004). "Development and validation of a fully modular platform for numerical modelling of air pollution: POLAIR". In: *Int. J. Environ. and Pollution* 22.1-2, pp. 17–28. DOI: 10.1504/IJEP.2004.005474 (cited on p. 24).

Casotti Rienda, I. and Alves, C. A. (2021). "Road dust resuspension: A review". In: *Atmos Res* 261, p. 105740. DOI: 10.1016/j.atmosres.2021.105740 (cited on p. 34).

CEU (1970). *Council Directive 70/220/EEC of 20 March 1970 on the approximation of the laws of the Member States relating to measures to be taken against air pollution by gases from positive-ignition engines of motor vehicles*. Tech. rep. Council of the European Union – DG III – Industry, DG03/D/01. URL: https://eur-lex.europa.eu/legal-content/EN/ALL/?uri=celex:31970L0220 (visited on 04/21/2023) (cited on p. 34).

— (1991). *Council Directive 91/441/EEC of 26 June 1991 amending Directive 70/220/EEC on the approximation of the laws of the Member States relating to measures to be taken against air pollution by emissions from motor vehicles*. Tech. rep. Council of the European Union – DG III – Industry, DG03. URL: https://eur-lex.europa.eu/legal-content/EN/ALL/?uri=CELEX:31991L0441 (visited on 04/21/2023) (cited on p. 34).

— (2018). *Consolidated text: Regulation (EC) No 443/2009 of the European Parliament and of the Council of 23 April 2009 setting emission performance standards for new passenger cars as part of the Community's integrated approach to reduce CO 2 emissions from light-duty vehicles (Text with EEA relevance)*. Tech. rep. Council of the European Union. URL: https://eur-lex.europa.eu/legal-content/EN/TXT/?uri=CELEX:02009R0443-20180517 (visited on 04/21/2023) (cited on p. 34).

Chen, C., McCabe, D. C., Fleischman, L. E., and Cohan, D. S. (2022). "Black Carbon Emissions and Associated Health Impacts of Gas Flaring in the United States". In: *Atmosphere* 13.3. DOI: 10.3390/atmos13030385 (cited on p. 21).

Chen, T.-M., Gokhale, J., Shofer, S., and Kuschner, W. G. (2007). "Outdoor air pollution: Nitrogen dioxide, sulfur dioxide, and carbon monoxide health effects". In: *Am. J. Med. Sci.* 333.4, pp. 249–256. DOI: 10.1097/MAJ.0b013e31803b900f (cited on p. 21).

Chen, Y., Schleicher, N., Fricker, M., Cen, K., Liu, X.-L., Kaminski, U., Yu, Y., Wu, X.-F., and Norra, S. (2016). "Long-term variation of black carbon and PM2.5 in Beijing, China with respect to meteorological conditions and governmental measures". In: *Environ. Pollut.* 212, pp. 269–278. DOI: 10.1016/j.envpol.2016.01.008 (cited on p. 20).

Chrit, M., Sartelet, K., Sciare, J., Majdi, M., Nicolas, J., Petit, J.-E., and Dulac, F. (2018). "Modeling organic aerosol concentrations and properties during winter 2014 in the northwestern Mediterranean region". In: *Atmos. Chem. Phys.* 18.24, pp. 18079–18100. DOI: 10.5194/acp-18-18079-2018 (cited on p. 64).

Cimorelli, A. J., Perry, S. G., Venkatram, A., Weil, J. C., Paine, R. J., Wilson, R. B., Lee, R. F., Peters, W. D., Brode, R. W., and Paumier, J. O. (2004). *AERMOD: description of model formulation, US Environmental Protection Agency.* Tech. rep. EPA-454/R-03-004. URL: https://gaftp.epa.gov/Air/aqmg/SCRAM/models/preferred/aermod/aermod_mfd_454-R-03-004.pdf (visited on 04/21/2023) (cited on p. 88).

Clenci, A., Berquez, J., Stoica, R., Niculescu, R., Cioc, B., Zaharia, C., and Iorga-Simăn, V. (2022). "Experimental investigation of the effect of an afterburner on the light-off performance of an exhaust after-treatment system". In: *Energy Rep.* 8. Technologies and Materials for Renewable Energy, Environment and Sustainability, pp. 406–418. DOI: 10.1016/j.egyr.2022.07.025 (cited on p. 70).

Coceal, O. and Belcher, S.E. (2004). "A canopy model of mean winds through urban areas". In: *Quart. J. Roy. Meteor. Soc.* 130, pp. 1349–1372. DOI: 10.1256/qj.03.40 (cited on p. 91).

Collett, R. S. and Oduyemi, K. (1997). "Air quality modelling: a technical review of mathematical approaches". In: *Meteorol. Appl.* 4.3, pp. 235–246. DOI: 10.1017/S1350482797000455 (cited on p. 88).

Compernolle, S., Ceulemans, K., and Müller, J.-F. (2011). "EVAPORATION: a new vapour pressure estimation method for organic molecules including non-additivity and intramolecular interactions". In: *Atmos. Chem. Phys.* 11.18, pp. 9431–9450. DOI: 10.5194/acp-11-9431-2011 (cited on p. 64).

Conti, G. O., Heibati, B., Kloog, I., Fiore, M., and Ferrante, M. (2017). "A review of AirQ Models and their applications for forecasting the air pollution health outcomes". In: *Environ. Sci. Pollut. Res.* 24.7, pp. 6426–6445. DOI: 10.1007/s11356-016-8180-1 (cited on p. 88).

Couvidat, F., Debry, E., Sartelet, K., and Seigneur, C. (2012). "A hydrophilic/hydrophobic organic (H2O) aerosol model: Development, evaluation and sensitivity analysis". In: *J. Geophys. Res. Atmos.* 117.D10. DOI: 10.1029/2011JD017214 (cited on p. 28).

Couvidat, F. and Sartelet, K. (2015). "The Secondary Organic Aerosol Processor (SOAP v1.0) model: a unified model with different ranges of complexity based on the molecular surrogate approach". In: *Geosci. Model Dev.* 8.4, pp. 1111–1138. DOI: 10.5194/gmd-8-1111-2015 (cited on p. 28).

Crippa, M., Guizzardi, D., Pisoni, E., Solazzo, E., Guion, A., Muntean, M., Florczyk, A., Schiavina, M., Melchiorri, M., and Hutfilter, A. F. (2021). "Global anthropogenic emissions in urban areas: patterns, trends, and challenges". In: *Environ. Res. Lett.* 16.7, p. 074033. DOI: 10.1088/1748-9326/ac00e2 (cited on p. 22).

Daellenbach, K. R. et al. (2020). "Sources of particulate-matter air pollution and its oxidative potential in Europe". In: *Nature* 587.7834, pp. 414–419. DOI: 10.1038/s41586-020-2902-8 (cited on p. 21).

Dai, P., Ge, Y., Lin, Y., Su, S., and Liang, B. (2013). "Investigation on characteristics of exhaust and evaporative emissions from passenger cars fueled with gasoline/methanol blends". In: *Fuel* 113, pp. 10–16. DOI: 10.1016/j.fuel.2013.05.038 (cited on p. 33).

Dai, Y., Cai, X., Zhong, J., and MacKenzie, A. R. (2021). "Modelling chemistry and transport in urban street canyons: Comparing offline multi-box models with large-eddy simulation". In: *Atmos. Environ.* 264, p. 118709. DOI: 10.1016/j.atmosenv.2021.118709 (cited on p. 97).

Denby, B. R., Sundvor, I., Johansson, C., Pirjola, L., Ketzel, M., Norman, M., Kupiainen, K., Gustafsson, M., Blomqvist, G., and Omstedt, G. (2013). "A coupled road dust and surface moisture model to predict non-exhaust road traffic induced particle emissions (NORTRIP). Part 1: Road dust loading and suspension modelling". In: *Atmos. Environ.* 77, pp. 283–300. DOI: 10.1016/j.atmosenv.2013.04.069 (cited on p. 56).

Dergaoui, H., Sartelet, K., Debry, E., and Seigneur, C. (2013). "Modeling coagulation of externally mixed particles: Sectional approach for both size and chemical composition". In: *J. Aerosol Sci.* 58, pp. 17–32. DOI: 10.1016/j.jaerosci.2012.11.007 (cited on p. 27).

Dios, M., Souto, J. A., and Casares, J. J. (2010). "Emissions inventory analysis for an urban (industrial)-rural (agricultural) environment". In: *SUSTAINABLE CITY VI: URBAN REGENERATION AND SUSTAINABILITY*. Ed. by CA Brebbia, S Hernandez, and E Tiezzi. Vol. 129. Sustainable City 2010: 6th International Conference on Urban Regeneration and Sustainability, A Coruna, SPAIN, APR 14-16, 2010. Univ Siena; Wessex Inst Technol, pp. 383–392. DOI: 10.2495/SC100331 (cited on p. 22).

Dons, E., Int Panis, L., Van Poppel, M., Theunis, J., and Wets, G. (2012). "Personal exposure to Black Carbon in transport microenvironments". In: *Atmos. Environ.* 55, pp. 392–398. DOI: 10.1016/j.atmosenv.2012.03.020 (cited on p. 21).

EC (2022). *Proposal for a REGULATION OF THE EUROPEAN PARLIAMENT AND OF THE COUNCIL on type-approval of motor vehicles and engines and of systems, components and separate technical units intended for such vehicles, with respect to their emissions and battery durability (Euro 7) and repealing Regulations (EC) No 715/2007 and (EC) No 595/2009*. Tech. rep. European Commission. URL: https://eur-lex.europa.eu/legal-content/EN/TXT/?uri=CELEX:52022PC0586 (visited on 04/21/2023) (cited on p. 35).

EEA (2016). *Explaining road transport emissions : a non-technical guide*. Publications Office. DOI: doi/10.2800/71804 (cited on p. 32).

— (2022). *Air quality in Europe 2021*. EEA Report no. 15/2021. European Environment Agency. DOI: 10.2800/549289 (cited on p. 49).

— (2023). *Air quality in Europe 2022*. EEA Report no. 05/2022. European Environment Agency. DOI: 10.2800/488115 (cited on pp. 21, 69).

EMEP/EEA (2019). *EMEP/EEA air pollutant emission inventory guidebook 2019*. EEA Report No 13/2019. European Environment Agency. URL: https://www.eea.europa.eu/publications/emep-eea-guidebook-2019 (cited on pp. 36, 44–46, 50, 51, 70).

EU (2015). *Consolidated text: Directive 2008/50/EC of the European Parliament and of the Council of 21 May 2008 on ambient air quality and cleaner air for Europe*. URL: http://data.europa.eu/eli/dir/2008/50/2015-09-18 (visited on 04/21/2023) (cited on pp. 22, 23).

Falasca, S. and Curci, G. (2018). "High-resolution air quality modeling: Sensitivity tests to horizontal resolution and urban canopy with WRF-CHIMERE". In: *Atmos. Environ.* 187, pp. 241–254. DOI: 10.1016/j.atmosenv.2018.05.048 (cited on pp. 23, 88).

Fares, S., Vargas, R., Detto, M., Goldstein, A. H., Karlik, J., Paoletti, E., and Vitale, M. (2013). "Tropospheric ozone reduces carbon assimilation in trees: estimates from analysis of continuous flux measurements". In: *Glob Chang Biol* 19.8, pp. 2427–2443. DOI: 10.1111/gcb.12222 (cited on p. 20).

Fitz, D. R. and Bufalino, C. (2002). "Measurement of PM10 emission factors from paved roads using on-board particle sensors". In: *US Environmental Protection Agency's 11th Annual Emission Inventory Conference, Emission Inventories—Partnering for the Future. Available: https://www3.epa.gov/ttnchie1/conference/ei11/dust/fitz.pdf. [accessed 12 April 2023]* (cited on p. 34).

Franco, V., Kousoulidou, M., Muntean, M., Ntziachristos, L., Hausberger, S., and Dilara, P. (2013). "Road vehicle emission factors development: A review". In: *Atmos. Environ.* 70, pp. 84–97. DOI: 10.1016/j.atmosenv.2013.01.006 (cited on p. 35).

Franzin, B. T., Guizellini, F. C., de Babos, D. V., Hojo, O., Pastre, I. A., Marchi, M. R.R., Fertonani, F. L., and Oliveira, C. M. R. R. (2020). "Characterization of atmospheric aerosol (PM10 and PM2.5) from a medium sized city in São Paulo state, Brazil". In: *J Environ Sci (China)* 89, pp. 238–251. DOI: 10.1016/j.jes.2019.09.014 (cited on p. 20).

Fuller, R., Landrigan, P. J., Balakrishnan, K., Bathan, G., Bose-O'Reilly, S., Brauer, M., Caravanos, J., Chiles, T., Cohen, A., Corra, L., Cropper, M, Ferraro, G, Hanna, J., Hanrahan, D., Hu, H., Hunter, D., Janata, G., Kupka, R., Lanphear, B., Lichtveld, M., Martin, K., Mustapha, A., Sanchez-Triana, E., Sandilya, K., Schaefli, L., Shaw, J., Seddon, J., Suk, W., Téllez-Rojo, M. M., and Yan, C. (2022). "Pollution and health: a progress update". In: *Lancet Planet. Health* 6.6, e535–e547. DOI: 10.1016/S2542-5196(22)00090-0 (cited on p. 88).

Gao, J., Chen, H., Liu, Y., Li, Y., Li, T., Tu, R., Liang, B., and Ma, C. (2021). "The effect of after-treatment techniques on the correlations between driving behaviours and NOx emissions of passenger cars". In: *J. Clean. Prod.* 288. DOI: 10.1016/j.jclepro.2020.125647 (cited on p. 32).

Gao, J., Tian, G., Sorniotti, A., Karci, A. E., and Di Palo, R. (2019). "Review of thermal management of catalytic converters to decrease engine emissions during cold start and warm up". In: *Appl. Therm. Eng.* 147, pp. 177–187. DOI: 10.1016/j.applthermaleng.2018.10.037 (cited on p. 70).

Gao, Z., Bresson, R., Qu, Y., Milliez, M., de Munck, C., and Carissimo, B. (2018). "High resolution unsteady RANS simulation of wind, thermal effects and pollution dispersion for studying urban renewal scenarios in a neighborhood of Toulouse". In: *Urban Clim.* 23. ICUC9: The 9th International Conference on Urban Climate, pp. 114–130. DOI: 10.1016/j.uclim.2016.11.002 (cited on pp. 23, 88).

Garg, B. D., Cadle, S. H., Mulawa, P. A., Groblicki, P. J., Laroo, C., and Parr, G. A. (2000). "Brake Wear Particulate Matter Emissions". In: *Env. Sc. and Tech.* 34.21, pp. 4463–4469. DOI: 10.1021/es001108h (cited on pp. 33, 34).

Gaudioso, D., Trozzi, C., Vaccaro, R., and Cirillo, M. C. (1994). "Sensitivity analysis of evaporative emission estimates from gasoline passenger cars". In: *Sci. Total Environ.* 147. 4th International Symposium on Highway Pollution, MADRID, SPAIN, MAY 18-22, 1992, pp. 325–332 (cited on p. 33).

Gautam, M., Miller, E. S., Ferguson, D. H., and Lyons, D. W. (1998). "Uncertainty in real-world particulate matter emission measurements from a transportable heavy-duty vehicle emissions testing laboratory". In: *International journal of vehicle design. Heavy vehicle systems.* 5.3-4, pp. 399–420 (cited on p. 31).

Gentner, D. R., Jathar, S. H., Gordon, T. D., Bahreini, R., Day, D. A., El Haddad, I., Hayes, P. L., Pieber, S. M., Platt, S. M., Gouw, J. de, Goldstein, A. H., Harley, R. A., Jimenez, J. L., Prévôt, A. S. H., and Robinson, A. L. (2017). "Review of Urban Secondary Organic Aerosol Formation from Gasoline and Diesel Motor Vehicle Emissions". In: *Env. Sc. and Tech.* 51.3, pp. 1074–1093. DOI: 10.1021/acs.est.6b04509 (cited on pp. 19, 49).

Grigoratos, T. and Martini, G. (2015). "Brake wear particle emissions: a review". In: *Environ. Sci. Pollut. Res.* 22.4, pp. 2491–2504. DOI: 10.1007/s11356-014-3696-8 (cited on pp. 33, 34).

Guevara, M., Jorba, O., Tena, C., Denier van der Gon, H., Kuenen, J., Elguindi, N., Darras, S., Granier, C., and Pérez García-Pando, C. (2021). "Copernicus Atmosphere Monitoring Service TEMPOral profiles (CAMS-TEMPO): global and European emission temporal profile maps for atmospheric chemistry modelling". In: *Earth Syst. Sci. Data* 13.2, pp. 367–404. DOI: 10.5194/essd-13-367-2021 (cited on p. 63).

Hanna, S. and Chang, J. (2012). "Acceptance criteria for urban dispersion model evaluation". In: *Meteorol. Atmospheric Phys.* 116.3, pp. 133–146. DOI: 10.1007/s00703-011-0177-1 (cited on pp. 47, 53).

El-Harbawi, M. (2013). "Air quality modelling, simulation, and computational methods: a review". In: *Environ. Rev.* 21.3, pp. 149–179. DOI: 10.1139/er-2012-0056 (cited on p. 88).

Herring, S. and Huq, P. (2018). "A Review of Methodology for Evaluating the Performance of Atmospheric Transport and Dispersion Models and Suggested Protocol for Providing More Informative Results". In: *Fluids* 3.1. DOI: 10.3390/fluids3010020 (cited on p. 53).

Hill, W. et al. (2023). "Lung adenocarcinoma promotion by air pollutants". In: *Nature* 616.7955, pp. 159–167. DOI: 10.1038/s41586-023-05874-3 (cited on p. 21).

Holnicki, P., Nahorski, Z., and Kałuszko, A. (2021). "Impact of Vehicle Fleet Modernization on the Traffic-Originated Air Pollution in an Urban Area - A Case Study". In: *Atmosphere* 12.12. DOI: 10.3390/atmos12121581 (cited on pp. 69, 70).

Hood, C., Stocker, J., Seaton, M., Johnson, K., O'Neill, J., Thorne, L., and Carruthers, D. (2021). "Comprehensive evaluation of an advanced street canyon air pollution model". In: *J. Air Waste Manag. Assoc.* 71.2, pp. 247–267. DOI: 10.1080/10962247.2020.1803158 (cited on pp. 24, 88).

Jang, J., Lee, J., Kim, J., and Park, S. (2015). "Comparisons of the nanoparticle emission characteristics between GDI and PFI vehicles". In: *J Nanopart Res* 17.12. DOI: 10.1007/s11051-015-3280-2 (cited on p. 32).

Jensen, S. S., Ketzel, M., Brandt, J., Becker, T., Plejdrup, M., Winther, M., Ellermann, T., Christensen, J. H., Nielsen, O.-K., Hertel, O., and Fuglsang, M. W. (2016). "04 - Air Quality at Your Street - Public Digital Map of Air Quality in Denmark". In: *Proceedings*. COST Association, Avenue Louise 149, 1050 Brussels, Belgium. DOI: 10.5162/6eunetair2016/04 (cited on p. 95).

Jeong, C. H., Wang, J. M., Hilker, N., Debosz, J., Sofowote, U., Su, Y., Noble, M., Healy, R. M., Munoz, T., Dabek-Zlotorzynska, E., Celo, V., White, L., Audette, C., Herod, D., and Evans, G. J. (2019). "Temporal and spatial variability of traffic-related PM2.5 sources: Comparison of exhaust and non-exhaust emissions". In: *Atmos. Environ.* 198, pp. 55–69. DOI: 10.1016/j.atmosenv.2018.10.038 (cited on p. 71).

Joback, K. G. and Reid, R. C. (1987). "ESTIMATION OF PURE-COMPONENT PROPERTIES FROM GROUP-CONTRIBUTIONS". In: *Chem Eng Commun* 57.1-6, pp. 233–243. DOI: 10.1080/00986448708960487 (cited on p. 64).

Joumard, R. and Andre, M. (1990). "Cold start emissions of traffic". In: *Sci. Total Environ.* 93, pp. 175–182. DOI: 10.1016/0048-9697(90)90106-5 (cited on p. 52).

Kamara, A. A. and Harrison, R. M. (2021). "Analysis of the air pollution climate of a central urban roadside supersite: London, Marylebone Road". In: *Atmos. Environ.* 258, p. 118479. DOI: https://doi.org/10.1016/j.atmosenv.2021.118479 (cited on p. 49).

Kampa, M. and Castanas, E. (2008). "Human health effects of air pollution". In: *Environ. Pollut.* 151.2, pp. 362–367. DOI: 10.1016/j.envpol.2007.06.012 (cited on p. 49).

Karl, M., Walker, S.-E., Solberg, S., and Ramacher, M. O. P. (2019). "The Eulerian urban dispersion model EPISODE – Part 2: Extensions to the source dispersion and photochemistry for EPISODE–CityChem v1.2 and its application to the city of Hamburg". In: *Geosci. Model Dev.* 12.8, pp. 3357–3399. DOI: 10.5194/gmd-12-3357-2019 (cited on p. 88).

Khan, S. and Quamrul, H. (2021). "Review of developments in air quality modelling and air quality dispersion models". In: *J. Environ. Eng. Sci.* 16.1, pp. 1–10. DOI: 10.1680/jenes.20.00004 (cited on p. 88).

Khaniabadi, Y. O., Goudarzi, G., Daryanoosh, S. M., Borgini, A., Tittarelli, A., and De Marco, A. (2017). "Exposure to PM10, NO2, and O-3 and impacts on human health". In: *Environ. Sci. Pollut. Res.* 24.3, pp. 2781–2789. DOI: 10.1007/s11356-016-8038-6 (cited on p. 21).

Khare, P., Machesky, J., Soto, R., He, M., Presto, A. A., and Gentner, D. R. (2020). "Asphalt-related emissions are a major missing nontraditional source of secondary organic aerosol precursors". In: *Sci. Total Environ.* 6.36, eabb9785. DOI: 10.1126/sciadv.abb9785 (cited on pp. 46–48, 50, 55, 57, 60).

Kim, H. J., Lee, S. H., Il Kwon, S., Park, S., Lee, J., Keel, J. H., Lee, J. T., and Park, S. (2020). "Investigation of the Emission Characteristics of Light-Duty Diesel Vehicles in Korea Based on EURO-VI Standards According to Type of After-Treatment System". In: *Energies* 13.18. DOI: 10.3390/en13184936 (cited on p. 32).

Kim, Y., Lugon, L., Maison, A., Sarica, T., Roustan, Y., Valari, M., Zhang, Y., André, M., and Sartelet, K. (2022). "MUNICH v2.0: a street-network model coupled with SSH-aerosol (v1.2) for multi-pollutant modelling". In: *Geosci. Model Dev.* 15.19, pp. 7371–7396. DOI: 10.5194/gmd-15-7371-2022 (cited on pp. 25, 26, 50–52, 54, 89, 90, 101, 104).

Kim, Y., Sartelet, K., Raut, J. C., and Chazette, P. (2013). "Evaluation of the Weather Research and Forecast/Urban Model Over Greater Paris". In: *Boundary Layer Meteorol* 149, pp. 105–132. DOI: 10.1007/s10546-013-9838-6 (cited on p. 50).

— (2015). "Influence of an urban canopy model and PBL schemes on vertical mixing for air quality modeling over Greater Paris". In: *Atmos. Environ.* 107, pp. 289–306. DOI: 10.1016/j.atmosenv.2015.02.011 (cited on p. 50).

Kim, Y., Wu, Y., Seigneur, C., and Roustan, Y. (2018). "Multi-scale modeling of urban air pollution: development and application of a Street-in-Grid model (v1.0) by coupling MUNICH (v1.0) and Polair3D (v1.8.1)". In: *Geosci. Model Dev.* 11.2, pp. 611–629. DOI: 10.5194/gmd-11-611-2018 (cited on pp. 25, 26, 45–47, 50, 51, 54, 89, 90, 95, 104).

Klimont, Z., Cofala, J., Bertok, I., Amann, M., Heyes, C., and Gyarfas, F. (2002). *Modeling Particulate Emissions in Europe. A Framework to Estimate Reduction Potential and Control Costs*. IIASA Interim Report. IIASA, Laxenburg, Austria. URL: https://pure.iiasa.ac.at/id/eprint/6712/ (cited on p. 34).

Koehler, K. A., DeMott, P. J., Kreidenweis, S. M., Popovicheva, O. B., Petters, M. D., Carrico, C. M., Kireeva, E. D., Khokhlova, T. D., and Shonija, N. K. (2009). "Cloud condensation

nuclei and ice nucleation activity of hydrophobic and hydrophilic soot particles". In: *Phys. Chem. Chem. Phys.* 11 (36), pp. 7906–7920. DOI: 10.1039/B905334B (cited on p. 20).

Krecl, P., Johansson, C., Targino, A. C., Ström, J., and Burman, L. (2017). "Trends in black carbon and size-resolved particle number concentrations and vehicle emission factors under real-world conditions". In: *Atmos. Environ.* 165, pp. 155–168. DOI: 10.1016/j.atmosenv.2017.06.036 (cited on p. 50).

Kuzmichev, A. A. and Loboyko, V. F. (2016). "Impact of the Polluted Air on the Appearance of Buildings and Architectural Monuments in the Area of Town Planning". In: *Procedia Engineering* 150. 2nd International Conference on Industrial Engineering (ICIE-2016), pp. 2095–2101. DOI: 10.1016/j.proeng.2016.07.244 (cited on p. 20).

Kwak, K.-H. and Baik, J.-J. (2012). "A CFD modeling study of the impacts of NOx and VOC emissions on reactive pollutant dispersion in and above a street canyon". In: *Atmos. Environ.* 46, pp. 71–80. DOI: 10.1016/j.atmosenv.2011.10.024 (cited on p. 97).

Kyriakis, N. A. and Andre, M. (1998). "Cold start of passenger cars". In: *Int. J. Veh. Des* 20.1-4, pp. 137–146. DOI: 10.1504/IJVD.1998.001826 (cited on pp. 32, 52).

Landrigan, P. J., Fuller, R., Acosta, N. J. R., Adeyi, O., Arnold, R., Basu, N., Baldé, A. B., Bertollini, R., Bose-O'Reilly, S., Boufford, J. I., Breysse, P. N., Chiles, T., Mahidol, C., Coll-Seck, A. M., Cropper, M. L., Fobil, J., Fuster, V., Greenstone, M., Haines, A., Hanrahan, D., Hunter, D., Khare, M., Krupnick, A., Lanphear, B., Lohani, B., Martin, K., Mathiasen, K. V., McTeer, M. A., Murray, C. J. L., Ndahimananjara, J. D., Perera, F., Potočnik, J., Preker, A. S., Ramesh, J., Rockström, J., Salinas, C., Samson, L. D., Sandilya, K., Sly, P. D., Smith, K. R., Steiner, A., Stewart, R. B., Suk, W. A., van Schayck, O. C. P., Yadama, G. N., Yumkella, K., and Zhong, M. (2018). "The Lancet Commission on pollution and health". In: *Lancet* 391.10119, pp. 462–512. DOI: 10.1016/S0140-6736(17)32345-0 (cited on p. 88).

Lateb, M., Meroney, R. N., Yataghene, M., Fellouah, H., Saleh, F., and Boufadel, M. C. (2016). "On the use of numerical modelling for near-field pollutant dispersion in urban environments - A review". In: *Environ. Pollut.* 208. Special Issue: Urban Health and Wellbeing, pp. 271–283. DOI: 10.1016/j.envpol.2015.07.039 (cited on p. 89).

Lawrence, S., Sokhi, R., Ravindra, K., Mao, H., Prain, H. D., and Bull, I. D. (2013). "Source apportionment of traffic emissions of particulate matter using tunnel measurements". In: *Atmos. Environ.* 77, pp. 548–557. DOI: 10.1016/j.atmosenv.2013.03.040 (cited on p. 71).

Leclercq, L., Laval, J., and Chevallier, E. (2007). "The Lagrangian coordinates and what it means for first order traffic flow models". In: *Proceedings of the 17 International Symposium on Transportation and Traffic Theoryth*, pp. 735–753 (cited on p. 52).

Lee, J. T., Son, J., Kim, J., Choi, Y., Yoo, H.-M., Kim, K. J., Kim, J. S., Park, S. W., Park, G., Park, T., Kang, S., and Lee, T. (2016). "Comparison of Chemical Composition of Particulate Matter Emitted from a Gasoline Direct Injected (GDI) Vehicle and a Port Fuel Injected (PFI) Vehicle using High Resolution Time of Flight Aerosol Mass Spectrometer (HR-ToF-AMS)". In: *Asian J. Atmos. Environ.* 10.1, pp. 51–56. DOI: 10.5572/ajae.2016.10.1.051 (cited on p. 32).

Leighton, P. A. (1961). *Photochemistry of air pollution*. New York: Academic Press (cited on pp. 26, 95).

Lejri, D., Can, A., Schiper, N., and Leclercq, L. (2018). "Accounting for traffic speed dynamics when calculating COPERT and PHEM pollutant emissions at the urban scale". In: *Transp*

Res D Transp Environ 63, pp. 588–603. DOI: 10.1016/j.trd.2018.06.023 (cited on p. 49).

Lelieveld, J., Evans, J. S., Fnais, M., Giannadaki, D., and Pozzer, A. (2015). "The contribution of outdoor air pollution sources to premature mortality on a global scale". In: *Nature* 525.7569, pp. 367–371. DOI: 10.1038/nature15371 (cited on p. 21).

Lemonsu, A., Grimmond, C. S. B., and Masson, V. (2004). "Modeling the Surface Energy Balance of the Core of an Old Mediterranean City: Marseille". In: *J. Applied Meteor.* 43.2, pp. 312–327. DOI: 10.1175/1520-0450(2004)043<0312:MTSEBO>2.0.CO;2 (cited on p. 26).

Li, N., Friedrich, R., and Schieberle, C. (2022a). "Exposure of Individuals in Europe to Air Pollution and Related Health Effects". In: *Front. Public Health* 10. DOI: 10.3389/fpubh.2022.871144 (cited on p. 69).

Li, W., Liu, X., Duan, F., Qu, Y., and An, J. (2022b). "A one-year study on black carbon in urban Beijing: Concentrations, sources and implications on visibility". In: *Atmos. Pollut. Res.* 13.2, p. 101307. DOI: 10.1016/j.apr.2021.101307 (cited on p. 20).

Liang, M., Chao, Y., Tu, Y., and Xu, T. (2023). "Vehicle Pollutant Dispersion in the Urban Atmospheric Environment: A Review of Mechanism, Modeling, and Application". In: *Atmosphere* 14.2. DOI: 10.3390/atmos14020279 (cited on pp. 23, 88).

Lin, C., Wang, Y., Ooka, R., Flageul, C., Kim, Y., Kikumoto, H., Wang, Z., and Sartelet, K. (2022). "Modelling of street-scale pollutant dispersion by coupled simulation of chemical reaction, aerosol dynamics, and CFD". In: *Atmos. Chem. Phys. Discuss.* 2022, pp. 1–32. DOI: 10.5194/acp-2022-365 (cited on pp. 23, 88, 89, 101).

Loaiza-Ceballos, M. C., Marin-Palma, D., Zapata, W., and Hernandez, J. C. (2021). "Viral respiratory infections and air pollutants". In: *Air Qual Atmos Health* 15.1, pp. 105–114. DOI: 10.1007/s11869-021-01088-6 (cited on pp. 21, 22).

Lugon, L. (July 2021). "Modélisation de la qualité de l'air dans les rues de Paris". Theses. École des Ponts ParisTech. URL: https://pastel.archives-ouvertes.fr/tel-03467496 (cited on p. 27).

Lugon, L., Kim, Y., Vigneron, J., Chrétien, O., André, M., André, J. M., Moukhtar, S., Redaelli, M., and Sartelet, K. (2022). "Effect of vehicle fleet composition and mobility on outdoor population exposure: A street resolution analysis in Paris". In: *Atmos. Pollut. Res.* 13.5, p. 101365. DOI: 10.1016/j.apr.2022.101365 (cited on pp. 28, 69, 70, 79, 80).

Lugon, L., Sartelet, K., Kim, Y., Vigneron, J., and Chrétien, O. (2020). "Nonstationary modeling of NO2, NO and NOX in Paris using the Street-in-Grid model: coupling local and regional scales with a two-way dynamic approach". In: *Atmos. Chem. Phys.* 20.13, pp. 7717–7740. DOI: 10.5194/acp-20-7717-2020 (cited on pp. 25, 45, 53, 54, 77, 88, 89).

— (2021a). "Simulation of primary and secondary particles in the streets of Paris using MUNICH". In: *Faraday Discuss.* 226.0, pp. 432–456. DOI: 10.1039/D0FD00092B (cited on pp. 50, 52, 57, 89, 101).

Lugon, L., Vigneron, J., Debert, C., Chrétien, O., and Sartelet, K. (2021b). "Black carbon modeling in urban areas: investigating the influence of resuspension and non-exhaust emissions in streets using the Street-in-Grid model for inert particles (SinG-inert)". In: *Geosci. Model Dev.* 14.11, pp. 7001–7019. DOI: 10.5194/gmd-14-7001-2021 (cited on pp. 25, 45–47, 52, 56, 59, 71, 90, 101).

Luhana, L., Sokhi, R., Warner, L., Mao, H., Boulter, P., McCrae, I., Wright, J., and Osborn, D. (2004). *Measurement of non-exhaust particulate matter*. Tech. rep. Deliverable 8. (last accessed 2022-06-16). EUROPEAN COMMISSION - Directorate General Transport and

Environment. URL: https://www.groundsmartrubbermulch.com/docs/resources/Measurement-%20of-non-exhaust-particulate-matter.pdf (cited on pp. 50, 56).

Lv, Z., Luo, Z., Deng, F., Wang, X., Zhao, J., Xu, L., He, T., Liu, H., and He, K. (2022). "Development and application of a multi-scale modelling framework for urban high-resolution NO_2 pollution mapping". In: *Atmos. Chem. Phys.* 2022, pp. 1–34. DOI: 10.5194/acp-2022-371 (cited on p. 50).

Mabahwi, N. A. B., Ling, O. H. L., and Dasimah, O. (2014). "Human Health and Wellbeing: Human Health Effect of Air Pollution". In: *Procedia Soc. Behav. Sci.* 153, pp. 221–229. DOI: 10.1016/j.sbspro.2014.10.056 (cited on p. 49).

Macdonald, R. W., Griffiths, R. F., and Hall, D. J. (1998). "An improved method for the estimation of surface roughness of obstacle arrays". In: *Atmos. Environ.* 32.11, pp. 1857–1864. DOI: 10.1016/S1352-2310(97)00403-2 (cited on p. 26).

Maison, A., Flageul, C., Carissimo, B., Tuzet, A., and Sartelet, K. (2022). "Parametrization of Horizontal and Vertical Transfers for the Street-Network Model MUNICH Using the CFD Model Code_Saturne". In: *Atmosphere* 13.4, p. 527. DOI: 10.3390/atmos13040527 (cited on pp. 26, 91, 93, 94).

Majdi, M., Sartelet, K., Lanzafame, G. M., Couvidat, F., Kim, Y., Chrit, M., and Turquety, S. (2019). "Precursors and formation of secondary organic aerosols from wildfires in the Euro-Mediterranean region". In: *Atmos. Chem. Phys.* 19.8, pp. 5543–5569. DOI: 10.5194/acp-19-5543-2019 (cited on pp. 28, 51, 64).

Malik, A. and Aggarwal, S.G. (2021). "A Review on the Techniques Used and Status of Equivalent Black Carbon Measurement in Two Major Asian Countries". In: *Asian J. Atmos. Environ.* 15.3. DOI: 10.5572/ajae.2021.044 (cited on p. 59).

Mallet, V., Quélo, D., Sportisse, B., Ahmed de Biasi, M., Debry, É., Korsakissok, I., Wu, L., Roustan, Y., Sartelet, K., Tombette, M., and Foudhil, H. (2007). "Technical Note: The air quality modeling system Polyphemus". In: *Atmos. Chem. Phys.* 7.20, pp. 5479–5487. DOI: 10.5194/acp-7-5479-2007 (cited on pp. 24, 50, 52, 88).

Malmqvist, P.-A. (1983). "Urban Stormwater Pollutant Sources - An Analysis of Inflows and Outflows of Nitrogen, Phosphorus, Lead, Zinc and Copper in Urban Areas". PhD thesis. Chalmers University of Technology (cited on p. 56).

Manisalidis, I., Stavropoulou, E., Stavropoulos, A., and Bezirtzoglou, E. (2020). "Environmental and Health Impacts of Air Pollution: A Review". In: *Front. Public Health* 8. DOI: 10.3389/fpubh.2020.00014 (cited on pp. 20, 21).

Marques, B., Kostenidou, E., Valiente, A. M., Vansevenant, B., Sarica, T., Fine, L., Temime-Roussel, B., Tassel, P., Perret, P., Liu, Y., Sartelet, K., Ferronato, C., and D'Anna, B. (2022). "Detailed Speciation of Non-Methane Volatile Organic Compounds in Exhaust Emissions from Diesel and Gasoline Euro 5 Vehicles Using Online and Offline Measurements". In: *Toxics* 10.4. DOI: 10.3390/toxics10040184 (cited on p. 55).

Masoud, F. S. (2014). "Modélisation de l'impact du trafic routier sur la pollution de l'air et des eaux de ruissellement". Theses. Université Paris-Est. URL: https://pastel.archives-ouvertes.fr/tel-01127301 (cited on p. 36).

Mathissen, M., Scheer, V., Kirchner, U., Vogt, R., and Benter, T. (2012). "Non-exhaust PM emission measurements of a light duty vehicle with a mobile trailer". In: *Atmos. Environ.* 59, pp. 232–242. DOI: 10.1016/j.atmosenv.2012.05.020 (cited on p. 31).

McHugh, C.A., Carruthers, D.J., and Edmunds, H.A. (1997). "ADMS and ADMS–Urban". In: *Int. J. Environ. and Pollution* 8.3-6, pp. 438–440. DOI: 10.1504/IJEP.1997.028193 (cited on pp. 24, 88).

Menut, L., Bessagnet, B., Briant, R., Cholakian, A., Couvidat, F., Mailler, S., Pennel, R., Siour, G., Tuccella, P., Turquety, S., and Valari, M. (2021). "The CHIMERE v2020r1 online chemistry-transport model". In: *Geosci. Model Dev.* 14.11, pp. 6781–6811. DOI: 10.5194/gmd-14-6781-2021 (cited on pp. 23, 88).

Milojevic, A., Niedzwiedz, C. L., Pearce, J., Milner, J., MacKenzie, I. A., Doherty, R. M., and Wilkinson, P. (2017). "Socioeconomic and urban-rural differentials in exposure to air pollution and mortality burden in England". In: *Environmental Health* 16.1. DOI: 10.1186/s12940-017-0314-5 (cited on p. 22).

Mu, Q., Denby, B. R., Wærsted, E. G., and Fagerli, H. (2022). "Downscaling of air pollutants in Europe using uEMEP_v6". In: *Geosci. Model Dev.* 15.2, pp. 449–465. DOI: 10.5194/gmd-15-449-2022 (cited on p. 50).

Myhre, G., Shindell, D., Bréon, F. M., Collins, W., Fuglestvedt, J., Huang, J., Koch, D., Lamarque, J. F., Lee, D., Mendoza, B., et al. (2013a). *Climate change 2013: the physical science basis. Contribution of Working Group I to the Fifth Assessment Report of the Intergovernmental Panel on Climate Change* (cited on p. 20).

Myhre, G., Shindell, D., Bréon, F.-M., Collins, W., Fuglestvedt, J., Huang, J., Koch, D., Lamarque, J.-F., Lee, D, Mendoza, B., Nakajima, T., Robock, A., Stephens, G., Takemura, T., and Zhang, H. (2013b). *Anthropogenic and Natural Radiative Forcing*. In: Climate Change 2013: The Physical Science Basis. Contribution of Working Group I to the Fifth Assessment Report of the Intergovernmental Panel on Climate Change [Stocker, T.F., D. Qin, G.-K. Plattner, M. Tignor, S.K. Allen, J. Boschung, A. Nauels, Y. Xia, V. Bex and P.M. Midgley (eds.)]. Cambridge University Press, Cambridge, United Kingdom and New York, NY, USA (cited on pp. 20, 21).

Myrdal, P. B. and Yalkowsky, S. H. (1997). "Estimating Pure Component Vapor Pressures of Complex Organic Molecules". In: *Ind. Eng. Chem. Res.* 36.6, pp. 2494–2499. DOI: 10.1021/ie9502421 (cited on p. 64).

Nannoolal, Y., Rarey, J., and Ramjugernath, D. (2008). "Estimation of pure component properties: Part 3. Estimation of the vapor pressure of non-electrolyte organic compounds via group contributions and group interactions". In: *Fluid Phase Equilib* 269.1, pp. 117–133. DOI: 10.1016/j.fluid.2008.04.020 (cited on p. 64).

Nannoolal, Y., Rarey, J., Ramjugernath, D., and Cordes, W. (2004). "Estimation of pure component properties: Part 1. Estimation of the normal boiling point of non-electrolyte organic compounds via group contributions and group interactions". In: *Fluid Phase Equilib* 226, pp. 45–63. DOI: 10.1016/j.fluid.2004.09.001 (cited on p. 64).

Nenes, A., Pandis, S.N., and Pilinis, C. (1998). "ISORROPIA: A New Thermodynamic Equilibrium Model for Multiphase Multicomponent Inorganic Aerosols". In: *Aquat Geochem* 4, pp. 123–152. DOI: 10.1023/A:1009604003981 (cited on p. 28).

Nilsson, P. T., Bergendorf, U., Tinnerberg, H., Nordin, E., Gustavsson, M., Strandberg, B., Albin, M., and Gudmundsson, A. (2018). "Emissions into the Air from Bitumen and Rubber Bitumen—Implications for Asphalt Workers' Exposure". In: *Ann. Work Expo. Health* 62.7, pp. 828–839. DOI: 10.1093/annweh/wxy053 (cited on p. 50).

Notter, B., Keller, M., Althaus, H. J., Cox, B., Knörr, W., Heidt, C., Biemann, K., Räder, D., and Jamet, M. (2019). *HBEFA 4.1 – Development Report*. Tech. rep. URL: https://www.hbefa.net/e/documents/HBEFA41_Development_Report.pdf (visited on 04/21/2023) (cited on p. 36).

Ntziachristos, L. and Boulter, P. (2019a). "1.A.3.b.vi-vii Road tyre and brake wear 2019". In: *EMEP/EEA air pollutant emission inventory guidebook 2019*. (last accessed 2023-04-11).

URL: https://www.eea.europa.eu/ds_resolveuid/755d02730336420b8c96ea20eceecea7 (cited on pp. 33, 34, 39, 41, 52).

Ntziachristos, L., Gkatzoflias, D., Kouridis, C., and Samaras, Z. (2009). "COPERT: A European Road Transport Emission Inventory Model". In: *Information Technologies in Environmental Engineering*. Springer Berlin Heidelberg, pp. 491–504. DOI: 10.1007/978-3-540-88351-7_37 (cited on p. 36).

Ntziachristos, L. and Samaras, Z. (2019b). "1.A.3.b.i-iv Road transport 2019". In: *EMEP/EEA air pollutant emission inventory guidebook 2019*. (last accessed 2023-04-11). URL: https://www.eea.europa.eu/ds_resolveuid/f27b3264edb247b4aea14eae9e81b706 (cited on pp. 37, 39, 41).

O'Meara, S., Booth, A. M., Barley, M. H., Topping, D., and McFiggans, G. (2014). "An assessment of vapour pressure estimation methods". In: *Phys. Chem. Chem. Phys.* 16 (36), pp. 19453–19469. DOI: 10.1039/C4CP00857J (cited on p. 64).

Olesen, H.R., Ketzel, M., Jensen, S.S., Løfstrøm, P., Im, U., and Becker, T. (2015). *User Guide to OML-Highway. A tool for air pollution assessments along highways.* Tech. rep. (last visited 2023-02-14). Aarhus University, DCE – Danish Centre for Environment and Energy. URL: https://dce2.au.dk/pub/TR59.pdf (cited on p. 95).

Ottosen, T.-B., Kakosimos, K. E., Johansson, C., Hertel, O., Brandt, J., Skov, H., Berkowicz, R., Ellermann, T., Jensen, S. S., and Ketzel, M. (2015). "Analysis of the impact of inhomogeneous emissions in the Operational Street Pollution Model (OSPM)". In: *Geosci. Model Dev.* 8.10, pp. 3231–3245. DOI: 10.5194/gmd-8-3231-2015 (cited on pp. 92, 94, 108).

Park, I., Kim, H., and Lee, S. (2018). "Characteristics of tire wear particles generated in a laboratory simulation of tire/road contact conditions". In: *J. Aerosol Sci.* 124, pp. 30–40. DOI: 10.1016/j.jaerosci.2018.07.005 (cited on p. 33).

Paz, D. de la, Borge, R., Vedrenne, M., Lumbreras, J., Amato, F., Karanasiou, A., Boldo, E., and Moreno, T. (2015). "Implementation of road dust resuspension in air quality simulations of particulate matter in Madrid (Spain)". In: *Front. Environ. Sci.* 3. DOI: 10.3389/fenvs.2015.00072 (cited on pp. 23, 88).

Pelkmans, L., Lenaers, G., Bruyninx, J., Scheepers, K., and De Vlieger, I. (2011). "Impact of biofuel blends on the emissions of modern vehicles". In: *Proceedings of the institution of mechanical engineers part D - journal of automobile engineering* 225.D9, SI, pp. 1204–1220. DOI: 10.1177/0954407011407254 (cited on p. 32).

Perry, R. and Gee, I. L. (1995). "Vehicule emissions in relation to fuel composition". In: *Sci. Total Environ.* 169.1-3. 3rd International Symposium on Transport and Air Pollution, AVIGNON, FRANCE, JUN 06-10, 1994, pp. 149–156. DOI: 10.1016/0048-9697(95)04643-F (cited on p. 32).

Pielecha, J., Skobiej, K., and Kurtyka, K. (2021). "Testing and evaluation of cold-start emissions from a gasoline engine in RDE test at two different ambient temperatures". In: *Open Eng.* 11.1, pp. 425–434. DOI: doi:10.1515/eng-2021-0047 (cited on pp. 32, 52).

Putaud, J.-P., Van Dingenen, R., Alastuey, A., Bauer, H., Birmili, W., Cyrys, J., Flentje, H., Fuzzi, S., Gehrig, R., Hansson, H. C., Harrison, R. M., Herrmann, H., Hitzenberger, R., Hüglin, C., Jones, A. M., Kasper-Giebl, A., Kiss, G., Kousa, A., Kuhlbusch, T. A. J., Löschau, G., Maenhaut, W., Molnar, A., Moreno, T., Pekkanen, J., Perrino, C., Pitz, M., Puxbaum, H., Querol, X., Rodriguez, S., Salma, I., Schwarz, J., Smolik, J., Schneider, J., Spindler, G., ten Brink, H., Tursic, J., Viana, M., Wiedensohler, A., and Raes, F. (2010). "A European aerosol phenomenology – 3: Physical and chemical characteristics of

particulate matter from 60 rural, urban, and kerbside sites across Europe". In: *Atmos. Environ.* 44.10, pp. 1308–1320. DOI: 10.1016/j.atmosenv.2009.12.011 (cited on p. 20).

Quaassdorff, C., Smit, R., Borge, R., and Hausberger, S. (2022). "Comparison of microscale traffic emission models for urban networks". In: *Environ. Res. Lett.* 17.9, p. 094030. DOI: 10.1088/1748-9326/ac8b21 (cited on p. 49).

Roberts, D. L. and Jones, A. (2004). "Climate sensitivity to black carbon aerosol from fossil fuel combustion". In: *J. Geophys. Res. Atmos.* 109.D16. DOI: 10.1029/2004JD004676 (cited on p. 20).

Rood, A. S. (2014). "Performance evaluation of AERMOD, CALPUFF, and legacy air dispersion models using the Winter Validation Tracer Study dataset". In: *Atmos. Environ.* 89, pp. 707–720. DOI: 10.1016/j.atmosenv.2014.02.054 (cited on p. 88).

Ropkins, K., Beebe, J., Li, H., Daham, B., Tate, J., Bell, M., and Andrews, G. (2009). "Real-World Vehicle Exhaust Emissions Monitoring: Review and Critical Discussion". In: *Crit Rev Environ Sci Technol* 39.2, pp. 79–152. DOI: 10.1080/10643380701413377 (cited on p. 31).

Roustan, Y., Pausader, M., and Seigneur, C. (2011). "Estimating the effect of on-road vehicle emission controls on future air quality in Paris, France". In: *Atmos. Environ.* 45.37, pp. 6828–6836. DOI: 10.1016/j.atmosenv.2010.10.010 (cited on pp. 28, 54, 69).

Saarikoski, S., Niemi, J. V., Aurela, M., Pirjola, L., Kousa, A., Rönkkö, T., and Timonen, H. (2021). "Sources of black carbon at residential and traffic environments obtained by two source apportionment methods". In: *Atmos. Chem. Phys.* 21.19, pp. 14851–14869. DOI: 10.5194/acp-21-14851-2021 (cited on p. 49).

Saliba, G., Saleh, R., Zhao, Y., Presto, A. A., Lambe, A. T., Frodin, B., Sardar, S., Maldonado, H., Maddox, C., May, A. A., Drozd, G. T., Goldstein, A. H., Russell, L. M., Hagen, F., and Robinson, A. L. (2017). "Comparison of Gasoline Direct-Injection (GDI) and Port Fuel Injection (PFI) Vehicle Emissions: Emission Certification Standards, Cold-Start, Secondary Organic Aerosol Formation Potential, and Potential Climate Impacts". In: *Env. Sc. and Tech.* 51.11, pp. 6542–6552. DOI: 10.1021/acs.est.6b06509 (cited on pp. 32, 63).

San Jose, R. and Perez-Camanyo, J. L. (2022). "High-resolution impacts of green areas on air quality in Madrid". In: *Air Qual Atmos Health*. DOI: 10.1007/s11869-022-01263-3 (cited on p. 50).

Sanchez, B., Santiago, J.-L., Martilli, A., Palacios, M., and Kirchner, F. (2016). "CFD modeling of reactive pollutant dispersion in simplified urban configurations with different chemical mechanisms". In: *Atmos. Chem. Phys.* 16.18, pp. 12143–12157. DOI: 10.5194/acp-16-12143-2016 (cited on p. 89).

Sanders, P. G., Xu, N., Dalka, T. M., and Maricq, M. M. (2003). "Airborne Brake Wear Debris: Size Distributions, Composition, and a Comparison of Dynamometer and Vehicle Tests". In: *Env. Sc. and Tech.* 37.18, pp. 4060–4069. DOI: 10.1021/es034145s (cited on pp. 33, 34).

Sarica, T. (2021). *Pollemission: computational tool for air pollutant emission factors from traffic*. Version 2.0. DOI: 10.5281/zenodo.5721253 (cited on pp. 36, 51).

Sarica, T., Maison, A., Roustan, Y., Ketzel, M., Jensen, S. S., Kim, Y., Chaillou, C., and Sartelet, K. (2023a). "Modelling concentration heterogeneities in streets using the street-network model MUNICH". In: *Geosci. Model Dev. Discuss.* 2023, pp. 1–34. DOI: 10.5194/gmd-2023-70 (cited on p. 88).

Sarica, T., Maison, A., Roustan, Y., Ketzel, M., Jensen, S. S., Kim, Y., and Sartelet, K. (2023b). *The Model of Urban Network of Intersecting Canyons and Highways (MUNICH)*. Version hete. DOI: 10.5281/zenodo.7778271 (cited on p. 107).

Sarica, T., Sartelet, K., Roustan, Y., Kim, Y., Lugon, L., André, M., Marques, B., D'Anna, B., Chaillou, C., and Larrieu, C. (2022). "Modelling Pollutant Concentrations in Streets: A Sensitivity Analysis to Asphalt and Traffic Related Emissions". In: *Air Pollution Modeling and its Application XXVIII*. Ed. by Clemens Mensink and Oriol Jorba. Cham: Springer International Publishing, pp. 287–293. DOI: 10.1007/978-3-031-12786-1_39 (cited on pp. 44, 101).

Sarica, T., Sartelet, K., Roustan, Y., Kim, Y., Lugon, L., Marques, B., D'Anna, B., Chaillou, C., and Larrieu, C. (2023c). "Sensitivity of pollutant concentrations in urban streets to asphalt and traffic-related emissions". In: *Environ. Pollut.* 332, p. 121955. DOI: 10.1016/j.envpol.2023.121955 (cited on pp. 44, 101).

Sartelet, K., Couvidat, F., Wang, Z., Flageul, C., and Kim, Y. (2020). "SSH-Aerosol v1.1: A Modular Box Model to Simulate the Evolution of Primary and Secondary Aerosols". In: *Atmosphere* 11.5. DOI: 10.3390/atmos11050525 (cited on pp. 27, 28, 45, 50, 89, 101).

Sartelet, K., Kim, Y., Couvidat, F., Merkel, M., Petäjä, T., Sciare, J., and Wiedensohler, A. (2022). "Influence of emission size distribution and nucleation on number concentrations over Greater Paris". In: *Atmos. Chem. Phys.* 22.13, pp. 8579–8596. DOI: 10.5194/acp-22-8579-2022 (cited on p. 50).

Sartelet, K., Zhu, S., Moukhtar, S., André, M., André, J. M., Gros, V., Favez, O., Brasseur, A., and Redaelli, M. (2018). "Emission of intermediate, semi and low volatile organic compounds from traffic and their impact on secondary organic aerosol concentrations over Greater Paris". In: *Atmos. Environ.* 180, pp. 126–137. DOI: 10.1016/j.atmosenv.2018.02.031 (cited on pp. 24, 45, 46, 48, 50, 52–54, 56, 72, 77, 88).

Sartelet, K. N., Couvidat, F., Seigneur, C., and Roustan, Y. (2012). "Impact of biogenic emissions on air quality over Europe and North America". In: *Atmos. Environ.* 53. AQMEII: An International Initiative for the Evaluation of Regional-Scale Air Quality Models - Phase 1, pp. 131–141. DOI: 10.1016/j.atmosenv.2011.10.046 (cited on p. 24).

Sartelet, K. N., Debry, E., Fahey, K., Roustan, Y., Tombette, M., and Sportisse, B. (2007). "Simulation of aerosols and gas-phase species over Europe with the Polyphemus system: Part I—Model-to-data comparison for 2001". In: *Atmos. Environ.* 41.29, pp. 6116–6131. DOI: 10.1016/j.atmosenv.2007.04.024 (cited on p. 53).

Schulte, N., Tan, S., and Venkatram, A. (2015). "The ratio of effective building height to street width governs dispersion of local vehicle emissions". In: *Atmos. Environ.* 112, pp. 54–63. DOI: 10.1016/j.atmosenv.2015.03.061 (cited on p. 26).

Seinfield, J. H. and Pandis, S. N. (2016). *Atmospheric Chemistry and Physics: From Air Pollution to Climate Change*. Ed. by Wiley Blackwell. 3rd ed. (cited on p. 20).

Singh, A. and Agrawal, M. (2008). "Acid rain and its ecological consequences". In: *J. Environ. Biol.* 29.1, pp. 15–24 (cited on p. 20).

Skamarock, W., Klemp, J., Dudhia, J., Gill, D., Barker, D., Wang, W., Huang, X.-Y., and Duda, M. (2008). *A Description of the Advanced Research WRF Version 3*. Tech. rep. UCAR/NCAR. DOI: 10.5065/D68S4MVH (cited on p. 95).

Solazzo, E., Cai, X., and Vardoulakis, S. (2008). "Modelling wind flow and vehicle-induced turbulence in urban streets". In: *Atmos. Environ.* 42.20, pp. 4918–4931. DOI: 10.1016/j.atmosenv.2008.02.032 (cited on p. 92).

Soulhac, L., Fellini, S., Vuong Nguyen, C., and Salizzoni, P. (2023). "Evaluation of Photostationary and Non-Photostationary Operational Models for NOX Pollution in a Street Canyon". In: *Atmos. Environ.* 297, p. 119589. DOI: 10.1016/j.atmosenv.2023.119589 (cited on p. 88).

Soulhac, L., Garbero, V., Salizzoni, P., Mejean, P., and Perkins, R. J. (2009). "Flow and dispersion in street intersections". In: *Atmos. Environ.* 43.18, pp. 2981–2996. DOI: 10.1016/j.atmosenv.2009.02.061 (cited on pp. 26, 89, 90, 92).

Soulhac, L., Perkins, R. J., and Salizzoni, P. (2008). "Flow in a Street Canyon for any External Wind Direction". In: *Boundary Layer Meteorol* 126, pp. 365–388. DOI: 10.1007/s10546-007-9238-x (cited on p. 26).

Soulhac, L., Salizzoni, P., Cierco, F.-X., and Perkins, R. (2011). "The model SIRANE for atmospheric urban pollutant dispersion; part I, presentation of the model". In: *Atmos. Environ.* 45.39, pp. 7379–7395. DOI: 10.1016/j.atmosenv.2011.07.008 (cited on pp. 24, 26, 88).

Sportisse, B. (2010). *Fundamentals in Air Pollution: From Processes to Modelling*. Springer Netherlands. DOI: 10.1007/978-90-481-2970-6 (cited on p. 24).

Stein, S. E. and Brown, R. L. (1994). "Estimation of normal boiling points from group contributions". In: *J Chem Inf Model* 34.3, pp. 581–587. DOI: 10.1021/ci00019a016 (cited on p. 64).

Stone, R. (1999). *Solutions Manual for Introduction to Internal Combustion Engines*. Macmillan Education UK. DOI: 10.1007/978-1-349-15079-3. URL: https://doi.org/10.1007/978-1-349-15079-3 (cited on p. 32).

Strosnider, H., Kennedy, C., Monti, M., and Yip, F. (2017). "Rural and Urban Differences in Air Quality, 2008–2012, and Community Drinking Water Quality, 2010–2015 — United States". In: *MMWR. Surveillance Summaries* 66.13, pp. 1–10. DOI: 10.15585/mmwr.ss6613a1 (cited on p. 22).

Tang, J., McNabola, A., Misstear, B., Pilla, F., and Alam, M. S. (2019). "Assessing the Impact of Vehicle Speed Limits and Fleet Composition on Air Quality Near a School". In: *Int. J. Environ. Res. Public Health* 16.1. DOI: 10.3390/ijerph16010149 (cited on pp. 69, 70).

Thorpe, A. and Harrison, R. M. (2008). "Sources and properties of non-exhaust particulate matter from road traffic: A review". In: *Sci. Total Environ.* 400.1, pp. 270–282. DOI: 10.1016/j.scitotenv.2008.06.007 (cited on pp. 33, 34, 56).

Trombetti, M., Thunis, P., Bessagnet, B., Clappier, A., Couvidat, F., Guevara, M., Kuenen, J., and López-Aparicio, S. (2018). "Spatial inter-comparison of Top-down emission inventories in European urban areas". In: *Atmos. Environ.* 173, pp. 142–156. DOI: 10.1016/j.atmosenv.2017.10.032 (cited on pp. 22, 31).

Tsanakas, N. (2019). *Emission estimation based on traffic models and measurements*. DOI: 10.3384/lic.diva-155771 (cited on p. 36).

Tsanakas, N., Ekström, J., and Olstam, J. (2020). "Estimating Emissions from Static Traffic Models: Problems and Solutions". In: *J. Adv. Transp.* DOI: 10.1155/2020/5401792 (cited on p. 49).

Twomey, S. (1977). "The Influence of Pollution on the Shortwave Albedo of Clouds". In: *J. Atmos. Sci.* 34.7, pp. 1149–1152. DOI: 10.1175/1520-0469(1977)034<1149:TIOPOT>2.0.CO;2 (cited on p. 20).

UN (1968). *Convention on road traffic*. Tech. rep. Economic Commission for Europe – Inland Transport Committee. URL: https://unece.org/DAM/trans/conventn/crt1968e.pdf (visited on 04/21/2023) (cited on p. 31).

United Nations (2019). *World Urbanization Prospects: The 2018 Revision*. Tech. rep. URL: https://population.un.org/wup/Publications/Files/WUP2018-Report.pdf (visited on 04/21/2023) (cited on p. 88).

Vardoulakis, S., Fisher, B. E. A., Pericleous, K., and Gonzalez-Flesca, N. (2003). "Modelling air quality in street canyons: a review". In: *Atmos. Environ.* 37.2, pp. 155–182. DOI: 10.1016/S1352-2310(02)00857-9 (cited on pp. 23, 88).

Vardoulakis, S., Solazzo, E., and Lumbreras, J. (2011). "Intra-urban and street scale variability of BTEX, NO2 and O3 in Birmingham, UK: Implications for exposure assessment". In: *Atmos. Environ.* 45.29, pp. 5069–5078. DOI: 10.1016/j.atmosenv.2011.06.038 (cited on p. 89).

Vehkamäki, H., Kulmala, M., Napari, I., Lehtinen, K. E. J., Timmreck, C., Noppel, M., and Laaksonen, A. (2002). "An improved parameterization for sulfuric acid–water nucleation rates for tropospheric and stratospheric conditions". In: *J. Geophys. Res. Atmos.* 107.D22, AAC 3-1-AAC 3–10. DOI: 10.1029/2002JD002184 (cited on p. 27).

Wan, J.-M., Lin, M., Chan, C.-Y., Zhang, Z.-S., Engling, G., Wang, X.-M., Chan, I.-N., and Li, S.-Y. (2011). "Change of air quality and its impact on atmospheric visibility in central-western Pearl River Delta". In: *Environ. Monit. Assess.* 172.1-4, pp. 339–351. DOI: 10.1007/s10661-010-1338-2 (cited on p. 20).

Wang, W. (2012). "An Analytical Model for Mean Wind Profiles in Sparse Canopies". In: *Boundary Layer Meteorol* 142, pp. 383–399. DOI: 10.1007/s10546-011-9687-0 (cited on p. 26).

— (2014). "Analytically modelling mean wind and stress profiles in canopies". In: *Boundary Layer Meteorol* 151, pp. 239–256. DOI: 10.1007/s10546-013-9899-6 (cited on pp. 26, 91).

Westerholm, R. and Egeback, K. E. (1994). "Exhaust emissions from ligh-duty and heavy-duty vehicles – chemical-composition, impact of exhaust after treatment, and fuel parameters". In: *Environ. Health Perspect.* 102.4. Symposium on Risk Assessment of Urban Air: Emissions, Exposure, Risk Identification and Risk Quantitation, STOCKHOLM, SWEDEN, MAY 31-JUN 03, 1992, pp. 13–23. DOI: 10.2307/3431926 (cited on p. 32).

WHO (Sept. 2021). *WHO global air quality guidelines: particulate matter (PM2.5 and PM10), ozone, nitrogen dioxide, sulfur dioxide and carbon monoxide*. World Health Organization. Genève, Switzerland: World Health Organization (cited on pp. 22, 23).

Wiesner, A., Pfeifer, S., Merkel, M., Tuch, T., Weinhold, K., and Wiedensohler, A. (2021). "Real World Vehicle Emission Factors for Black Carbon Derived from Longterm In-Situ Measurements and Inverse Modelling". In: *Atmosphere* 12.1. DOI: 10.3390/atmos12010031 (cited on p. 50).

Wik, A. and Dave, G. (2009). "Occurrence and effects of tire wear particles in the environment – A critical review and an initial risk assessment". In: *Environ. Pollut.* 157.1, pp. 1–11. DOI: 10.1016/j.envpol.2008.09.028 (cited on p. 33).

Wolf, T., Pettersson, L. H., and Esau, I. (2020). "A very high-resolution assessment and modelling of urban air quality". In: *Atmos. Chem. Phys.* 20.2, pp. 625–647. DOI: 10.5194/acp-20-625-2020 (cited on p. 88).

Wong, D.C., Pleim, J., Mathur, R., Binkowski, F., Otte, T., Gilliam, R., Pouliot, G., Xiu, A., and Kang, D. (2012). "WRF-CMAQ two-way coupled system with aerosol feedback:

software development and preliminary results." In: *Geosci. Model Dev.* 5, pp. 299–312. DOI: 10.5194/gmd-5-299-2012 (cited on pp. 23, 88).

Xia, T., Nitschke, M., Zhang, Y., Shah, P., Crabb, S., and Hansen, A. (2015). "Traffic-related air pollution and health co-benefits of alternative transport in Adelaide, South Australia". In: *Environ Int* 74, pp. 281–290. DOI: 10.1016/j.envint.2014.10.004 (cited on p. 69).

Xie, H. and Zhang, Y. (2013). "The Research Status of Acid Rain". In: *ADVANCES IN ENVIRONMENTAL TECHNOLOGIES, PTS 1-6*. Vol. 726-731. Advanced Materials Research, pp. 4033–4036. DOI: 10.4028/www.scientific.net/AMR.726-731.4033 (cited on p. 20).

Xie, S., Zhang, Y., Qi, L., and Tang, X. (2003). "Spatial distribution of traffic-related pollutant concentrations in street canyons". In: *Atmos. Environ.* 37.23, pp. 3213–3224. DOI: 10.1016/S1352-2310(03)00321-2 (cited on p. 89).

Yarwood, G., Rao, S., Yocke, M., and Whitten, G. (2005). "Updates to the Carbon Bond Chemical Mechanism: CB05". In: *RT-04-00675*. URL: https://camx-wp.azurewebsites.net/Files/CB05_Final_Report_120805.pdf (visited on 04/21/2023) (cited on pp. 28, 51).

Yue, T., Yue, X., Chai, F., Hu, J., Lai, Y., He, L., and Zhu, L. (2017). "Characteristics of volatile organic compounds (VOCs) from the evaporative emissions of modern passenger cars". In: *Atmos. Environ.* 151, pp. 62–69. DOI: 10.1016/j.atmosenv.2016.12.008 (cited on p. 33).

Zallinger, M. S., Tate, J., and Hausberger, S. (2008). "An Instantaneous Emission Model for the Passenger Car Fleet". In: *VKM-THD Mitteilungen*. Vol. 91. ISBN: 987-3-85125-016-9; 16th Symposium Transport and Air Pollution ; Conference date: 16-06-2008 Through 17-06-2008. Verlag der Technischen Universität Graz, pp. 117–128 (cited on p. 36).

Zhang, H. (2015). "Simulation-Based Estimation of Fuel Consumption and Emissions of Asphalt Paving Operations". In: *J. Comput. Civ. Eng.* 29.2, p. 04014039. DOI: 10.1061/(ASCE)CP.1943-5487.0000326 (cited on p. 50).

Zhang, J., Wei, Y., and Fang, Z. (2019). "Ozone Pollution: A Major Health Hazard Worldwide". In: *Front. Immunol.* 10. DOI: 10.3389/fimmu.2019.02518 (cited on p. 21).

Zhang, X., Fung, J. C. H., Zhang, Y., Lau, A. K. H., Leung, K. K. M., and Huang, W. (2020). "Assessing PM2.5 emissions in 2020: The impacts of integrated emission control policies in China". In: *Environ. Pollut.* 263, p. 114575. DOI: 10.1016/j.envpol.2020.114575 (cited on p. 69).

Zhao, Y., Nguyen, N. T., Presto, A. A., Hennigan, C. J., May, A. A., and Robinson, A. L. (2016). "Intermediate Volatility Organic Compound Emissions from On-Road Gasoline Vehicles and Small Off-Road Gasoline Engines". In: *Env. Sc. and Tech.* 50.8, pp. 4554–4563. DOI: 10.1021/acs.est.5b06247 (cited on p. 56).

Zheng, X., He, L., He, X., Zhang, S., Cao, Y., Hao, J., and Wu, Y. (2022). "Real-Time Black Carbon Emissions from Light-Duty Passenger Vehicles Using a Portable Emissions Measurement System". In: *Engineering* 16, pp. 73–81. DOI: 10.1016/j.eng.2020.11.009 (cited on p. 31).

Zhong, J., Cai, X. M., and Bloss, W. J. (2017). "Large eddy simulation of reactive pollutants in a deep urban street canyon: Coupling dynamics with O3-NOx-VOC chemistry". In: *Environ. Pollut.* 224, pp. 171–184. DOI: 10.1016/j.envpol.2017.01.076 (cited on p. 97).

Zhu, S., Sartelet, K., Zhang, Y., and Nenes, A. (2016a). "Three-dimensional modeling of the mixing state of particles over Greater Paris". In: *J. Geophys. Res. Atmos.* 121.10, pp. 5930–5947. DOI: 10.1002/2015JD024241 (cited on p. 24).

Zhu, S., Sartelet, K. N., Healy, R. M., and Wenger, J. C. (2016b). "Simulation of particle diversity and mixing state over Greater Paris: a model–measurement inter-comparison". In: *Faraday Discuss.* 189 (0), pp. 547–566. DOI: 10.1039/C5FD00175G (cited on pp. 24, 50).

Zhu, S., Sartelet, K. N., and Seigneur, C. (2015). "A size-composition resolved aerosol model for simulating the dynamics of externally mixed particles: SCRAM (v 1.0)". In: *Geosci. Model Dev.* 8.6, pp. 1595–1612. DOI: 10.5194/gmd-8-1595-2015 (cited on p. 27).